The Role of Cilia in Inner Ear Development and Otolith Formation in the Zebrafish Embryo

Georgina Alexandra Stooke-Vaughan

MRC Centre for Developmental and Biomedical Genetics
Department of Biomedical Science
The University of Sheffield

Thesis submitted for the degree of Doctor of Philosophy
September 2013

Abstract

The inner ear is the vertebrate organ of hearing and balance. The ear structures required for vestibular function are well conserved across vertebrates. Here the zebrafish is used as a model of inner ear development, with a focus on the role of cilia in this process.

Otoliths are biomineralised structures required for the sensation of gravity, linear acceleration and sound in the zebrafish ear. Otolith precursor particles, initially distributed throughout the otic vesicle lumen, become tethered to the tips of hair cell kinocilia at the otic vesicle poles, forming two otoliths. I have used high-speed videomicroscopy to investigate the role of hair cells, cilia and ciliary motility in otolith formation. I provide a careful description of the distribution of motile and non-motile cilia in the wild-type otic vesicle. I find that hair cells are essential for the tethering of otoliths within the otic vesicle. Absent cilia or defective ciliary motility lead to the formation of defective otoliths; this suggests that normally cilia help the process of otolith formation. I also show that embryonic movement plays a minor role in the formation of normal otoliths.

After 1 day postfertilisation motile cilia within the otic vesicle disappear. Non-motile cilia remain and have a role in relaying developmental signals. Zebrafish otic vesicles developing in the absence of cilia show defects in morphogenesis associated with an incomplete repression of the hedgehog signalling pathway. Hair cells are capable of differentiating and polarising at both cellular and tissue level in the absence of cilia or ciliary motility. However, a decrease in hair cell number is seen in zebrafish mutants with cilia defects.

This work increases our understanding of the mechanistic and signalling functions of cilia in development of the zebrafish ear. Some aspects of otolith formation in the zebrafish embryo are also clarified.

Acknowledgements

I would first like to thank Dr. Tanya Whitfield, for being an excellent PhD supervisor who was always happy to give advice and discuss ideas and experimental plans. I am very grateful for her nearly always open office door.

The past and present members of Dr. Whitfield's lab have been invaluable in their advice, willingness to help, and willingness to have coffee breaks. Thank you Kate, Leila, Laina, Fansuo, Lauren, Esther, Sarah, CJ, Ryan and Rachael. I would also like to say an extra thank you to Kate Hammond for sharing her thoughts about the role of embryonic movement in otolith formation.

Our collaborators on this project, Dr. Peng Huang and Prof. Alexander Schier, generously shipped maternal zygotic mutant embryos to us so I could investigate ear formation in the absence of cilia.

My advisors, Dr. Andrew Furley and Dr. Freek van Eeden, provided valuable discussion and advice at advisory meetings, which I mostly listened to and followed.

Dr. Robert Forrester went beyond the call of duty as departmental manager, picking up a desk lamp at the weekend to save me headaches and eyestrain while writing this thesis.

The excellent zebrafish care provided by the team of staff working at the CDBG aquarium facility has ensured that working with these animals has been as simple as it could be.

My funding was provided by the BBSRC, and has allowed me to learn by attending scientific courses and conferences as well as supporting me in the lab.

I would like to thank the teams of people who work to make and maintain the free software that has made my PhD thesis and research possible, particularly the people behind Fiji Is Just ImageJ, LaTeX, Texmaker and Mendeley Desktop. I also want to thank the people who built and contributed to the fantastic online communities providing documentation and support for these programs, without which I would have been lost.

Finally, I would like to thank my family and my fiancé, Stuart. They always look interested when I decide to talk science, but also know how to give me a break from lab life. We all need to be shown the bigger picture sometimes.

List of Abbreviations

AP	Alkaline phosphatase
BCIP	5-bromo-4-chloro-3'-indolyphosphate p-toluidine salt
BDP	BSA, DMSO, PBS
BSA	Bovine serum albumin
DAB	Diaminobenzidine
dH_2O	Distilled water
DIC	Differential interference contrast
DIG	Digoxigenin
DMSO	Dimethyl sulfoxide
DNA	Deoxyribonucleic acid
dpf	days post fertilisation
DTT	Dithiothreitol
E3	Embryo Medium
EDTA	Ethylenediaminetetraacetic acid
EtOH	Ethanol
FCS	Fetal calf serum
FITC	Fluorescein isothiocyanate
GFP	Green fluorescent protein
hpf	hours post fertilisation
HRP	Horseradish peroxidase
Hyb+	Hybridisation solution with tRNA and heparin

Hyb–	Hybridisation solution without tRNA and heparin
IgG	Immunoglobulin G
MO	Morpholino
NBT	nitro-blue tetrazolium chloride
OV	Otic vesicle
PBS	Phosphate buffered saline
PCP	Planar cell polarity
PFA	Paraformaldehyde
PTW	PBS Tween
RNA	Ribonulceic acid
S	Somite stage
SSC	Saline-sodium citrate buffer
TRITC	Tetramethylrhodamine isothiocyanate
tRNA	Transfer RNA

Contents

1 Introduction **7**

1.1 Significance of the project . . . 7
1.2 Cilia . . . 9
1.2.1 Ciliogenesis . . . 9
1.2.2 Structure of cilia . . . 11
1.2.3 Genes involved in ciliogenesis and cilia function relevant to this study 13
1.2.4 Functions of cilia . . . 16
1.2.5 Diseases of cilia . . . 17
1.3 Inner ear function, structure and development . . . 18
1.3.1 Overview of inner ear function and structure . . . 18
1.3.2 Ear development in the zebrafish embryo . . . 19
1.3.3 Signalling pathways involved in patterning the zebrafish ear . . . 20
1.3.4 Hair cells . . . 21
1.3.5 Otolith formation in the zebrafish . . . 25
1.4 The role of cilia in otolith formation in the zebrafish embryo . . . 27
1.5 The role of cilia in inner ear patterning and morphogenesis in the zebrafish embryo . . . 30
1.6 Objectives of PhD research . . . 30

2 Materials and Methods **31**

2.1 Zebrafish husbandry . . . 31
2.1.1 Zebrafish care . . . 31
2.1.2 Embryo collection . . . 31
2.1.3 Embryo staging . . . 31
2.1.4 Embryo raising . . . 31
2.2 Zebrafish lines . . . 32
2.3 Microscopy . . . 33
2.3.1 DIC and epifluorescence microscopy . . . 33
2.3.2 Confocal microscopy . . . 33
2.3.3 High-speed videomicroscopy . . . 33
2.4 Immunohistochemistry . . . 34

2.4.1 Double anti-acetylated tubulin/phalloidin stains . . . 34
2.4.2 Anti-acetylated tubulin stain using HRP conjugated secondary antibody . . . 34
2.4.3 Double anti-acetylated tubulin anti-GFP stains . . . 35
2.4.4 Immunohistochemistry solutions . . . 35
2.4.5 Preparation of embryos for examination of hair-cell polarity in sensory maculae . . . 35
2.5 Whole mount *in situ* hybridisation . . . 36
2.5.1 Solutions for *in situ* hybridisation . . . 37
2.6 Morpholino injections . . . 38
2.7 Molecular biology . . . 38
2.7.1 Transformation of plasmid DNA . . . 38
2.7.2 Plasmid purification . . . 38
2.7.3 Restriction enzyme digestion of plasmid DNA . . . 38
2.7.4 Synthesis of DIG labelled RNA probes . . . 38
2.8 Movement restriction and forced motion experiments . . . 39
2.8.1 Movement restriction . . . 39
2.8.2 Forced motion . . . 39
2.8.3 Otolith scoring . . . 39
2.9 Image analysis . . . 41
2.9.1 Estimates of total cilia number in the otic vesicle . . . 41
2.9.2 Movie processing . . . 41
2.9.3 Counts of total motile cilia in otic vesicle . . . 41
2.9.4 Calculation of ciliary beat frequency . . . 41
2.9.5 Time-to-colour images . . . 41
2.9.6 Polarity patterns . . . 42
2.9.7 Polarity graphs . . . 42
2.10 Statistics . . . 43

3 Description of Cilia in the Wild-Type Otic Vesicle 44
3.1 Introduction . . . 44
3.2 Results . . . 44
3.2.1 Cilia presence and number in the wild-type otic vesicle . . . 44
3.2.2 Motility of cilia in the wild-type otic vesicle . . . 47
3.2.3 Tether cilia are immotile in the absence of otolith binding . . . 49
3.3 Discussion . . . 50

4 Mechanisms of Otolith Tethering in the Zebrafish Embryo 54
4.1 Introduction . . . 54
4.2 Results . . . 55
4.2.1 The effect of a complete loss of cilia (MZ*ovl*) on otolith formation . 55

4.2.2 The effect of a zygotic loss of *ift88* on otolith formation (Z*ovl*) . . . 57
4.2.3 The effect of a partial loss of cilia (*iguana*) on otolith formation . . . 57
4.2.4 Otolith defects in embryos lacking cilia are unlikely to be due to misexpression of genes required for otolith formation 60
4.2.5 The effect of a loss of ciliary motility (*lrrc50*) on otolith formation . 61
4.2.6 The effects of otolith tethering and ciliary flow on the visible length of kinocilia 62
4.2.7 The effect of ectopic hair cells and tether cilia on otolith tethering (*mindbomb*) 63
4.2.8 The effect of hair cell loss on otolith tethering (*atoh1b* morpholino injection) 64
4.2.9 The effect of loss of cilia and gain of hair cells on otolith tethering (MZ*ovl* injected with *Su(H)1+2* morpholino) 66
4.2.10 The effect of loss of both cilia and hair cells on otolith tethering (MZ*ovl* injected with *atoh1b* morpholino) 66
4.2.11 The role of embryonic movement in otolith tethering 67
4.2.12 Cilia and ciliary motility are normal in the *sloth* mutant 70
4.2.13 Normal development can rescue otolith defects in mutants lacking cilia (igu^{ts294e}) or ciliary motility (*lrrc50*) 71
4.3 Discussion 71
4.3.1 Ciliary flow helps to prevent the formation of untethered otoliths . . 72
4.3.2 The first hair cells produce a factor or factors essential for otolith tethering 74
4.3.3 Embryonic movement plays a minor role in normal otolith formation 75
4.4 Conclusion 76

5 The Role of Cilia in Inner Ear Patterning and Morphogenesis 78
5.1 Introduction 78
5.2 Results 79
5.2.1 Sensory patch polarity is not affected in mutants completely lacking cilia (MZ*ovl*) 79
5.2.2 Sensory patch polarity is not affected in mutants with a severe loss of cilia (Z*ovl*) 81
5.2.3 Sensory patch polarity is not affected in mutants with a reduced number of cilia (*iguana*) 83
5.2.4 Sensory patch polarity is not affected in mutants lacking ciliary motility (*lrrc50*) 84
5.2.5 Hair cell number is reduced in the posterior maculae of all ciliary mutants, and reduced in both the anterior and posterior macula of zygotic or maternal zygotic *ovl* mutants 85

5.2.6 The establishment of sensory patch polarity is not dependent on ciliary flow . . . 89
5.2.7 The hair cell cuticular plate is nearly normal in mutants lacking cilia or ciliary motility . . . 90
5.2.8 The number of hair cells in the posterior macula of a mutant completely lacking cilia is reduced from 48hpf . . . 93
5.2.9 Mutants with a partial or complete loss of cilia have defects in the development of dorsolateral ear structures . . . 94
5.2.10 Polarity graphs may aid the comparison of macular polarity between different zebrafish lines . . . 96
5.3 Discussion . . . 97
5.4 Conclusion . . . 99

6 Discussion **100**
6.1 Overview of results . . . 100
6.2 Finding the otolith precursor binding factors . . . 101
6.3 The role of cilia in zebrafish hair cell development . . . 104
6.4 Cilia-mediated signalling in the otic vesicle . . . 106
6.5 Imaging cilia in the otic vesicle . . . 108
6.6 Relation of my research to the understanding of ciliopathies, hearing loss, and vestibular disease . . . 109
6.7 Ventral axis curvature in zebrafish cilia mutants . . . 110
6.8 Concluding remarks . . . 110

A Movie Legends **112**

Chapter 1

Introduction

1.1 Significance of the project

The importance of studying development of sensory systems

Developmental biology is the study of how a fertilised egg develops into an organism. It encompasses fertilisation of the egg cell by a sperm, co-ordination of the initial cell divisions, specification of different fates and competencies in the early embryo, the processes of gastrulation, the formation of tissues and organs within the embryo and their maturation into functional structures in the adult.

All animals are capable of sensing their external environment to some degree, and it is important that they are able to do so. Animals need to be able to find food and mates (if the animal reproduces sexually), and avoid noxious stimuli and predation in order to survive and reproduce. Most complex animals sense their environment using specialised sensory organs, adapted to maximise the animal's fitness in its environment. For example, humans sense light (sight), sound (hearing), chemical stimuli (smell and taste), gravity (balance), touch, body position (proprioception), temperature and pain.

Throughout the animal kingdom the range of stimuli sensed by animals is highly varied; some water based animals can sense electric fields, aiding in prey detection and navigation in a silty environment with low visibility. Other animals, particularly birds and arthropods, see different ranges of wavelengths of the electro-magnetic spectrum or can detect the polarisation of light. Some birds sense magnetic fields, aiding them in long distance migrations.

The vertebrate inner ear is the sensory organ that detects sound, linear and angular accelerations. The sensory capability of the inner ear varies enormously across the vertebrates, both in the ability to sense sound intensity and frequency, and in the ability to sense linear and angular accelerations. Animals are often most sensitive to sound frequencies that are used for within species communication and that aid them in hunting or avoiding predation. The structure of the semicircular canals will vary depending on how fine a sense of balance an animal requires. For example, tree-dwelling primates that

move fast, jumping between trees, have elongated semicircular canals compared to ground-dwelling or slow-moving mammals. This allows them to detect much smaller changes in angular acceleration, helping them to maintain balance (Spoor et al., 2007; Yang and Hullar, 2007). This huge variation in the variety and sensitivity of sensory systems across animals makes understanding the development and function of sensory organs a fascinating area of study.

The zebrafish as a model for development and disease

The zebrafish has grown immensely in popularity as a model for researching development and disease in the last two decades. This is for a number of reasons. The adults are small, hardy, and easy to breed. They are also relatively cheap to maintain when compared to other vertebrate model organisms such as the mouse. Zebrafish development occurs entirely outside the mother, allowing easy observation and manipulation of embryos at any developmental stage. Embryonic wild-type zebrafish are transparent for the first day of development, and pigmentation mutant lines exist which are transparent in most tissues through to adulthood. This allows easy *in vivo* observation of development of the embryo and development of organs, even if they are inside the embryo. Zebrafish develop quickly; within 5 days of fertilisation the larvae are capable of sensing and responding to their environment, and able to feed. The generation time of zebrafish is reasonably short at three to six months.

Zebrafish are genetically tractable. Mutagenesis screens and forward genetics can be undertaken to isolate genetic mutations. The development of ZFNs, TALENs (reviewed in Huang et al., 2012), and most recently, CRISPRs (Chang et al., 2013; Hwang et al., 2013), means that reverse genetics is getting much easier, despite the lack of embryonic stem cell lines in zebrafish. Transgenic zebrafish lines allow a tissue or cell type of interest to be labelled by fluorescent proteins, thus aiding visualisation of a process of interest.

Many labs are now using zebrafish to model human diseases. As a vertebrate, the zebrafish shares many developmental signalling pathways with humans, making it a good model for researching congenital diseases. In addition, the zebrafish also has a high capacity for regenerating damaged tissue, making it valuable for understanding the process of tissue regrowth after damage. Relevant to ear development research is the use of zebrafish as a model for hair cell regeneration (Brignull et al., 2009). Zebrafish are also an emerging model for drug and toxicity screening. For example, screens to identify potential therapeutics for human diseases such as epilepsy (Baxendale et al., 2012), or to assess ototoxic affects of existing drugs or drugs in development (Buck et al., 2012), are being developed.

Impact of research into inner ear development and cilia

As mentioned above the development of sensory systems is fascinating. The senses of hearing and balance are very important to humans. Hearing loss and associated conditions

are thought to affect upwards of 250 million people worldwide, and hearing loss is the third most common chronic condition in older people (Vio and Holme, 2005). Balance problems and vertigo affect many people as they age, and are the cause of many falls in older people (Oghalai et al., 2000; Wetmore et al., 2011). The molecular mechanisms behind ear development are highly conserved across vertebrates. The zebrafish is a relevant model for the investigation of ear development; molecular pathways identified in the zebrafish are likely to also be important for human ear development and function (Whitfield, 2002).

The study of cilia is currently a rapidly growing field, due to the recent finding that cilia are involved in many signalling pathways during development, and that dysfunctional cilia lead to the ciliopathies, serious diseases with a broad spectrum of symptoms (see Section 1.2). Therefore research into the basic biology and understanding of cilia is relevant to increasing our understanding of human ciliopathies.

The practical advantages of studying the role of cilia in zebrafish ear development are that the embryonic zebrafish ear develops close to the surface of the embryo, making it very amenable to *in vivo* microscopy. As the ear is a vesicle with a lumen, cilia on the cells making up the vesicle epithelium protrude into the lumen, making them easy to observe by microscopy with DIC optics when compared to cilia on cells in tissues without a lumen, or cilia on lumenal cells deeper within the embryo.

Structure of this introduction chapter

The rest of the introduction to this thesis has been split into three main sections; a general overview of cilia, including ciliogenesis and structure and functions of cilia (Section 1.2); an overview of ear development, structure, and function, with a focus on the vestibular system (Section 1.3); and the final sections address what is already known about the role of cilia in zebrafish ear development and otolith formation (Sections 1.4 – 1.5).

1.2 Cilia

Cilia are organelles present on the apical surface of most vertebrate cells. They were first described in Zimmermann (1898) and it was postulated early on that they may have a function for sensing the extracellular environment (reviewed in Wheatley, 2005). Until recently, the study of cilia was a low-key affair. However, the discovery that non-motile cilia (also known as primary cilia) did indeed play an important role in regulating developmental signalling pathways in vertebrates as well as in sensing the extracellular environment has led to a resurgence in the study of this organelle (reviewed in Eggenschwiler and Anderson, 2007).

1.2.1 Ciliogenesis

An early description of the formation of cilia observed by transmission electron microscopy (TEM) was published in 1962 (Sorokin, 1962). It described the process of ciliogenesis in

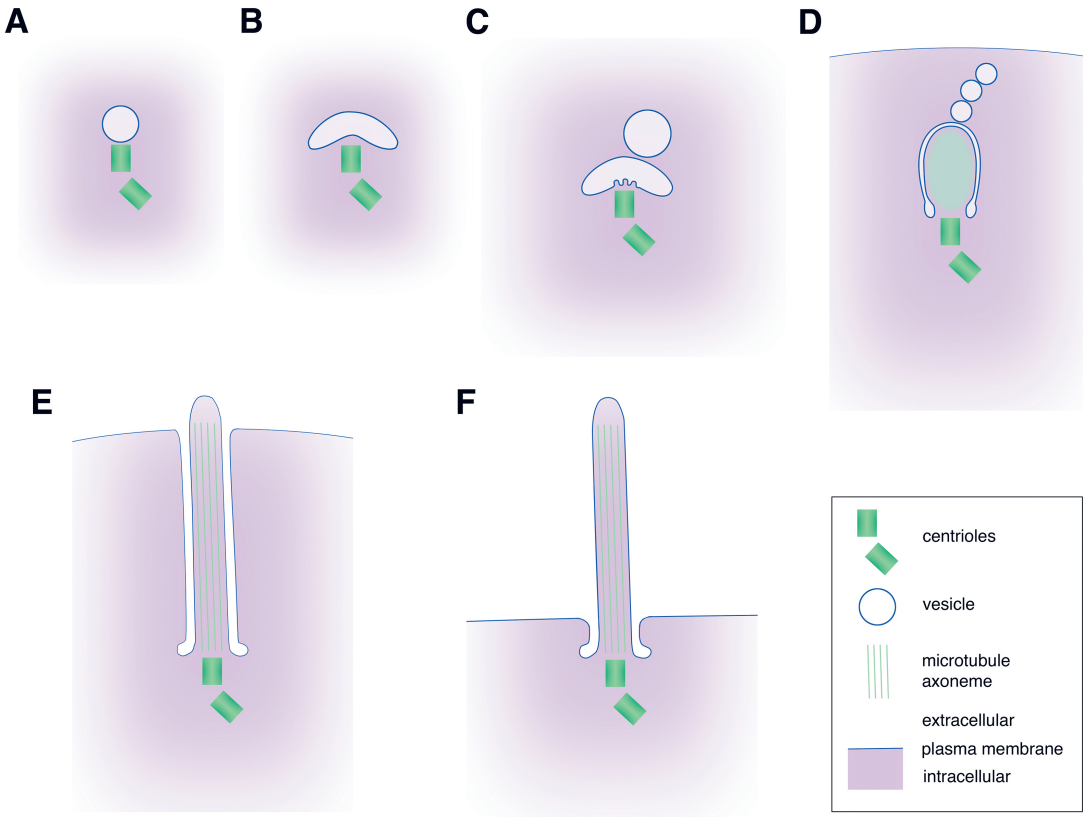

Figure 1.1: Cartoon of primary ciliogenesis, based on Sorokin (1962). A. The first observed stage of ciliogenesis is the docking of the cell's centriole (basal body) to the ciliary vesicle. **B**. The ciliary vesicle flattens and forms a ciliary bud adjacent to the centriole. **C**. The ciliary vesicle grows by addition of secondary vesicles. The ciliary bud may form a fluted shape over the docked centriole. **D**. As the developing cilium grows, the microtubule axoneme is not immediately visible, but there is denser material in the cilium (represented by green shading). There may also be vesicles or membrane-bound structures within the developing cilium at this stage. Secondary vesicles continue to fuse with the ciliary vesicle, which is now known as the ciliary sheath. The secondary vesicles enable the sheath to grow with the cilium and may guide the cilium towards the cell surface. **E**. The cilium has formed a microtubule axoneme and the ciliary vesicle has fused with the plasma membrane, forming the ciliary pocket. The cilium may remain mostly within the cell as pictured in this panel. **F**. Alternatively, the cilium may protrude from the cell into an extracellular lumen or matrix. A ciliary pocket remains at the base of the cilium. This contains the ciliary necklace, a specialised structure that controls protein trafficking into and out of the cilium.

fibroblasts and smooth muscle cells from chicken and rat; the findings are summarised in Figure 1.1. Cilia are formed when the mother centriole docks to a membrane-bound vesicle within a cell, known as the ciliary vesicle. The ciliary axoneme grows as an invagination into the ciliary vesicle. As the cilium lengthens, the ciliary vesicle grows with it by addition of secondary vesicles and becomes the ciliary sheath. The ciliary sheath then goes on to fuse with the plasma membrane (the apical plasma membrane in an epithelium), a process that may involve secondary vesicles that help guide the ciliary sheath to the plasma membrane. The cilium is left protruding from the apical surface of the cell. The ciliary sheath does

not flatten out completely upon docking with the plasma membrane; the cilium is left surrounded by a ciliary pocket, a specialised site involved in endocytosis and exocytosis and trafficking of membrane proteins into and out of the cilium (Molla-Herman et al., 2010).

1.2.2 Structure of cilia

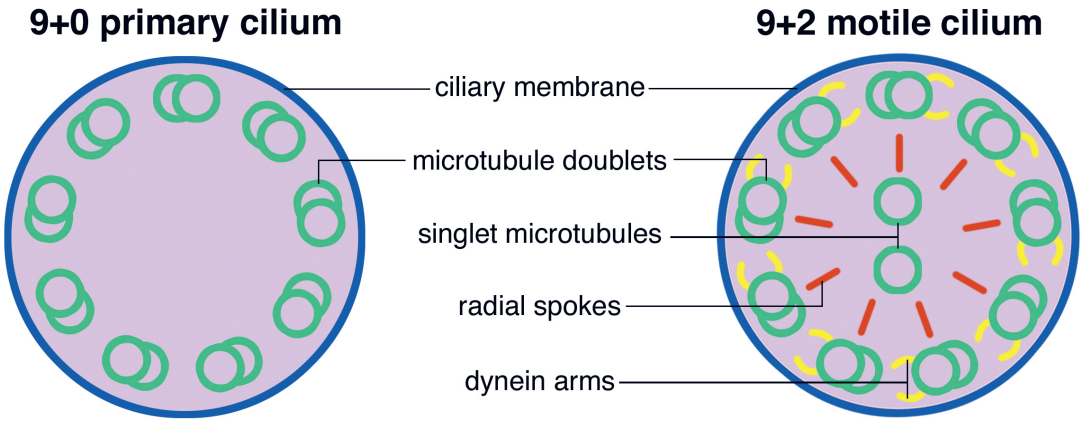

Figure 1.2: Structure of the axoneme in a stereotypical primary and motile cilium. Typically the immotile primary cilium (left) has a 9+0 microtubule axoneme when observed in cross-section by TEM and is approximately 200nm in diameter. A motile cilium (right) has a more complex 9+2 axoneme, with dynein arms attached to the microtubule doublets allowing them to slide relative to each other, producing a beating motion.

There are two main types of cilia, immotile cilia and motile cilia. Cells with an immotile cilium (also known as a primary cilium) are mono-ciliated. A typical immotile cilium has a microtubule axoneme with a "9+0" structure. The "9" refers to the presence of 9 microtubule doublets around the periphery of the axoneme. The "0" refers to the absence of any singlet microtubules in the centre of the ciliary axoneme.

A typical motile cilium has a microtubule axoneme with a "9+2" structure. Here, the "2" refers to the presence of two singlet microtubules at the centre of the axoneme, known as the central pair. In addition to the central pair, a motile cilium also has radial spokes. These join the central pair to the outer microtubule doublets. Dynein arms are present on the microtubule doublets of a motile cilium, and consist of motor proteins that confer motility to the cilium. The dynein arms cause sliding of the microtubule doublets relative to each other in a co-ordinated way, leading to a ciliary beat pattern. Cells with motile cilia may be either mono-ciliated or multi-ciliated (reviewed in Satir and Christensen, 2007).

Other microtubule axoneme structures have been described for both motile and non-motile cilia. For example: motile cilia in the mouse node have been shown to have a 9+0 axonemal structure, lacking the central pair but still having dynein arms (Nonaka et al., 1998), while rabbit nodal cilia have been found which have a 9+4 axonemal structure (Feistel and Blum, 2006). Hair cell kinocilia have a 9+2 axoneme structure (Flock and

Duvall, 1965; Yu et al., 2011), but are immotile (Yu et al., 2011; Stooke-Vaughan et al., 2012).

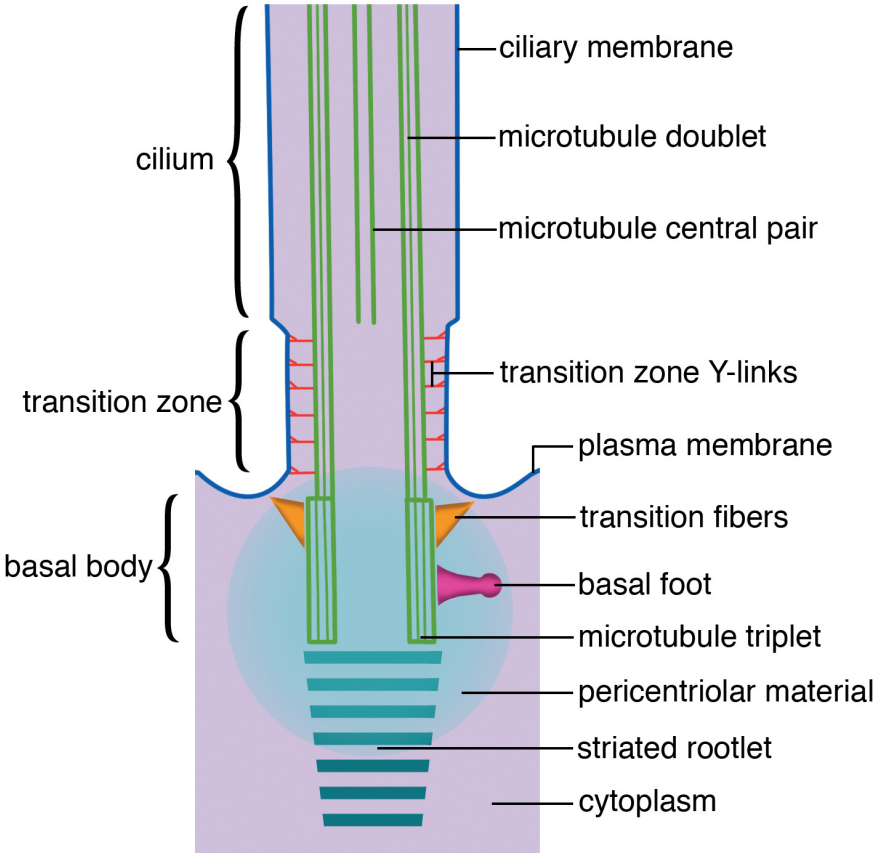

Figure 1.3: Longitudinal cross section of a cilium with detail of basal body and transition zone. A cilium with a 9+2 axoneme is shown, based on the diagram of a vestibular hair cell kinocilium given in Figure 8 of Flock and Duvall (1965). The basal body has a microtubule axoneme consisting of 9 sets of triplet microtubules. A basal foot, transition fibres and a striated rootlet are associated with the basal body, and help to anchor and orient it within the apical cell cytoplasm. Pericentriolar material (PCM) surrounds the basal body and is where many centrosome associated proteins are localised, including those associated with some ciliopathies such as Bardet-Biedl Syndrome (BBS) and those required for organisation of the microtubule cytoskeleton of the cell. The transition zone of the cilium is where the triplet structure of the basal body is converted to the doublet structure of the ciliary axoneme. Y-links link the microtubule axoneme of the transition zone to the ciliary membrane and organise membrane proteins required for regulation of ciliary import and export.

The mother centriole that docks with the ciliary vesicle at the start of ciliogenesis (Figure 1.1) is known as the basal body once the cilium is formed. Figure 1.3 shows the structure of the basal body in more detail. The centriole/basal body has a different microtubule cytoskeleton to the ciliary axoneme, with 9 sets of radially arranged triplet microtubules. The basal body is linked to the apical plasma membrane of the cell by transition fibres. The microtubule doublets of the ciliary axoneme are constructed from the microtubule triplets of the basal body, this change in microtubule organisation occurs in a specialised part of the cilium known as the transition zone. Transition zone Y-links

link the microtubule doublet axoneme of the transition zone to the ciliary membrane. The transition zone fibres and Y-links are associated with membrane localised protein particles that form the ciliary necklace, a structure that helps to regulate the import and export of proteins to and from the cilium (reviewed in Seeley and Nachury, 2010; Verhey et al., 2011; Hoey et al., 2012b).

A structure called the basal foot is associated with the basal body. The basal foot interacts with the apical microtubule cytoskeleton, and indicates the plane of ciliary beating in multi-ciliated cells (Kunimoto et al., 2012). The basal foot of the hair cell kinocilium always points directly away from the stereocilliary bundle (Flock and Duvall, 1965) (Hair cell structure is discussed further in Section 1.3.4). A striated rootlet anchors the basal body in the cell, aiding stability of the cilium (Yang et al., 2005). The basal body is surrounded by the pericentriolar material (PCM). Many centrosome associated proteins are localised to this area, including those required for organisation of the microtubule cytoskeleton of the cell (reviewed in Bärenz et al., 2011). The basal body structures associated with primary cilia with a 9+0 axoneme are slightly different to those associated with motile or sensory cell cilia with a 9+2 axoneme. A primary cilium will have multiple basal feet and multiple striated rootlets associated with the basal body (Hoey et al., 2012b).

Vertebrate sensory cells often carry a modified cilium or cilia as part of the sensory apparatus. Hair cells have a kinocilium with a 9+2 axoneme on their apical surface, surrounded by the mechanosensitive stereociliary bundle (discussed further in Section 1.3.4). Photoreceptor cells in the retina have a modified 9+0 cilium, the connecting cilium, which joins the photoreceptor cell body to the photoreceptor outer segments. Olfactory receptor neurons have a tuft of immotile 9+2 cilia where odour receptors localise (reviewed in Afzelius, 2004; Louvi and Grove, 2011).

1.2.3 Genes involved in ciliogenesis and cilia function relevant to this study

The number of proteins required for ciliogenesis and normal cilia function is currently thought to be over 600 (Inglis et al., 2006). Here I will only discuss cilia genes that are relevant to this study.

Gene products required for ciliogenesis

Intraflagellar transport (IFT) proteins are required for ciliogenesis and maintenance of cilia (Rosenbaum and Witman, 2002). Null mutations of IFT genes result in a failure of ciliogenesis. This leads to ciliopathy phenotypes, including situs inversus, cystic kidneys, and phenotypes associated with misregulation of Hedgehog (Hh) signalling (see Sections 1.2.4 and 1.2.5). IFT particles occur in two complexes; complex A IFTs and complex B IFTs. Complex A contains higher molecular weight IFT particles, whereas complex B contains the lower molecular weight IFT particles. IFT complexes are thought to carry components

required for assembly of the ciliary axoneme, and associate with the motor proteins that shuttle them up and down the cilium (Rosenbaum and Witman, 2002).

One of the most studied IFT proteins is IFT88. Mutations in mouse IFT88 are associated with polycystic kidney disease (Yoder et al., 2002), retinal degeneration (Pazour et al., 2002), situs inversus (Murcia et al., 2000), and misregulation of Hedgehog signalling (Huangfu et al., 2003). In the zebrafish maternal-zygotic *ift88* mutant, ciliogenesis fails completely; however, the basal body still docks to the cell plasma membrane. The complete lack of cilia in zebrafish maternal zygotic *ift88* mutants results in a mis-regulation of Hh signalling (Huang and Schier, 2009). Degeneration of sensory cells of the retina, otic vesicle and olfactory pit is also seen in zebrafish zygotic *ift88* mutants (Tsujikawa and Malicki, 2004).

Different proteins are required for the processes of motile and immotile ciliogenesis. Dzip1 (DAZ (deleted in azoospermia) interacting protein 1) localises to the centriole of primary cilia. Study of the zebrafish *dzip1* mutant (*iguana*) has shown that Dzip1 is required for primary ciliogenesis in the zebrafish. Motile ciliogenesis can still occur in *iguana* mutants, although fewer motile cilia are made in *iguana* mutants than in wild-type embryos (Glazer et al., 2010; Kim et al., 2010; Tay et al., 2010). The exact function of DZIP1 is not yet known. In humans, the DZIP1 protein interacts with DAZ, an RNA binding zinc-finger protein with a role in spermatogenesis (Tsui et al., 2000).

Small GTPases in cilia

A number of small GTPases have been found to be localised to cilia, and are necessary for the normal function of cilia (reviewed in Li and Hu, 2011). One of these small GTPases is the arl protein, Arl13b (ADP-ribosylation factor-like 13b). Mutations in Arl13b lead to Joubert Syndrome in humans (Cantagrel et al., 2008). The *hennin* mutant mouse has a null mutation in Arl13b, which leads to short cilia and a constitutively low level of Gli activator activity (Caspary et al., 2007). The *arl13b* mutant zebrafish line (*scorpion*) was identified due to a cystic kidney phenotype (Duldulao et al., 2009). Defects in ciliogenesis are seen in *arl13b* mutant and morphant embryos, and use of anti-Arl13b antibody staining has confirmed the ciliary localisation of Arl13b in the zebrafish (Duldulao et al., 2009). Although little is understood about the function of small GTPases in cilia (Li and Hu, 2011), it has been shown in *C. elegans* that Arl13b is required for association of the IFTA and IFTB complexes within the cilium (Li et al., 2010). The localisation of Arl13b to all cilia in the zebrafish has been taken advantage of by the creation of the *Tg(βactin2:Arl13b-GFP)* line, which fluorescently labels all cilia in the developing embryo (Borovina et al., 2010).

Proteins that are required for ciliary motility

As shown in Figure 1.2, motile cilia have a more complex structure than immotile cilia. The production of effective dynein arms, radial spokes and central pair apparatus requires the expression of further genes in a motile-ciliated cell. Here I discuss motile-ciliogenesis genes that are relevant to this study.

The winged-helix/forkhead domain-containing *foxj1* transcription factors, *foxj1a* and *foxj1b* in the zebrafish, are expressed in ciliated tissues in the zebrafish embryo (Aamar and Dawid, 2008). *foxj1a* and *foxj1b* expression is coordinated by Sonic-hedgehog signalling (Yu et al., 2008). Knock-down of *foxj1a* by morpholino injection prevents motile ciliogenesis, while overexpression of *foxj1a* is sufficient to produce ectopic motile cilia (Yu et al., 2008). Only *foxj1b* is expressed in the otic vesicle of the zebrafish embryo, making it the subject of a recent study on the role of motile cilia in otolith formation (Yu et al., 2011) (see Section 1.4).

Genes with protein products that are either part of, or regulate, the axonemal dynein arm motor proteins cause defects in cilia motility if knocked down. For example *gas8* (*growth arrest-specific 8*) was knocked down in a study of ciliary motility in the zebrafish otic vesicle to investigate the effect of disrupting ciliary motility on otolith formation (Colantonio et al., 2009) (see Section 1.4). In the zebrafish, *gas8* is expressed in motile-ciliated tissues during organogenesis (Colantonio et al., 2009). *gas8* is the vertebrate homologue of the protist *trypanin*, a subunit of the Dynein Regulatory Complex that binds microtubules, and is thought to be involved in the regulation of axonemal dynein activity by regulation of signals from the radial spokes and central pair of the motile cilium (Colantonio et al., 2009). Zebrafish embryos in which *gas8* has been knocked down by morpholino injection lack motile cilia (Colantonio et al., 2009).

A component of the outer dynein arm of motile cilia is the protein encoded by *lrrc50* (*leucine-rich repeat-containing 50*), also known as *dnaaf1* (*dynein, axonemal, assembly factor 1*). Zebrafish mutants that have either a premature stop mutation, or missense mutation in a conserved residue of *lrrc50*, fail to produce motile cilia. As a result *lrrc50* mutants have pronephric cysts (Sullivan-Brown et al., 2008; van Rooijen et al., 2008). The *Chlamydomonas* orthologue of *lrrc50* is *oda7*. A mutation in the *Chlamydomonas oda7* locus that deletes the first exon results in a failure of outer row dynein assembly. This is due to blockage of the association of dynein heavy and intermediate chains in the cell cytoplasm (Freshour et al., 2007). TEM observation of *oda7* or *lrrc50* mutant cilia shows that mutant axonemes lack dynein arms or have incomplete dynein arms (Freshour et al., 2007; van Rooijen et al., 2008).

1.2.4 Functions of cilia

Functions of motile cilia

In single-celled organisms such as *Chlamydomonas* and *Tetrahymena*, and also in the spermatozoa of animals, motile cilia, also known as flagella, are used for propulsion (Satir and Christensen, 2007). In multi-cellular organisms, motile cilia are involved in moving extra-cellular fluid. A subset of cells lining the mammalian trachea are multi-ciliated and required for moving mucus up and out of the airways. Mice that have a deletion of exons 6 and 7 of *Odf2* are still able to form motile cilia in the trachea. However, the basal bodies of the mutant motile cilia lack basal feet and beat in an uncoordinated manner in the trachea. This leads to problems with mucus clearance in the mice, and models the human ciliopathy, Primary Ciliary Dyskinesia (Kunimoto et al., 2012).

Specialised 9+0 motile cilia in the embryonic mouse node have been shown to have a role in left-right asymmetry determination (reviewed in Hirokawa et al., 2006). Mouse mutants that lack cilia have randomization of left-right asymmetry (Nonaka et al., 1998). It is even possible to determine the establishment of left-right asymmetry by artificially producing a directional nodal flow (Nonaka et al., 2002). Observation of cilia in the wild-type mouse node has shown that a subset of nodal cilia are motile, and produce a leftward fluid flow due to a biased rotation caused by a posterior tilt of the cilia (Nonaka et al., 2005). This leftward flow is thought to push a signalling cue over to the left side of the node, resulting in asymmetrical Calcium signalling around the node (McGrath et al., 2003), which leads to the asymmetrical gene expression in the embryo required for development of left-right asymmetry. The zebrafish equivalent of the node, Kupffer's Vesicle, also contains motile cilia that are required for establishment of left-right asymmetry (Essner et al., 2005).

It is possible that motile cilia also have a sensory function. Mouse ependymal cilia (motile cilia present on multi-ciliated cells lining the brain ventricle) require both fluid flow and the planar cell polarity protein Vangl2 in order to correctly orient and coordinate ciliary beating (Guirao et al., 2010).

In zebrafish, motile cilia are required for normal development of the pronephros (the embryonic fish kidney) (Kramer-Zucker et al., 2005). Zebrafish mutants that fail to form motile cilia or that lack ciliary motility form cysts in the pronephros, due to the lack of fluid flow (Sullivan-Brown et al., 2008; van Rooijen et al., 2008). Motile cilia are also involved in normal ear development and otolith formation in the zebrafish embryo; this is discussed in Section 1.4.

Functions of immotile cilia

Multi-cellular organisms have adopted immotile cilia as devices for sensing the environment. Highly adapted immotile cilia are found on sensory cells, including photoreceptor cells, mechanosensitive hair cells, and olfactory sensory cells (reviewed in Satir and Chris-

tensen, 2007). The immotile primary cilia found on most vertebrate cell types are involved in transducing signalling pathways during development (reviewed in Eggenschwiler and Anderson, 2007; Goetz and Anderson, 2010). The Hedgehog signalling pathway is the pathway for which the role of primary cilia has been most studied.

Other signalling pathways that the primary cilium appears to be involved in include the platelet-derived growth factor receptor α (PDGFRα) pathway (Eggenschwiler and Anderson, 2007). The role of primary cilia in both the canonical and non-canonical (planar cell polarity) Wnt pathways is still uncertain. Most evidence suggests that Wnt pathways act upstream of ciliogenesis. The canonical β-catenin Wnt signalling pathway appears to be required for expression of *foxj1a*, a transcription factor required for motile ciliogenesis, in the zebrafish (Caron et al., 2012). Non-canonical planar cell polarity Wnt signalling may have a role in positioning the cilium on the apical cell surface in an epithelium (Wallingford, 2010; Wallingford and Mitchell, 2011).

Immotile cilia are also capable of directly sensing the extracellular environment. For example, cilia in the tubules of the mammalian kidney play an important role in sensing fluid flow. Ciliary defects in mammals lead to Polycystic Kidney Disease (PKD); if primary cilia are absent, or missing the correct receptors for fluid flow, there is no rise in intracellular $[Ca^{2+}]$ in response to fluid flow, leading to over-proliferation of the epithelial cells and kidney cyst formation (reviewed in Bisgrove and Yost, 2006; Satir and Christensen, 2007; Veland et al., 2009; Pan et al., 2012). Immotile cilia also have a proposed role in sensing bile flow in the liver (reviewed in Larusso and Masyuk, 2011), and flow in blood vessels (reviewed in Nauli et al., 2011). It is also thought that primary cilia on chondrocytes and osteocytes have a role in normal cartilage and bone formation (reviewed in Hoey et al., 2012a).

The cell centriole is required for the formation of the primary cilium. As centrioles are also required for mitosis this means that ciliogenesis and mitosis are mutually exclusive; only cells in G or S phases can have a primary cilium. As many genes associated with ciliogenesis are also involved in the cell cycle this implies a link between ciliogenesis and tumorigenesis (reviewed in Basten and Giles, 2013).

1.2.5 Diseases of cilia

Diseases caused by ciliary dysfunction are known as ciliopathies. Ciliopathies range in severity. The mildest forms include Primary Ciliary Dyskinesia (PCD), caused by mutations affecting the motility of motile cilia (the 'primary' in the syndrome name refers to the heritability of this genetic disorder). Symptoms of PCD include coughs and lung problems caused by failure to clear airways effectively, infertility, and situs inversus (Satir and Christensen, 2007; Waters and Beales, 2011).

The ciliopathies affecting the function of non-motile cilia are more severe due to the important role that non-motile cilia have in transducing developmental signals. Diseases such as Bardet-Biedl Syndrome (BBS), Alström Syndrome, Joubert Syndrome and Meckel-

Gruber Syndrome are caused by failure to form correctly functioning primary cilia in some or all tissues. Ciliopathy symptoms include retinal degeneration, brain abnormalities, mental retardation, obesity, craniofacial defects, kidney failure, heart problems, and diabetes. Deafness is only reported as a symptom in two ciliopathies, BBS and Alström syndrome, and no ciliopathy has any vestibular defect reported as a symptom (Waters and Beales, 2011).

1.3 Inner ear function, structure and development

1.3.1 Overview of inner ear function and structure

Ears are the vertebrate organ of hearing and balance (Purves et al., 2001; Chapters 14 and 15). The vertebrate inner ear consists of three orthogonally arranged semicircular canals, which sense angular acceleration. The semicircular canals sense angular acceleration via a swelling at the end of each canal, the ampulla, which contains a sensory epithelium called the crista. The cristae and all other sensory patches within the ear contain mechanosensitive hair cells (Section 1.3.4). Ventral to the semicircular canals are the vestibular sensory patches, the utricle and saccule. These patches sense gravity and linear acceleration. In mammals these sensory patches have associated otoconia embedded in the jelly-like otoconial membrane that sits above the apical surface of the sensory hair cells. The otoconia act as an inertial mass in the vestibular sensory system, moving in response to gravity or linear acceleration with respect to the hair cells. This differential movement activates the mechanosensitive hair cells in the sensory patch (Purves et al., 2001; Chapter 14). Instead of otoconia, teleost fish have a single calcified otolith (ear stone) associated with each sensory patch (see Section 1.3.5). In addition to the utricle and saccule, teleosts also have a third sensory patch, the lagena, which has a corresponding third otolith (reviewed in Abbas and Whitfield, 2010).

In mammals, sound is detected by a specialised hearing organ called the cochlea; however, the vestibular apparatus has been implicated in sensing low-frequency tones in mice (Jones et al., 2010). In teleosts, sound is detected by a combination of the lagena and saccule (Platt, 1993). Hearing specialist teleosts (ostariophysans, including the zebrafish) have a set of bones, known as the Weberian apparatus, or Weberian ossicles, connecting their swim bladder to the inner ear. The Weberian apparatus allows the swim bladder to act as an auditory amplifier. The structure of the adult zebrafish ear and its association to the Weberian apparatus has been described by serial-sectioning of the zebrafish inner ears and weberian ossicles (Bang et al., 2001). An overview of zebrafish and mouse inner ear structure is given in Figure 1.4.

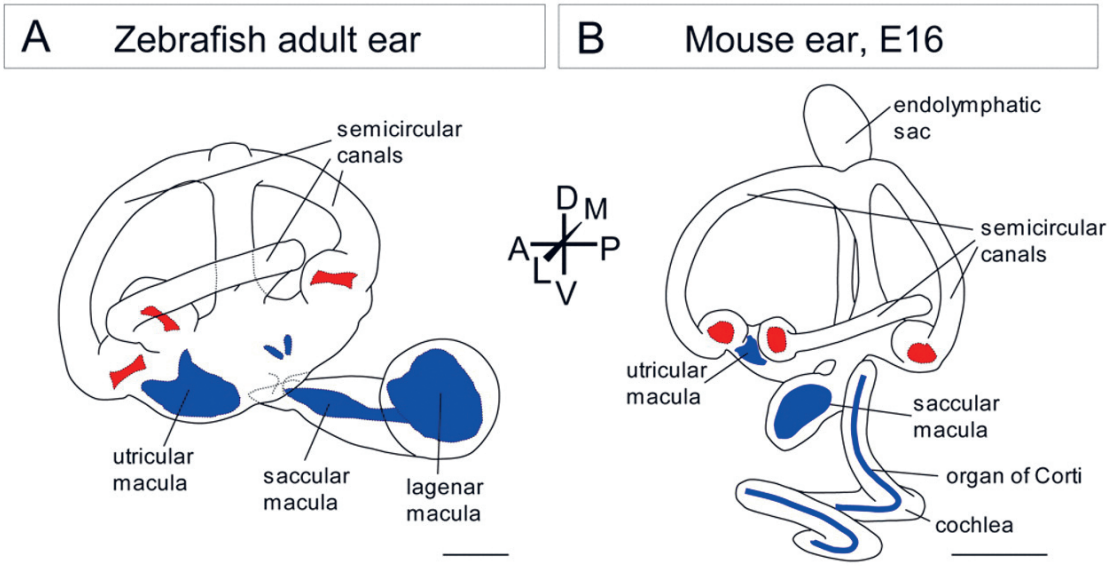

Figure 1.4: Comparison of adult zebrafish and E16 mouse ear structure. A. Lateral view of an adult zebrafish left inner ear. The sensory patches of the semicircular canals, the cristae, are shown in red. The sensory patches of the utricle, saccule and lagena are shown in blue. **B**. Lateral view of an E16 (Embryonic day 16) mouse left inner ear. The cristae are in red and the vestibular sensory patches of the utricle and saccule are shown in blue. The specialised hearing sensory apparatus, the organ of Corti within the cochlea, is also shown in blue. Scale bars: 500μm. Reproduced and modified with permission from The International Journal of Developmental Biology (Int. J. Dev. Biol.) (2007) 51: 507–20 (Whitfield and Hammond, 2007), and from Development 137: 1361–71 (Hammond et al., 2010).

1.3.2 Ear development in the zebrafish embryo

Zebrafish ear development begins when the otic placode is specified by interactions of various signalling pathways, including FGF3/8, Retinoic Acid and Sox transcription factors (reviewed in Whitfield et al., 2002). The otic placode becomes visible *in vivo* with DIC optics at 14S (14 somites stage) (Haddon and Lewis, 1996). At 18–19S (∼18.5hpf) the otic placode opens up by cavitation to form the otic vesicle (OV). At this stage the OV is a hollow ovoid structure with a lumen (Haddon and Lewis, 1996; Riley et al., 1997). The anterior pole of the OV cavitates before the posterior pole of the OV, allowing the anterior otolith to begin forming slightly before the posterior otolith (Riley et al., 1997). The presumptive utricle is specified at the anterior pole of the OV and the presumptive saccule at the posterior pole of the OV. The OV expands to form a hollow vesicle, forming a thick ventral epithelium with a high density of cells compared to the thinner dorsal epithelium. The ventral epithelium gives rise to the utricle and saccule, also referred to as the anterior and posterior sensory maculae.

At 42–48hpf the four semicircular canal projections (anterior, posterior, lateral and ventral) form and push into the OV, growing towards the centre of the OV and fusing by 72hpf in a specific pattern to form the anterior, posterior and ventral semicircular canal pillars, which define the anterior, posterior and lateral semicircular canals (Haddon and

Lewis, 1996). A dorsolateral septum is also formed, separating the lumens of the anterior and posterior canals. Meanwhile the three cristae (anterior, lateral and posterior) form from 48hpf (Haddon and Lewis, 1996). See Figure 1.5 for an illustration of the larval zebrafish ear. The ear is functional from 3–4dpf; larval zebrafish can orient themselves correctly with respect to gravity, showing a functional vestibular-ocular reflex from 72hpf (Mo et al., 2010), and showing a startle response to auditory stimuli at 5dpf (Kimmel et al., 1974; Zeddies and Fay, 2005; Buck et al., 2012). At approximately 12dpf an otolith associated with the third sensory patch, the lagena, forms (Riley and Moorman, 2000). Little is known about the development and formation of the zebrafish lagena and its associated otolith.

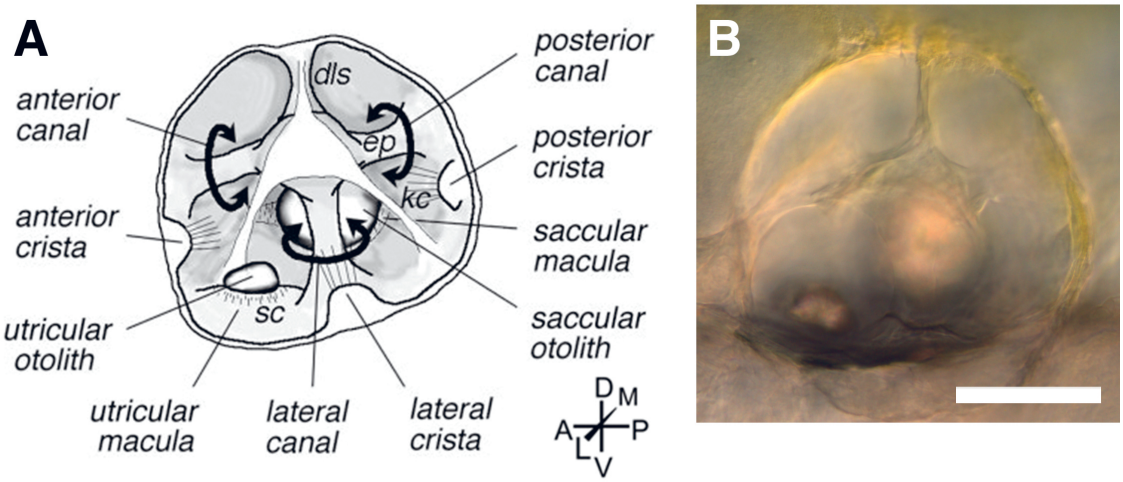

Figure 1.5: Structure of the larval zebrafish inner ear. A. Illustration of lateral view of a 4dpf zebrafish ear. The anterior, posterior and ventral epithelial pillars (ep) project into the centre of the ear, and the semicircular canal lumens run around them (black arrows). The dorsolateral septum (dls) separates that anterior and posterior semicircular canals. Kinocilia (kc) project from the hair cells of the cristae into the semicircular canal lumens. The anterior and posterior otoliths appear to sit directly on the stereocilia (sc) of the hair cells of the utricular and saccular maculae at this stage. Reproduced, with permission, from Whitfield et al. (2002); Figure 1. **B**. Lateral view of 5dpf phenotypically wild-type zebrafish inner ear. Several structures illustrated in panel A can be seen; particularly the utricular and saccular otoliths, the dorsolateral septum, and anterior and posterior semicircular canal pillars. Scale bar: 100μm.

1.3.3 Signalling pathways involved in patterning the zebrafish ear

Correct ear morphogenesis is coordinated by the interaction of several signalling pathways. Ear specification is highly dependent on *fgf3* and *fgf8*; zebrafish *fgf8* mutant embryos form small and abnormally patterned otic vesicles (Brand et al., 1996; Whitfield et al., 1996), as do *fgf3* morphant embryos (Phillips et al., 2001). *Fgf3* and *fgf8* are thought to work together to specify the otic placode; homozygous *fgf8* mutants injected with a morpholino against *fgf3* fail to form an otic placode (Phillips et al., 2001).

Retinoic acid signalling is required for the formation of posterolateral ear structures.

If retinoic acid signalling is pharmaceutically inhibited, non-neurogenic posterolateral ear domains are lost, and neurogenic anterior domains expand (Radosevic et al., 2011).

Hedgehog (Hh) signalling plays an important early role in specification of the anterior and posterior of the zebrafish OV. In zebrafish embryos with a severe upregulation of Hh signalling, a double-posterior ear results, with a centro-medial saccular macula, whereas in embryos with strong repression of Hh signalling, a double anterior ear is seen, with duplicated utricular maculae and partial or complete loss of the saccular macula (Hammond et al., 2003). Hh signalling also plays a role in morphogenesis of dorsolateral structures in the zebrafish ear. Zebrafish mutants that fail to repress Hh signalling fully often fail to form the dorsolateral septum and lateral crista (Hammond et al., 2010).

1.3.4 Hair cells

Hair cell structure

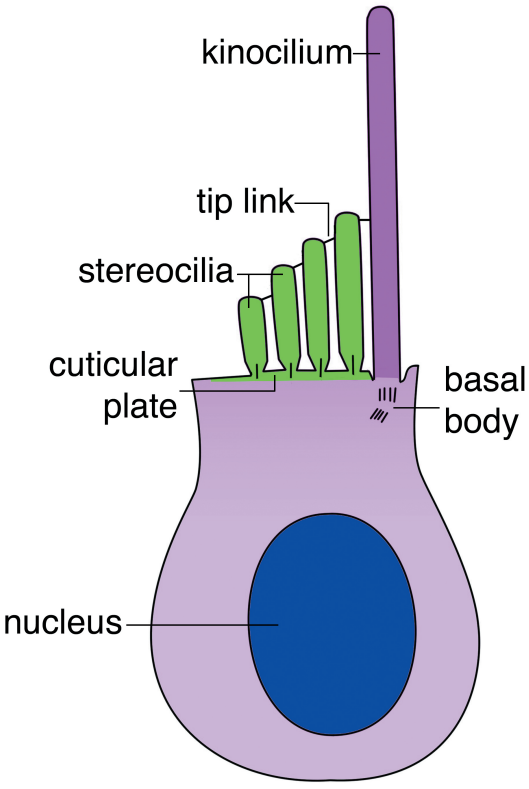

Figure 1.6: Structure of a vertebrate vestibular hair cell. Simplified cartoon of a vertebrate mechanosensory hair cell. The single kinocilium (purple) is located eccentrically on the apical surface and has a microtubule axoneme and a basal body. The kinocilium is surrounded by a stereociliary bundle (green) that is graded in height so as to be tallest next to the kinocilium. The stereocilia have an actin-rich cytoskeleton and are held in place in the actin-rich cuticular plate by rootlets. Tip links join together the stereocilia and kinocilial links join stereocilia to the kinocilium. Deflection of the bundle towards the kinocilium tensions the tip links, opening mechanotransduction channels in the stereocilia. This allows K^+ ions to enter the hair cell from the surrounding endolymph, depolarising it.

Hair cells are the mechanosensitive cells of the inner ear, allowing the detection of movement, gravity and sound (reviewed in Schwander et al., 2010; Purves et al., 2001, Chapter 13). Hair cells are a neural cell subtype and have a specialised apical domain capable of detecting nanometer scale movements. The apical surface of a mature vestibular hair cell consists of a single kinocilium (a modified 9+2 cilium) with a surrounding stereociliary bundle (see Figure 1.6).

The stereocilia of the stereociliary bundle are not true cilia, but modified microvilli with a filamentous actin cytoskeleton. The stereocilia comprising the sensory bundle are linked to each other by tip-links, visible by Scanning electron microscopy (SEM) and known to contain Cadherin23 and Protocadherin15 (Siemens et al., 2004; Ahmed et al., 2006; Kazmierczak et al., 2007). The tip links open mechanosensitive membrane ion channels in the stereociliary membranes when the stereocilia move, allowing K^+ ions to enter the hair cell, depolarising it.

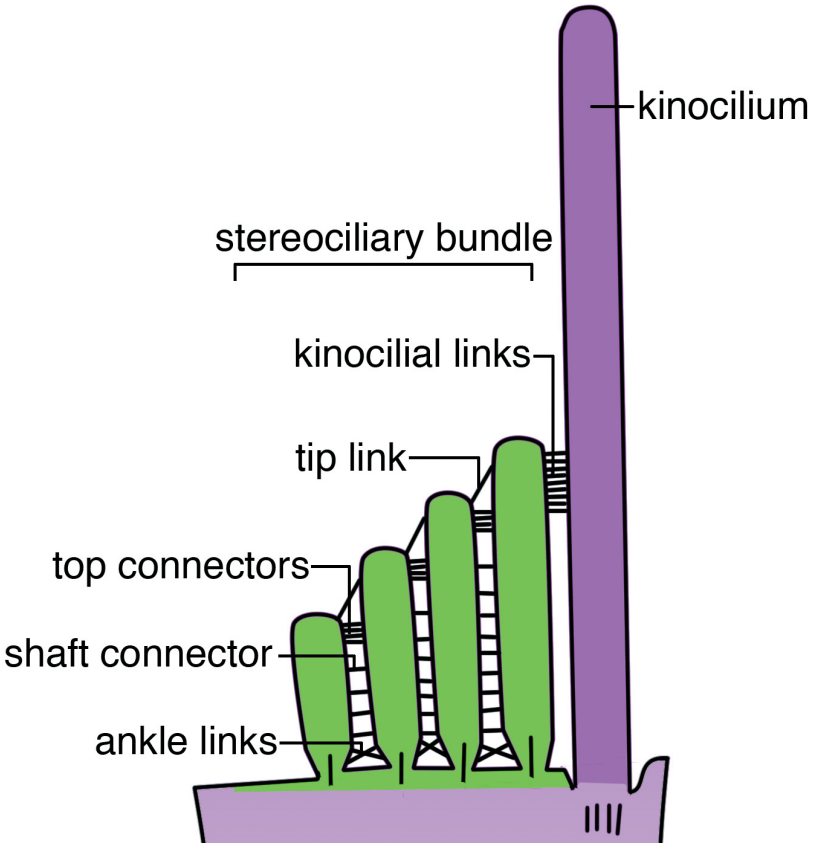

Figure 1.7: Structure of a vertebrate vestibular hair cell bundle. Simplified cartoon showing detail of the sensory bundle of a mechanosensory hair cell. In addition to the mechanosensitive tip links between individual stereocilia, the top connectors, shaft connectors and ankle links that join the stereocilia are shown. These links are known collectively as lateral links and are not thought to play a role in mechanotransduction. Instead, lateral links are thought to play a structural role in the stereociliary bundle, transmitting the force of bundle movement between stereocilia and helping to maintain bundle integrity. Kinocilial links join the tallest stereocilia in the bundle to the kinocilium. This cartoon is based on Figure 1 of Nayak et al. (2007).

In addition to the tip links, stereociliary bundles are also connected to each other by top connectors, shaft connectors and ankle links; these are known collectively as lateral links (Figure 1.7). The role of these links is thought to be in helping to transmit movement of the kinocilium or the tallest row of stereocilia through the entire stereociliary bundle. The lateral links are also thought to have a role in maintaining structural integrity of the stereociliary bundle (Nayak et al., 2007). The tallest stereocilia of the stereociliary bundle are connected to the kinocilium by kinocilial links. It is uncertain if the kinocilial links have a purely structural role in the hair cell bundle or if they also have a mechanosensitive role. Antigens raised against Cadherin23 and Protocadherin15 localise to kinocilial links as well as to the tip links (Goodyear and Richardson, 2003; Nayak et al., 2007). In addition, it appears that kinocilial links have a mechanosensitive role during development of zebrafish lateral line hair cells (Kindt et al., 2012).

The hair cells in each sensory patch have an associated extracellular membrane, the cupula for hair cells of the crista, the otolithic/otoconial membrane for hair cells of the utricle and saccule (and lagena in fish), and additionally the tectorial membrane for the hair cells of the organ of Corti in the mammalian cochlea. These extracellular membranes are thought to mechanically couple the hair cell sensory bundles to their stimulus, improving the sensitivity of the hair cell response (Goodyear and Richardson, 2002).

Hair cell development and maturation

Hair cells and supporting cells develop from a patch of tissue within the otic vesicle known as the prosensory domain. Expression of the proneural gene *Atoh1* is required for establishment of the prosensory domain and hair cell differentiation in the mouse cochlea; mouse null mutants for *Atoh1* do not develop either hair cells or supporting cells in the cochlea (Woods et al., 2004). The zebrafish has two homologues of *Atoh1*, *atoh1a* and *atoh1b*. Expression of zebrafish *atoh1b* is induced in the prosensory domain of the otic placode at 10.5hpf, downstream of otic placode induction by Fgf3 and Fgf8. The competence factors *foxi1* and *dlx* are also required upstream of *atoh1b* expression in the otic placode. Initially *atoh1b* is expressed throughout the otic placode. By 12hpf the *atoh1b*-expressing prosensory domain has become restricted to areas at the anterior and posterior of the otic placode, a process that requires *pax2*-, *pax8*- and *atoh1b*-dependent activation of the Notch pathway. At approximately 14hpf *atoh1b* expression is restricted to the tether cells (first hair cells) at each pole of the otic placode, and *atoh1a* expression is also detectable in the tether cells. From 20hpf Notch and FGF signalling pathways act to increase the area of *atoh1a* expression, allowing differentiation of more hair cells and supporting cells. As hair cells differentiate they express *atoh1b* as well as *atoh1a*. Beyond 24hpf expansion of the domain of *atoh1a* expression is regulated by Notch and FGF. Terminally differentiated hair cells downregulate expression of the *atoh1* genes (Millimaki et al., 2007).

Millimaki et al. (2007) knocked down expression of *atoh1a* and *atoh1b* in the zebrafish embryo by morpholino injection. They found that *atoh1b* expression was required for

specification of the tether cells (the first hair cells in the OV which tether the newly formed otoliths), but the second wave of hair cell generation could take place in *atoh1b* morphants. *atoh1a* expression is required for differentiation of the second and subsequent waves of hair cells: *atoh1a* morphants fail to differentiate any hair cells after the formation of the first tether hair cells. If both *atoh1a* and *atoh1b* expression is knocked down, no hair cells differentiate, until the morpholinos begin to lose their effectiveness at 48hpf (Millimaki et al., 2007).

Hair cell specification during the development of the sensory epithelium is a process that requires Notch-Delta signalling. The zebrafish *mindbomb* mutant is a mutation in an E3 ubiquitin-ligase required for activation of the Notch signal by Delta (Itoh et al., 2003). *mib* mutant embryos form supernumerary neural cells (Jiang et al., 1996; Schier et al., 1996), including sensory hair cells (Haddon et al., 1998). These supernumerary hair cells are formed at the expense of supporting cells in the sensory epithelium. In the absence of supporting cells, hair cells are unable to adhere to non-sensory epithelial cells and maintain their place in the OV epithelium, becoming extruded from the zebrafish OV by 60hpf (Haddon et al., 1998, 1999).

Specification of hair cells leads to the expression of transcription factors necessary for hair cell development. *pou4f3* (previously *brn3c*) is a transcription factor expressed in all hair cells in the zebrafish. A transgenic reporter line, *pou4f3:mGFP*, has made it possible to visualise fluorescently labelled hair cells in the developing zebrafish (Xiao et al., 2005). Mice with a homozygous targeted deletion of *Pou4f3* are deaf and have vestibular defects due to a complete loss of auditory and vestibular hair cells in late embryonic and postnatal development (Xiang et al., 1997).

Hair cell maturation consists of several steps and has been best studied in the chick auditory epithelium (Tilney et al., 1992). Apical specialisation of the hair cell starts at 8 days when the hair cell has a single kinocilium surrounded by several short microvilli-like immature stereocilia. At this stage the kinocilium is placed randomly on the apical surface. Over the next few days the stereocilia form a bundle round the kinocilium and mature, first increasing in length and then getting wider. During this time the kinocilium becomes located at one edge of the hair cell apical domain, with the stereociliary bundle adjacent to it, positioned closer towards the centre of the apical surface; this gives the apical surface of the hair cell a within-cell polarity. Formation of tip links between the stereocilia occurs as they change from a semi-circular pattern to a straight staircase, oriented towards the kinocilium; this step is seen in 12–14 day embryos.

The process in mammalian embryos is very similar to chick embryos, though the lengthening and widening of stereocilia occurs simultaneously as opposed to the two separate steps in chick (Denman-Johnson and Forge, 1999). In the mammalian vestibular epithelia, kinocilia remain in the mature hair cells, and the stereociliary bundle has a more triangluar shape. Vestibular hair cell maturation occurs in a similar manner in mammalian to chick auditory hair cells; a kinocilium appears randomly on the hair cell apical surface (E12.5 in

mouse), and stereocilia mature around or next to it (E13.5). The hair cell then becomes polarised and the kinocilium moves to one side of the apical surface, with a height-graded stereociliary bundle forming adjacent to it (Denman-Johnson and Forge, 1999).

Hair cell maturation has not been studied in as much detail in the zebrafish, or in teleost fish in general. Sokolowski and Popper (1987) studied the development of the toadfish (*Opsanus tau*) saccule by SEM, and illustrated hair cells at different stages of maturation. There appears to be no stage of hair cell maturation where the apical surface of the hair cell is covered in short microvilli with a randomly placed kinocilium as in chick and mouse. Rather, it appears that the kinocilium develops before microvillar projections of the apical surface, and that a stereociliary bundle forms adjacent to the kinocilium, in a manner that suggests the apical surface of the hair cell is already polarised.

No study of zebrafish inner ear hair cells has been done using SEM at a high enough resolution to see the steps involved in the processes of zebrafish hair cell maturation. However, a study of the zebrafish lateral line hair cells, focused on the role of the kinocilium in establishing directional bundle depolarisation, has shown that stereocilia only ever appear to form on one side of an already present kinocilium on the apical surface of the hair cell (Kindt et al., 2012). This study also shows that tip links form very quickly on the maturing zebrafish lateral line hair cell, with the first stereocilia connecting to the kinocilium via kinocilial links before more stereocilia have formed. This is in contrast to the chick embryonic cochlea, where tip link formation occurs after formation of all the stereocilia that will make up the sensory bundle (Tilney et al., 1992).

1.3.5 Otolith formation in the zebrafish

A review on the formation of otoliths and otoconia, Hughes et al. (2006), splits the formation of these biomineralised structures into six steps: 1. The formation of a normal otocyst/otic vesicle; 2. Formation of normal macular compartments and non-sensory epithelium; 3. Establishment of the correct ionic environment in the endolymph; 4. Correct production and export of the otolith matrix proteins; 5. Assembly and attachment of matrix proteins in the correct places in the inner ear; and 6. Local increase of calcium and carbonate concentration to initiate growth of the otolith (Hughes et al., 2006). Steps that are relevant to this study are the formation of normal macular compartments (the utricle and saccule in the zebrafish <5.2dpf), the correct production and export of otolith matrix proteins, and the assembly and attachment of matrix proteins within the otic vesicle.

Formation of the sensory maculae in zebrafish is covered in Section 1.3.4. As mentioned above, *mib* mutant zebrafish produce supernumerary hair cells at the expense of supporting cells. The lack of supporting cells affects otolith formation in the *mib* mutant. Otoliths initially tether within the OV, but without supporting cells the otoliths fail to biomineralise as normal and remain in an immature, non-calcified state (Haddon et al., 1998, 1999); also see Section 4.2.7.

Zebrafish otoliths form from otolith precursor particles. These are secreted into the

OV immediately after cavitation, and start to adhere to the tether cilia at the anterior and posterior poles of the OV as soon as the tips of the tether cilia appear when the pole cavitates (Riley et al., 1997). Otolith precursor particles are denser than the surrounding OV fluid, and capable of adhering to one another. Riley et al. (1997) used laser tweezers to trap otolith precursor particles in one place in the OV lumen, and observed the formation of an ectopic, untethered otolith as the otolith precursor particles adhered to each other. The complete composition of either otolith precursor particles or the developed otoliths is not yet known; a summary of proteins known to be involved in zebrafish otolith development is provided in Table 1.1.

Table 1.1: Proteins involved in teleost otolith formation

Protein	**Function**	**Mutant/morphant phenotype**	**Reference**
Cadherin-11 (Cdh11)	Adhesion of otolith component containing vesicles during otolith growth	Reduced or absent otoliths	Clendenon et al. (2009)
Otoconin90 (Oc90)	Component of the otolith core	Otoliths small, missing, ectopic or fused	Petko et al. (2008)
Otolin1a	Involved in placement and stabilisation of the otolith matrix	Otoliths form normally but then fuse together	Murayama et al. (2002, 2005)
Otolith matrix protein (Otomp)	Component of the otolithic matrix; the most abundant protein in teleost otoliths	Small otoliths	Murayama et al. (2005)
Otopetrin1 (Otop1)	Transmembrane protein required for secretion of otolith components into the OV	Absent otoliths (*backstroke* mutant line)	Hughes et al. (2004); Söllner et al. (2004)
Sparc	Component of the otolith protein matrix, also involved in bone development	Otoliths small, missing, ectopic or fused	Kang et al. (2008)
Starmaker (Stm)	Organises calcium carbonate into aragonitic crystal form	Otoliths vary from slightly abnormally shaped to calcitic crystals	Söllner et al. (2003)

In addition, it is thought that glycogen may play a role in early otolith nucleation as a component of the core of the early otolith, potentially making a matrix that the glycoprotein collagen can interact with, thereby organising calcium fixation (Pisam et al., 2002). Collagen is not a known component of fish otoliths, although Otolin is a collagen-like protein thought to be required for stabilisation of calcium carbonate within the otolith matrix, and adherence of the otolith to the sensory patch (though not adherence to the hair cell kinocilia). Zebrafish embryos injected with a morpholino against *otolin1a* initially form normal otoliths, but they fuse together during growth, losing adherence with the sensory

patch (Murayama et al., 2005). This suggests that Otolin1a is likely to be a component of the otolithic membrane in zebrafish, required for maintenance of adhesion between a sensory macula and its associated otolith.

After otolith precursor particles have adhered to tether cilia (see Section 1.4) at the anterior and posterior poles of the OV, the otoliths continue growth by biomineralisation, incorporating layers of calcium carbonate in the aragonitic crystal form. The calcium carbonate is organised into layers of aragonitic crystal by various proteins, as detailed in Table 1.1. The process of biomineralisation appears to require supporting cells. The zebrafish *mindbomb* mutant, which lacks supporting cells due to the presence of ectopic hair cells, fails to mineralise otolith precursor particles successfully (Haddon et al., 1999). Supporting cells may also be required for normal otolith tethering as transplanted wild-type cells that become support cells in the *monolith* mutant can rescue otolith formation, such that two normal otoliths are formed as opposed to the single otolith characteristic of the *monolith* mutant (Riley and Grunwald, 1996).

An otolithic membrane is likely to be important for continued adhesion of the otolith to the sensory patch in the zebrafish, as it is in other teleosts, and as the otoconial membrane is required for maintenance of otoconia in mammals (Hughes et al., 2006). Little is currently known about the composition and formation of the zebrafish otolithic membrane; it is known to be present at 4dpf and has been observed by SEM (Hughes et al., 2004). Observation by TEM in another teleost, the Mummichog *Fundulus heteroclitus*, has revealed that the otolithic membrane consists of two layers, the subcupular meshwork immediately above the hair cell epithelium, and a gelatinous layer between the subcupular meshwork and the otolith (Dunkelberger et al., 1980).

Otolith accretion continues throughout the life of a fish. A new layer of $CaCO_3$ is laid down every day, in zebrafish and all other bony fish species. Growth of the otolith is retarded on the surface nearest the hair cells by secretion of H^+ from the hair cells, acidifying the local endolymphatic environment (Shiao et al., 2005). This acidification is thought to prevent outward growth of the otolith towards the hair cells from crushing the apical sensory epithelium. The daily deposition of $CaCO_3$ leaves the otolith with growth rings, which provide a means of aging fish.

1.4 The role of cilia in otolith formation in the zebrafish embryo

When I started my PhD research there were two studies dealing with the role of cilia in otolith formation in the zebrafish embryo:

The first study to describe cilia in the otic vesicle and propose that they had a role in tethering the forming otoliths was Riley et al. (1997). Using anti-acetylated tubulin antibody staining, they showed that the OV had a large number of cilia projecting into the lumen as soon as cavitation occurred. They also described the presence of, typically

two, longer 'tether cilia' at each pole of the OV, which bind the otolith precursor particles at their tips to form the otolith. The new otolith is bound very strongly to the tips of the tether cilia, and cannot be removed by pulling with laser tweezers. As OV cavitation continues, the majority of cilia in the OV shrink and are no longer observable by anti-acetylated tubulin antibody stain. This leaves just the longer tether cilia in the OV, bound to the newly formed otolith (Riley et al., 1997). Based on observations of the cilia lining the OV, and of the movement of otolith precursor particles within the OV, Riley et al. (1997) proposed that the tether cilia were immotile, thus forming stable platforms within the OV for nucleation of the two otoliths. All the other cilia in the zebrafish otic vesicle were hypothesised to be motile, preventing premature or ectopic aggregation of the dense and sticky otolith precursor particles, and helping to guide the otolith precursor particles to the poles of the otic vesicle, where they could aggregate to form the otoliths on the stable platform formed by the immotile tether cilia (Riley et al., 1997).

Riley et al. (1997) also suggested that the tether cilia were the kinocilia of the first hair cells, which have not yet completed maturation when the OV cavitates. This has since been confirmed by observing the appearance (at 22hpf) and gain of function (at 23hpf) of stereociliary bundles on the apical surface of the tether cells (Tanimoto et al., 2011).

Colantonio and colleagues proposed a new model for the role of cilia in otolith formation after observation of the otic vesicle with high-speed videomicroscopy (Colantonio et al., 2009). They reported that the tether cilia were motile, and suggested that these motile tether cilia produce a fluid vortex within the OV fluid, thus drawing in the otolith precursor particles until they stick to the tips of the tether cilia. They also disrupted the motility of cilia by injecting *gas8* morpholino (see Section 1.2.3 for a description of *gas8* gene function), and showed that a disruption in ciliary motility led to defects in otolith formation. Although Colantonio et al. (2009) was the first study to use high-speed videomicroscopy to observe motility of cilia within the OV, their model did not explain the presence of what were termed 'ectopic' motile cilia away from the polar tether cilia within the OV, which were also seen in the *gas8* morphant embryos. Also, their model did not address the presence of motile cilia next to the nucleating otolith which did not appear to be attached to it.

These two initial models for the role of cilia in otolith formation in Zebrafish are summarised in Figure 1.8. One of the aims of my PhD research when I started was to resolve the controversy between these two models. However, further research on the role of cilia in otolith formation in the zebrafish embryo has been published during my PhD, and I discuss this reasearch below.

The group that published the first videomicrosopy study (Colantonio et al., 2009) revised the initial model after further research (Wu et al., 2011). Careful observation showed that tether cilia are immotile and the cilia that surround the otolith, but do not tether it are motile. These motile cilia near the otolith are hypothesised to produce fluid flow that biases otolith growth, giving the developing otoliths a flat surface facing the

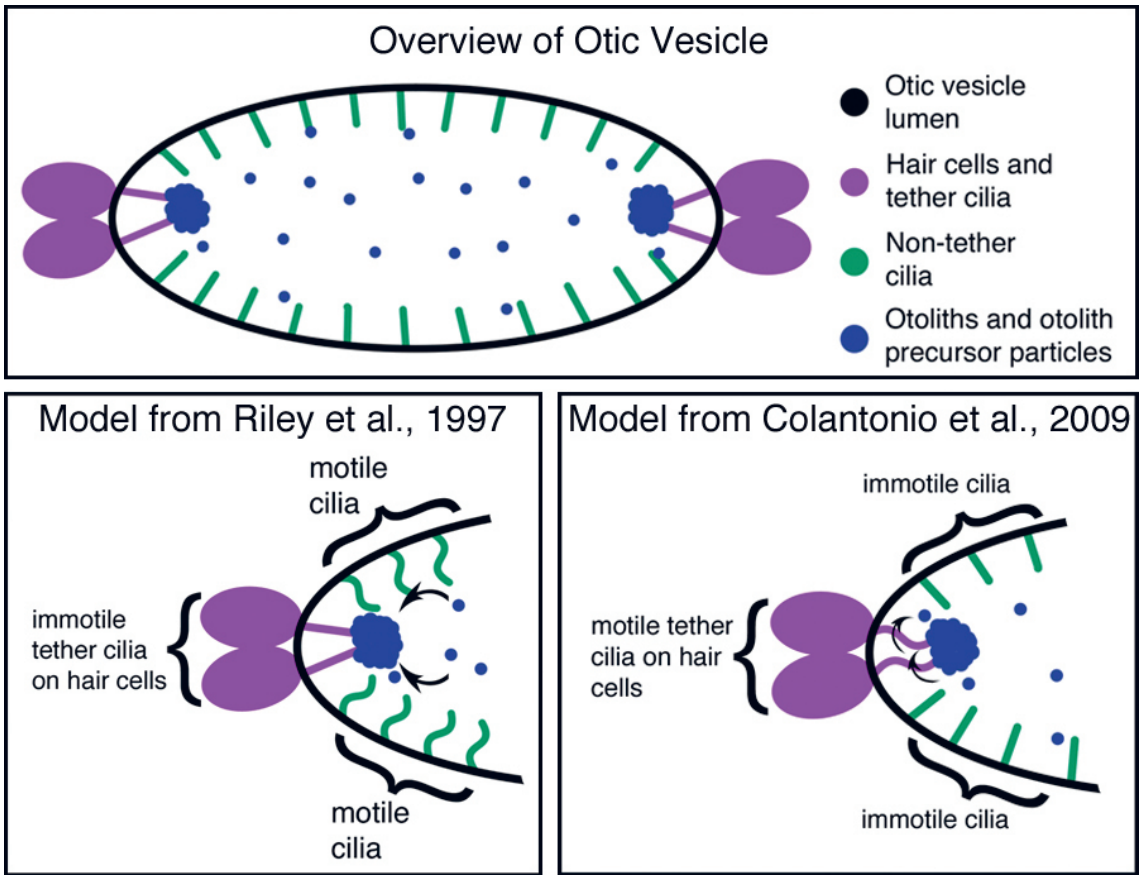

Figure 1.8: Models for the role of cilia in otolith formation. The top panel shows a sketch of the <24hpf zebrafish otic vesicle. The OV lumen is outlined in black. The first hair cells (pink) have kinocilia protruding into the OV lumen that tether the otoliths (blue), earning the hair cells and kinocilia the alternative names of tether cells and tether cilia. Numerous other cilia protrude into the OV lumen (green) from the apical surface of cells making up the OV epithelium (not shown). The otoliths are formed by the aggregation of numerous small otolith precursor particles (blue dots). Riley et al. (1997) suggested that the tether cilia were immotile, forming a stable platform for nucleation of the otolith. All non-tether cilia within the OV were proposed to be motile, guiding the otolith precursor particles towards the tether cilia and the developing otolith. This hypothesis was supported by the findings of Yu et al. (2011). Colantonio et al. (2009) suggested a new model based on observation with high-speed videomicroscopy: tether cilia were motile and could produce a fluid vortex, drawing otolith precursor particles towards the tips of the tether cilia, where they could stick to form the otolith. Motility was not observed in the other cilia lining the OV, or if observed was thought to be ectopic and not necessary for otolith formation.

sensory epithelium and a rounded surface on the lumenal side. The flat side of the otolith becomes rounded if cilia motililty is laser ablated (Wu et al., 2011). Wu et al. (2011) did not address cilia in the otic vesicle away from the poles of the OV in their revised model.

Another study has been published that supports the hypothesis of Riley et al. (1997). Yu et al. (2011) reported that the tether cilia are immotile and that all the other cilia in the OV are initially motile, using observation with high-speed videomicroscopy. Further, they showed that expression of the transcription factor, *foxj1b* (see Section 1.2.3 for details of *foxj1b* gene function) is required for ciliary motility within the otic vesicle (Yu et al.,

2011). *Foxj1b* is expressed throughout the OV at 10hpf, and is restricted to the OV poles by 22hpf, leading Yu et al. (2011) to suggest that ciliary motility within the OV follows the pattern of *foxj1b* expression.

1.5 The role of cilia in inner ear patterning and morphogenesis in the zebrafish embryo

Although several studies on zebrafish models of ciliary dysfunction have reported defects in otolith formation (Panizzi et al., 2007; Colantonio et al., 2009; Neugebauer et al., 2009; Serluca et al., 2009; Wilkinson et al., 2009; Gao et al., 2010; Wu et al., 2011; Yu et al., 2011), no studies have been done to see if cilia have a role in other aspects of zebrafish ear development. Defects in the formation of dorsolateral ear structures have been reported in *iguana* (*dzip1*) mutants (Hammond et al., 2010); however, this study was focused on the role of Hedgehog signalling in patterning the zebrafish OV and not on cilia.

In chick and mammals the hair cell kinocilium is thought to play a role in polarising the hair cell stereociliary bundle (Tilney et al., 1992; Denman-Johnson and Forge, 1999). The kinocilium has been shown to be important for both polarising the apical surface of the hair cell and for establishing a coordinated hair cell polarity across the auditory epithelium. In conditional *Ift88* null mice, where *Ift88* function is knocked down in the cochlea, some hair cells fail to produce a correctly polarised hair cell bundle, and there is a disorganisation of hair cell polarity across the sensory surface of the cochlea (Jones et al., 2008).

1.6 Objectives of PhD research

There is a lack of agreement in the scientific literature over the role of cilia and ciliary motility in otolith formation. In particular, no study has yet thoroughly described the distribution of motile cilia across the entire wild-type zebrafish otic vesicle from cavitation to 24hpf, when the majority of cilia within the OV have receded, with the exception of the hair cell kinocilia (Riley et al., 1997).

The work in this thesis sets out to carefully describe the role of cilia in otolith formation in the wild-type zebrafish embryo (Chapter 3). In addition, the effect of ciliary loss and dysfunction on otolith formation and the role of hair cells in otolith tethering are also investigated (Chapter 4).

There are at present no studies looking at the role of cilia in zebrafish ear development beyond the stages of initial otolith formation. The roles of cilia in morphogenesis of the zebrafish ear were investigated by looking at zebrafish mutants with a loss or complete lack of cilia. In addition, zebrafish mutants either lacking cilia or with a loss of ciliary motility were used to see if the requirement for kinocilia in polarising the apical surface of hair cells at both the cell and tissue level in mammals holds true for zebrafish (Chapter 5).

Chapter 2

Materials and Methods

2.1 Zebrafish husbandry

2.1.1 Zebrafish care

All adult fish were kept in a re-circulating system with a 14 hours light to 10 hours dark light cycle. Temperature was regulated at 28.5°C.

2.1.2 Embryo collection

Embryos were collected by marbling a tank of adult zebrafish the afternoon before the day newly laid embryos were wanted. To marble a tank of zebrafish, a small tank containing a mesh insert with marbles on top was placed carefully into the tank of fish. Zebrafish fertilised eggs over the marbles when the light comes on. The eggs fell through the marbles and mesh into the collection tank so that they were not eaten. Eggs were collected at 10–11am and sorted according to developmental stage.

Alternatively, embryos were collected by pair-mating adult fish. Pairs were set up the afternoon before embryo collection with a barrier between the male and female. The next morning the barrier was lifted between 8.30am and 9am and embryos were collected between 10am and 12noon and sorted according to developmental stage.

2.1.3 Embryo staging

Embryos were staged according to the staging series published in Kimmel et al. (1995)

2.1.4 Embryo raising

Embryos were raised in E3 embryo medium (5mM NaCl, 0.17mM KCl, 0.33mM $CaCl_2$, 0.33mM $MgSO_4$, 0.0001% methylene blue) in 90mm Petri dishes at 28.5°C. For some experiments embryos were slowed at between 20–23°C overnight from 70% epiboly to allow study of stages younger than 24hpf.

2.2 Zebrafish lines

The following two tables detail the zebrafish lines other than wild-types used in this research:

Table 2.1: Mutant zebrafish lines

Mutant	Description	Reference
keinstein: kei^{m219}	Fails to form otoliths, currently uncloned	Malicki et al. (1996); Whitfield et al. (1996)
oval: ovl^{tz288b}	Mutation in *ift88*, cilia initially form but start to disappear in sensory organs from 3dpf	Tsujikawa and Malicki (2004)
MZovl^{tz288b}	Maternal Zygotic mutation of *ift88*, ciliogenesis fails after the basal body docks to the cell membrane	Huang and Schier (2009)
iguana: igu^{ts294e} and igu^{tm79a}	Mutation in *dzip1* leading to a partial loss of cilia, evidence that there is a loss of primary cilia but not a loss of motile cilia	Brand et al. (1996); Sekimizu et al. (2004); Wolff et al. (2004); Glazer et al. (2010); Kim et al. (2010); Tay et al. (2010)
$lrrc50^{hu255H}$	Mutation in *dynein, axonemal assembly factor 1* (*dnaaf1*), cilia form normally but are immotile	Sullivan-Brown et al. (2008); van Rooijen et al. (2008)
mindbomb: mib^{ta52b}	Mutation in an E3 ubiquitin ligase required for Notch-Delta signalling	Jiang et al. (1996); Itoh et al. (2003)
sloth: slo^{tu44c}	Mutation in *hsp90aa1.1* required for skeletal muscle development and function	Granato et al. (1996); Hawkins et al. (2008)

Table 2.2: Transgenic zebrafish lines

Transgenic	Description	Reference
Tg(βactin2:Arl-13b-GFP)	The Arl13b-GFP fusion protein localises to all cilia in the zebrafish embryo, marking them fluorescently	Borovina et al. (2010)
Tg(pou4f3:m-GFP)	The pou4f3 promoter drives membrane targeted GFP expression in hair cells of the inner ear and lateral line, and retinal ganglion cells	Xiao et al. (2005)

2.3 Microscopy

2.3.1 DIC and epifluorescence microscopy

Live embryos or fixed specimens were examined using an Olympus BX-51 compound microscope with DIC and epifluorescence optics. Pictures were acquired using CellB software.

2.3.2 Confocal microscopy

Fluorescently stained embryos or transgenic embryos were visualised on either a Leica SP1 confocal microscope or Olympus FV1000. Images were processed either with the native confocal software or Fiji (Fiji Is Just ImageJ; Schindelin et al., 2012).

2.3.3 High-speed videomicroscopy

Embryos were anaesthetized in 4% tricaine in E3 medium at 18.5–26hpf and mounted in 3% Methyl Cellulose in a cavity made by cutting a hole in two layers of electrical insulation tape. A cover slip was carefully placed on the embryo to give a dorsolateral mount with the otic vesicle close to the cover slip. The cover slip was held in place with nail varnish. The mounted embryos on slides were stored flat at 25–28°C using heat packs in a polystyrene box. Embryos were imaged with an Olympus SPlan Apo 100× oil immersion objective with NA of 1.40, using an optical zoom of 1.6× on an inverted Olympus IX81 microscope. Movies were recorded at approximately 300 frames per second with a Basler A504k camera. Software was Video Savant.

Embryos of mutant lines that were too young to be phenotyped were then carefully dismounted by soaking the slide in E3 until the coverslip could be removed. Each embryo was then individually put into E3 in a 24-well dish and incubated at 28.5°C overnight and the genotype determined by phenotypic appearance the next day.

2.4 Immunohistochemistry

2.4.1 Double anti-acetylated tubulin/phalloidin stains

Dechorionated embryos were fixed overnight at 4°C in 4%PFA and stored at 4°C in PBS until required.

Embryos were permeabilised in Triton-X 100 in PBS according to stage: <24hpf, 0.5% Triton-X 100 in PBS; 24–48hpf, 1.0% Triton-X 100 in PBS; 48–72hpf, 1.5% Triton-X 100 in PBS; >72pf, 2.0% Triton-X 100 in PBS. The embryos were left in the Triton solution until otoliths dissolved, typically 4 days at 4°C or 3 hours at room temperature.

The Triton-X 100 solution was removed by rinsing 3 × 5min in PBS, before blocking embryos in BDP+5%FCS for 1 hour at room temperature. Embryos were then incubated overnight at 4°C in BDP+5%FCS with 1:100 dilution of anti-acetylated tubulin antibody (Sigma T6739). The next day unbound primary antibody was removed by rinsing for at least 3 × 1 hour at room temperature in BDP+5%FCS. Embryos were then incubated at room temperature for 2 hours in the dark in secondary antibody (1:50 dilution of TRITC labeled goat anti-mouse (Sigma T5393) in BDP+5%FCS. After secondary antibody binding, unbound secondary antibody was removed by rinsing overnight at 4°C in the dark in BDP+5%FCS. Block solution was removed by rinsing 2 × 20min in PBS at room temperature. *The protocol was stopped here for only an anti-acetylated tubulin stain.* 100μl FITC-phalloidin (Sigma P5282) was diluted in 2ml PBS and used to stain embryos in the dark for at least 3 hours at 4°C. Excess FITC-phalloidin was removed by rinsing for at least 3 × 30mins in PBS at 4°C in the dark.

After staining, embryos were dissected in a drop of PBS to provide an unobstructed view of the otic vesicle. They were then equilibrated from PBS into 100% Vectashield (Vector Laboratories Cat No. H-1000), and mounted in 100% Vectashield for confocal microscopy.

2.4.2 Anti-acetylated tubulin stain using HRP conjugated secondary antibody

The anti-acetylated tubulin stain was carried out as above until addition of the secondary antibody:

Embryos were incubated overnight at 4°C in a 1:200 dilution of HRP conjugated goat anti-mouse IgG (Sigma A4416) in BDP+5%FCS. Then unbound secondary antibody was removed by rinsing overnight at 4°C in BDP+5%FCS. Block solution was then removed by rinsing for 2 × 20min in PBS at room temperature. Embryos were then stained in a 24-well plate using Vector Laboratories DAB substrate kit for peroxidase (Cat No. SK-4100), following the standard manufacturer's protocol. Better results were achieved without nickel enhancer solution.

After staining, yolks were dissected from embryos in a drop of PBS and then embryos were equilibrated to and mounted in 100% glycerol for examination with an Olympus

BX-51 compound microscope.

2.4.3 Double anti-acetylated tubulin anti-GFP stains

Embryos were fixed and permeabilised as for anti-acetylated tubulin stain. Then the embryos were blocked in BDP+5%FCS for 1 hour at room temperature. Binding of the primary antibodies was achieved by incubating overnight at 4°C in BDP+5%FCS with a 1:100 dilution of mouse anti-acetylated tubulin and 1:500 dilution of rabbit anti-GFP (Torrey Pines Biolabs Inc TP401). Unbound primary antibody was removed by rinsing in BDP+5%FCS for 3 × 1 hour at room temperature. Secondary antibodies were bound by incubating overnight at 4°C in BDP+5%FCS with 1:50 dilution TRITC conjugated anti-mouse IgG (Sigma T5393) and 1:200 dilution FITC conjugated anti-rabbit IgG (Sigma F9887). Excess secondary antibody was removed by rinsing overnight in BDP+5%FCS. Block was then removed by rinsing 2 × 20mins in PBS. Stained embryos were dissected and mounted in 100% Vectashield for examination by confocal microscopy.

2.4.4 Immunohistochemistry solutions

BDP+5%FCS (10ml)

10ml	PBS
0.1g	BSA
10μl	DMSO

Mix the above and wait for the BSA to dissolve, then replace 0.5ml of this solution with 0.5ml Fetal Calf Serum or Bovine Serum.

2.4.5 Preparation of embryos for examination of hair-cell polarity in sensory maculae

4dpf embryos were fixed overnight in 4%PFA at 4°C and then permeabilised in 2% Triton-X 100 at either room temperature or 4°C until the otoliths dissolved. After permeabilisation the embryos were dissected to remove fins, eyes, jaw, yolk and brain in a drop of PBS to facilitate penetration of the ear tissue by the antibodies and FITC-phalloidin. They were then stained with both anti-acetylated tubulin antibody and FITC-phalloidin as described in Section 2.4.1. After staining, ears were dissected out, mounted and coverslipped for visualisation of either the anterior or posterior macula in Vectashield mounting medium. The maculae were then imaged using a Leica SP1 confocal microscope (typically using a 60× water immersion objective and 2× zoom), taking optical sections approximately 0.5μm apart through the entire apical surface of the maculae.

2.5 Whole mount *in situ* hybridisation

All stages of the protocol were carried out in 1.5ml tubes until the BCIP/NBT staining step on Day 3.

Day 1

Embryos that had been fixed overnight in 4%PFA and then stored in 100% methanol at –20°C were rehydrated through a methanol series into 100%PBS. The embryos were then digested in 10μg/ml proteinase K in PTW for a time dependent on age of the embryo: <20 somite stage (S) → 1min; 20S–25S → 2–3min; 25S–24hpf → 3–5min; 24–30hpf → 7.5–10min; 30–36hpf → 10–15min; >36hpf → 15–20min. After proteinase K digestion the embryos were re-fixed in 4%PFA for 20mins at room temperature to de-activate the proteinase K, before being rinsed with 4 × 5min washes in PTW. The embryos were then pre-hybridised in Hyb+ for at least 1 hour in a water bath at 65–70°C. DIG labelled RNA probes, diluted 1:450 in Hyb+, were pre-heated at 80°C for 2–3mins to denature any secondary structure, and then put on ice. RNA probe was added to the pre-hybridised embryos. RNA was hybridised to the embryos overnight at 65–70°C in a water bath.

Day 2

The RNA probe was removed from embryos and stored at –20°C for re-use. Hot washes were then carried out at the hybridisation temperature (65–70°C) to remove any un-hybridised probe: 20mins in 50% Hyb– : 50% 2×SSC; 20mins in 50% Hyb– : 50% 2×SSC; 20mins in 2×SSC; 2 × 1 hour washes in 0.2×SSC. After the hot washes embryos were then washed at room temperature: 10mins in 50% 0.2×SSC : 50% PTW; 3 × 10–15min washes in PTW. Embryos were then blocked in block solution for at least 1 hour before the hybridised probes were labelled by overnight incubation at 4°C with Anti-Digoxigenin-AP Fab fragments (Roche 11 093 274 910) diluted 1:2000 in block solution.

Day 3

Any unbound anti-digoxigenin antibody was removed by 8 room temperature washes over 3.5–4 hours in PTW. *Optional:* Embryos can be rinsed overnight in PTW at 4°C. Embryos were then equilibrated in Alkaline phosphatase (AP) staining buffer 3–4 times over 15–20 mins and then transferred to a 24-well plate (one well for each 1.5ml tube of embryos). Next, embryos were stained in the dark in 3.5μl/ml BCIP and 4.5μl/ml NBT diluted in AP staining buffer, until developed. Once the stain was visible and before background staining appeared the reaction was stopped by washing in PTW or PBS for at least 3 × 5min. Embryos were fixed overnight at 4°C in 4%PFA and then transferred to 1.5ml tubes for storage until they were mounted for microscopy.

Day 4

Embryos were mounted by first dissecting off the yolk in a drop of PBS. For embryos 2dpf and older, eyes, fins, and jaw may also have been removed for a clean mount allowing visualization of the ear. Embryos were then passed through a stage series of glycerol until equilibrated into 100% glycerol, then mounted in 100% glycerol and coverslipped.

2.5.1 Solutions for *in situ* hybridisation

PTW

0.1% Tween in PBS

Hyb+ (50ml)

Formamide	25ml
20×SSC	12.5ml
tRNA 25mg/ml	1ml
Heparin 50mg/ml	50μl
Tween 20 10%	0.5ml
Citric Acid	0.46ml
dH_2O	10ml

Hyb– (50ml)

Formamide	25ml
20×SSC	12.5ml
Tween 20 10%	0.5ml
Citric Acid	0.46ml
dH_2O	11.54ml

Block solution (10ml)

PTW	9.8ml
Bovine serum	200μl
BSA	20mg

AP staining buffer (50ml)

1M Tris pH 9.5	5ml
1M $MgCl_2$	2.5ml
5M NaCl	1ml
Tween 20 10%	0.5ml
dH_2O	41ml

2.6 Morpholino injections

Embryos were injected with morpholino at the 1–4 cell stage. For injections of *atoh1b* morpholino (5'–TCATTGCTTGTGTAGAAATGCATAT–3' (Millimaki et al., 2007)), approximately 5nl of 1mM morpholino dissolved in dH_2O with 25% phenol red was injected. For injections of *Su(H) 1+2* morpholino (5'–CAAACTTCCCTGTCACAACAGG–3' (Sieger et al., 2003; Echeverri and Oates, 2007)), approximately 0.5nl of 0.5mM morpholino dissolved in dH_2O with 25% phenol red was injected. 1–4 hours after injection embryos were checked for normal development and incorporation of phenol red into cells.

2.7 Molecular biology

2.7.1 Transformation of plasmid DNA

DH5α competent cells were thawed on ice and 50μl competent cells were aliquoted into prechilled 1.5ml tubes for each transformation reaction. 2μl of mini or midi-prepped plasmid DNA was pipetted into the competent cells and mixed by gentle flicking. Cells were then incubated on ice for 30mins, before being heat-shocked at 42°C for 40s in a water bath. The cells were then allowed to recover on ice for 2mins before adding 200μl LB and incubating for 1 hour at 37°C with shaking. 100μl of each transformation was plated on LB-agar plates with the appropriate antibiotic, then incubated overnight at 37°C. Colonies were then picked for plasmid purification.

2.7.2 Plasmid purification

Purification of plasmid DNA was performed using either the QIAprep Spin Miniprep Kit (Qiagen 27106), or HiSpeed Plasmid Midi Kit (Qiagen 12643), following the manufacturer's standard protocol.

2.7.3 Restriction enzyme digestion of plasmid DNA

To produce a template for RNA transcription plasmid DNA was digested with a restriction enzyme that cut the plasmid once, at the opposite side of the clone to the transcription start site. Restriction enzymes manufactured by Promega, Roche or NEB were used according to the manufacturer's instructions.

2.7.4 Synthesis of DIG labelled RNA probes

The following were mixed in an RNAse free 1.5ml tube: 1–5μg template DNA; 4μl 5x transcription buffer (Promega); 1μl 0.1mM DTT; 2μl DIG labelling mix; 1μl RNAse inhibitor; 2μl RNA polymerase (T7, T3 or SP6 (Promega)); fresh milliQ water to 20μl. Reactions were incubated at 37°C for 2 hours and then 0.2μl 0.2M EDTA was added to stop the reaction. RNA was precipitated by adding 2.5μl 4M LiCl or 2.5μl 3M NH_4OAc

and 75μl cold EtOH before incubating for at least 2 hours at –20°C or 30mins at –80°C. The precipitated RNA was pelleted by centrifuging at 13000rpm for 10mins at 4°C. The pellet was then washed in cold 70% EtOH, and re-centrifuged at 13000rpm for 2mins at 4°C. The EtOH was removed and the pellet air-dried for 10–15mins. The RNA was then resuspended in 50μl 50% Formamide in fresh milliQ water and stored at –20°C. RNA synthesis was confirmed by running a 2μl aliquot on a 1% agarose gel.

2.8 Movement restriction and forced motion experiments

2.8.1 Movement restriction

Embryos were sorted and raised at 28.5°C until shield stage. Embryos were then slowed overnight at 21°C. The next day embryos were dechorionated with forceps at the 15–18 somite stage and placed in a layer of 3% methyl cellulose in the bottom of a Petri dish. A layer of E3 was then carefully pipetted on top to prevent the embryos drying out. Embryos were incubated at 28.5°C and otolith phenotypes scored for both ears 28–30 hours later. Control embryos had the same incubation temperature changes as restricted embryos but were not dechorionated and were grown in E3 without any methyl cellulose.

2.8.2 Forced motion

At 2–3hpf batches of 40 embryos were sorted into 25ml E3 in 50ml Falcon tubes and placed on a roller mixer at approximately 26.5°C. Otolith phenotypes for both ears were scored at approximately 30hpf. Control embryos were incubated in Petri dishes at 28.5°C. Embryos grown in Falcon tubes showed no discernible age difference to their non-rolled siblings, despite the difference in incubation temperature. This may be because better aeration in the rolled tubes compensated for the lower incubation temperature, though this was not investigated.

2.8.3 Otolith scoring

Ears were scored based on their otolith phenotype by examination on a dissecting stereomicroscope. Otoliths were scored based on their position and number; otolith size and shape was not scored. Both left and right ears were scored for each embryo. The scoring system used for otoliths is described in Table 2.3, and example otic vesicles and their score are shown in Figure 2.1.

Table 2.3: Otolith scoring system

Score	Description
N	normal otic vesicle with one anterior and one posterior otolith
3AF	three otoliths, with a fusion of the two anterior otoliths
3PF	three otoliths, with a fusion of the two posterior otoliths
3S	three separate otoliths, with one untethered otolith
1FA	a single anterior otolith, which may be a fusion of multiple otoliths
1FP	a single posterior otolith, which may be a fusion of multiple otoliths
1U	a single untethered otolith
other	other defect in otolith number and position

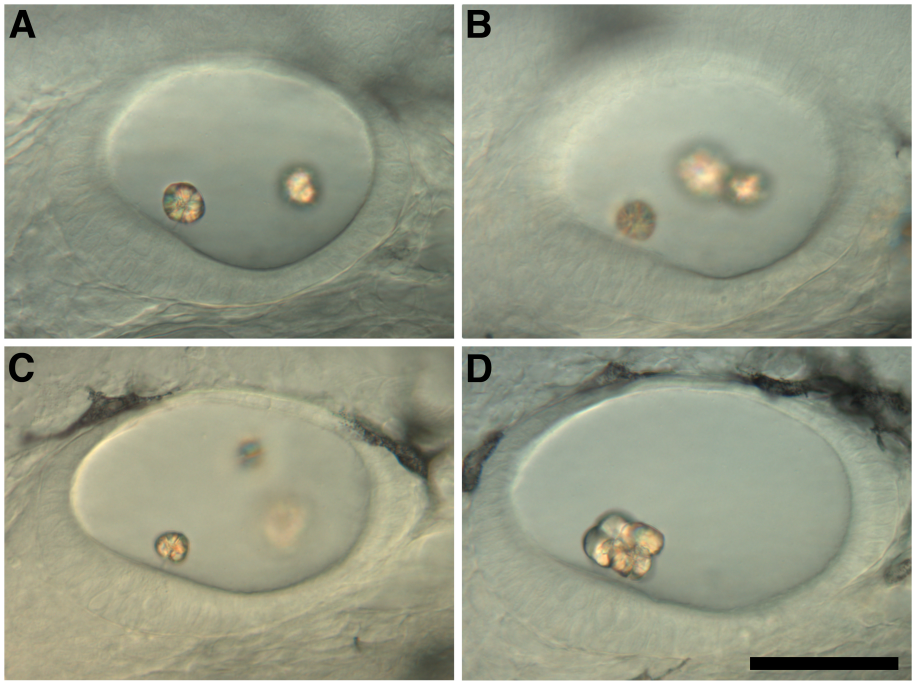

Figure 2.1: Example otic vesicles and their otolith phenotype. All panels show left OV with anterior to left. **A**. DIC image of a 32hpf igu^{tm79a} sibling OV with an otolith phenotype that would be scored as 'N'. **B**. DIC image of a 32hpf igu^{tm79a} mutant OV with an otolith phenotype that would be scored as '3PF'. **C**. DIC image of a 32hpf igu^{tm79a} mutant OV with an otolith phenotype that would be scored as '3S'. **D**. DIC image of a 32hpf igu^{tm79a} mutant OV with an otolith phenotype that would be scored as '1FA'. Scale bar: 50μm, applies to all panels.

2.9 Image analysis

2.9.1 Estimates of total cilia number in the otic vesicle

A maximum projection of a confocal stack through an entire otic vesicle (OV), stained with anti-acetylated tubulin antibody, was opened in Fiji. The image was converted to a binary image using the threshold tool. The paintbrush tool was used to manually separate any large area consisting of several cilia into a number of separate areas that equalled the number of cilia; the number of cilia in a large area was determined by referring back to the original image stack. The 'Analyze Particles' tool was then used to count the total cilia in the image. Total cilia count had to be taken as an estimate since some cilia may have been missed due to being hidden beside others in the stack and background signal may have led to extra counts.

2.9.2 Movie processing

Movies from high-speed videomicroscopy experiments were saved as .tiff stacks using Video Savant. Fiji was then used to convert the tiff stack to a .avi file with a frame rate of 15 frames per second (20 times slower than the 300 frames per second recording speed) and to put arrowheads on movies. iSquint was used to convert .avi files to a compressed .mp4 format for publication.

2.9.3 Counts of total motile cilia in otic vesicle

A high-speed movie was taken over the entire OV by changing the microscope focal plane from the medial to the lateral wall of the OV whilst recording a high-speed video (example: Movie 9). These videos were then used to count the total number of motile cilia in the OV by eye.

2.9.4 Calculation of ciliary beat frequency

Ciliary beat frequency was estimated by counting the number of rotations made by a cilium during a 99 frame movie lasting 0.33s. The counts were multiplied by 3 to estimate ciliary beats per second (Hz). Beat frequencies of several cilia were averaged to get a mean beat frequency for each age group.

2.9.5 Time-to-colour images

Six consecutive frames of a high-speed movie were opened as layers in the GIMP (GNU Image Manipulation Program). Each layer was assigned a different colour using the 'colorify tool' (Hues of 0, 60, 120, 180, 240 and 300). The top five layer modes were changed to 'difference'. This had the result that parts of the original grey-scale movie frames that did not change in intensity (because there was no moving object) remained grey-scale, while parts of the movie frames that did change in intensity (because there was a moving

object) were coloured. The layers forming the image were then flattened and saved as a .jpg. Adobe Photoshop CS5 was used to boost saturation of the time-to-colour images.

2.9.6 Polarity patterns

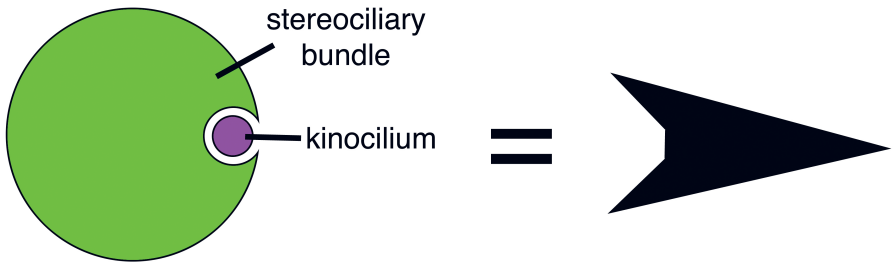

Figure 2.2: Cartoon of hair cell bundle and its corresponding polarity. When making polarity patterns the arrow to show the polarity of the hair cell is drawn from the stereociliary bundle and points towards the kinocilium.

A confocal stack of a sensory macula was opened in Fiji and channels were merged into a two-coloured stack. Using the arrow tool, arrows were drawn over each stereociliary bundle, indicating the relative position of the kinocilium in the bundle (Figure 2.2) and added to an overlay. If a stereociliary bundle lacked a kinocilium the arrow was drawn pointing towards the gap for the kinocilium instead. A dot was used to indicate the position of any hair cells where polarity could not be determined. Once all the hair cells had been marked, a new slice was added to the end of the stack and painted white, and the overlay was flattened onto it to give the polarity patterns. Hair cell counts were achieved by using the 'Analyze particles' tool on the polarity pattern.

Polarity patterns were made for imperfectly mounted maculae by scrolling through slices of the confocal stack in Fiji, allowing stereociliary bundles from different z positions to be incorporated into a polarity pattern of the whole stack. It was occasionally possible to determine the polarity of a stereociliary bundle by comparing its image across 2–3 optical sections, although its polarity could not be determined from a single image.

2.9.7 Polarity graphs

Circular graphs to represent the polarity of a macula were made by measuring the angle of each arrow (angle measured from tail to point) in a polarity pattern with respect to a fixed 0° line using Fiji. These data were then saved into a Microsoft Excel spreadsheet and grouped into 20° bins. The number of arrows in each bin was then plotted on a modified donut chart using Microsoft Excel, using the method described on the webpage: *http://www.excelcharts.com/blog/the-consultants-chart-revisited/*.

2.10 Statistics

Graphpad Prism was used to carry out statistical tests and plot graphs, with the exception of graphs showing the % proportion of ears with different otolith defects, which were plotted using Microsoft Excel.

Chapter 3

Description of Cilia in the Wild-Type Otic Vesicle

3.1 Introduction

The wild-type zebrafish otic vesicle (OV) is known to be ciliated from the point of cavitation (between 18 and 18.5hpf) until at least 30hpf. At 24hpf all cilia apart from the kinocilia of the hair cells have receded and are not easily visible in fixed embryos stained with anti-acetylated tubulin antibody (Riley et al., 1997). More recently it has been shown that these cilia do not disappear completely; they are still visible in *Tg(βactin2:Arl13b-GFP)* embryos (see Table 2.2, page 33) at 30hpf as shown in Borovina et al. (2010) and Figure 3.1B. However, the total number of cilia in the OV, and whether cells lining the OV are monociliated or multiciliated, have not been previously described.

Previous descriptions of ciliary motility in the wild-type OV and the role of motile cilia in otolith tethering were incomplete, with conflicting evidence and conclusions (see Section 1.4, page 27). A full description of wild-type OV cilia and ciliary motility based on observations with confocal and high-speed videomicroscopy imaging follows.

3.2 Results

3.2.1 Cilia presence and number in the wild-type otic vesicle

The presence of cilia in the wild-type OV from the cavitation stage was confirmed by anti-acetylated tubulin antibody stain to mark the microtubule axonemes of all cilia (Figure 3.1). In addition the cell bodies of hair cells were marked as differentiation into a neural cell type progressed. The nerve bundle that sits medial to the OV was also marked by the anti-acetylated tubulin stain (asterisk, Figure 3.1A).

Cilia were present from the earliest stage examined, the 17 somite stage (S), at which point they were located along the seam from which the OV cavitates. As cavitation progressed more cilia were present in the OV, reflecting the greater number of cells lining the

OV lumen. By 21S denser patches of cilia became apparent at the anterior and posterior poles of the OV where the otoliths tether (arrowheads, Figure 3.1A). On the medial wall of the OV, there were between one and six cilia that appeared longer and thicker when stained with anti-acetylated tubulin antibody.

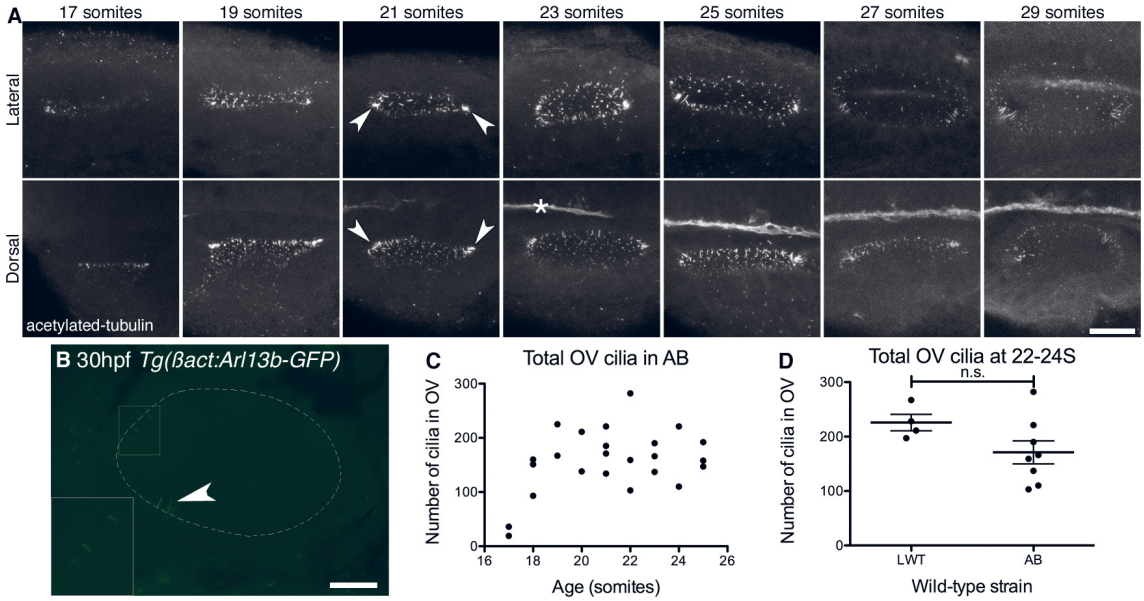

Figure 3.1: Cilia in the wild-type otic vesicle. **A**. Stage series of confocal projections through entire otic vesicle (OV) of wild-type (AB strain) zebrafish embryos stained with anti-acetylated tubulin antibody. Arrowheads indicate denser patches of cilia found at the anterior and posterior poles of the OV, where the sensory maculae form. Asterisk indicates position of nerve bundle medial to the OV. Scale bar: 25μm. **B**. Epifluorescence picture of 30hpf *Tg(βactin2:Arl13b-GFP)* embryo showing that short cilia are still present (inset) away from the tether cilia (arrowhead). Dotted line indicates OV lumen. Scale bar: 25μm. **C**. Scatter plot showing the change in total number of cilia found in the OV of wild-type (AB strain) embryos with age. **D**. No significant difference was found between the total number of OV cilia in 22-24S wild-type strains LWT and AB (2-tailed t-test; p=0.1196, t=1.702 d.f.=10). Bars show mean ±s.e.m.

In fixed embryos stained with anti-acetylated tubulin antibody, non-tether cilia seem to disappear from the OV beyond 24hpf (Riley et al., 1997). However, observation of 30hpf *Tg(βactin2:Arl13b-GFP)* embryos revealed that short non-tether cilia were still present in the OV at this stage; see Figure 3.1B and supplementary material in Borovina et al. (2010).

The 'Analyze Particles' tool in Image J was used to estimate the total number of cilia in wild-type OVs from 17S to 25S. The number of cilia in the OV increased from approximately 30 in 17S embryos to approximately 200 in 21S embryos. After this initial rapid increase the number of cilia remained steady until 25S (Figure 3.1C). The total number of OV cilia was very variable from one embryo to another. This may reflect an uncoupling between OV development and somite stage from one individual to the next. Alternatively, OVs could vary a lot in number of ciliated cells lining the lumen from one individual to the next. There did not appear to be a strong correlation between extent of

OV cavitation and total number of cilia within the OV when OV cavitation was compared within each somite stage by eye. No significant difference was found in the number of OV cilia present between 22-24S in wild-type strains LWT and AB (Figure3.1D).

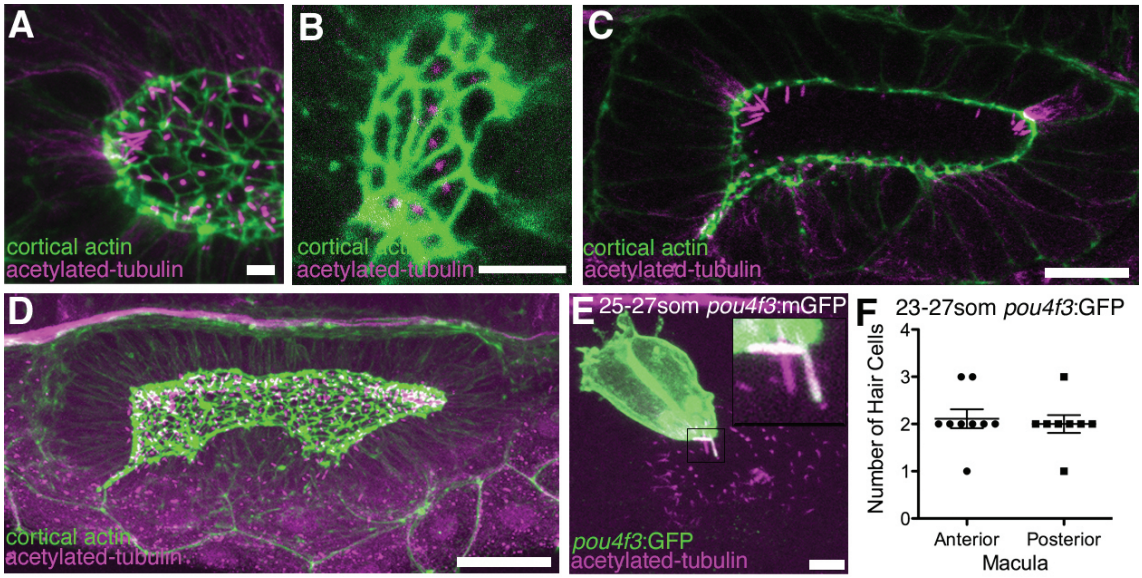

Figure 3.2: Wild-type otic vesicle morphology. A. Confocal projection showing 21S stage wild-type (LWT strain) embryo stained with anti-acetylated tubulin antibody (magenta) and FITC-phalloidin (green). Lateral view with anterior to left. Cells lining the OV lumen are monociliated. Scale bar: 5μm. **B**. Confocal projection showing transverse view of 20-22S wild-type (AB strain) (dorsal up, medial left). Cells supporting the denser cluster of cilia at the OV pole are still monociliated. Scale bar: 5μm. **C**. Single confocal section that shows clusters of cilia at the anterior and posterior poles in a 21S stage wild-type (AB strain) embryo (dorsal view; anterior left, medial up). Scale bar: 20μm. **D**. Confocal projection of entire OV of a 19-21S LWT embryo (dorsal view; anterior left, medial up). The medial wall of the OV is well defined, while the lateral wall is less well defined at this stage. Scale bar: 20μm. **E**. Confocal projection of anti-GFP antibody and anti-tubulin antibody stain of *Tg(pou4f3:mGFP)*. GFP marks hair cells and their kinocilia: tether cilia appear white (inset); other cilia are magenta. Scale bar: 5μm. **F**. The early OV had between one and three hair cells at each pole, most commonly two. Cells were counted in either fixed or live 23-27S *Tg(pou4f3:mGFP)* embryos. Bars show mean ± s.e.m.; anterior maculae n=9, posterior maculae n=8.

OVs were stained with both anti-acetylated tubulin antibody and phalloidin, marking the axonemes of cilia and cortical actin localised to cell boundaries respectively; this revealed that all cells lining the OV are monociliated (Figure 3.2A). Even the denser patches of cilia at the anterior and posterior poles of the OV occur on monociliated cells with smaller apical domains than cells in the middle region of the OV. This was observed by transverse mounting the OV (Figure 3.2B).

The phalloidin stains also revealed that initially the medial wall and poles of the OV are well defined, whereas the lateral wall of the OV appears less well organised (Figure 3.2C, D). This has interesting parallels to epithelialisation of the OV in other species, and is discussed in Section 3.3.

The *pou4f3:mGFP* transgenic line, which marks all hair cells in the embryo (Xiao

et al., 2005), was used to visualise how many hair cells and kinocilia are present at the OV poles, where the denser patch of cilia is located (see Section 1.3.4 and Table 2.2 for details of *pou4f3* function). In *tg(pou4f3:mGFP)* embryos, GFP is localised to the membranes of both the hair cells and their kinocilia. A double stain with anti-GFP and anti-acetylated tubulin antibodies revealed that between one and three, typically two, hair cells are present (Figure 3.2E and F). Hair cell kinocilia are labelled with both the anti-GFP antibody and the anti-acetylated tubulin antibody and appear white, whereas non-hair cell cilia are only labelled by the anti-acetylated tubulin antibody and appear purple (see inset, Figure 3.2E). Therefore a subset of between one and three of the patch of four to six cilia at the OV pole are the kinocilia of the first hair cells, which are known to tether the forming otolith (Riley et al., 1997; Yu et al., 2011)

Ciliary length was not measured as it was impossible to tell when cilia were truly in the plane of focus, or to determine their angle relative to the focal plane to allow calculation of cilium length.

3.2.2 Motility of cilia in the wild-type otic vesicle

High-speed videomicroscopy was used to investigate the *in vivo* motility of OV cilia in anaesthetised wild-type embryos from 18S to 25hpf. Colantonio et al. (2009) reported that anaesthetising embryos had no effect on the motility of OV cilia. I was unable to test this in my set-up by recording movies from unanaesthetised embryos, as 3% methyl cellulose was used as the mounting medium. This meant that unanaesthetised embryos could twitch, moving too much to allow recording of ciliary motility within the OV. The study by Colantonio and colleagues was able to look at ciliary motility in unanaesthetised embryos because they used agarose as the mounting medium.

All movies appeared to show motile cilia rotating as opposed to beating. This is most similar to the reported rotating motion of cilia in the mouse embryonic node (Nonaka et al., 2005) and zebrafish Kupffer's vesicle (Kramer-Zucker et al., 2005). See Kramer-Zucker et al. (2005), Supplementary Movie 10, for an example of zebrafish Kupffer's vesicle cilia. An example of beating cilia in the zebrafish pronephros can be seen in Kramer-Zucker et al. (2005), Supplementary Movie 2.

Observation of the OV before 21S was impaired as the OV was not fully cavitated at these stages, making it difficult to determine the full extent of the lumen. However, it appears that ciliary motility starts very soon after a lumen is present; the youngest embryo in which motile cilia could be seen was 18S and had a single motile cilium on the medial wall of the OV, alongside several immotile cilia (Figure 3.3A, Movie 1).

As soon as the OV cavitates otolith precursor particles appear in the OV lumen. These start to stick to the tips of the tether cilia (kinocilia of the first hair cells) as soon as the poles of the OV have cavitated (Riley et al., 1997). I saw otolith precursor particles bound to tether cilia in embryonic OVs from 19S. Motile cilia were seen next to the otolithic material nucleating on the tips of the tether cilia (Figure 3.3B, Movie 2).

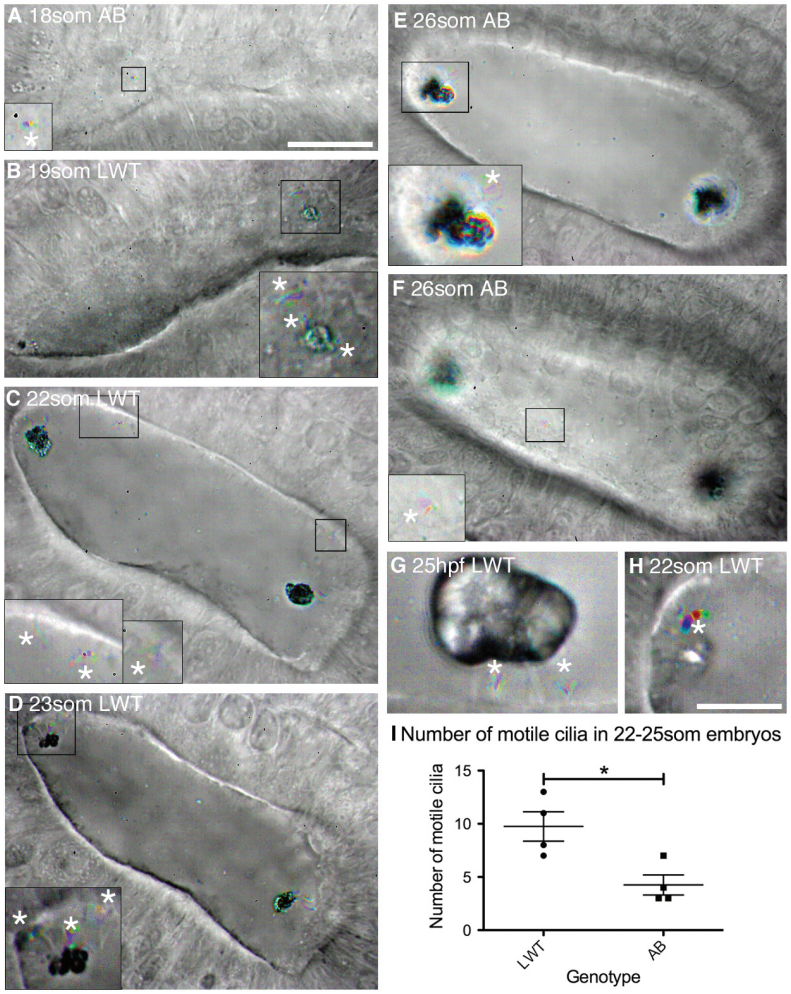

Figure 3.3: Ciliary motility in the developing wild-type zebrafish otic vesicle. All panels are dorsolateral views of the left ear, with anterior to the right, and are merged time-to-colour composites of six consecutive frames of a high-speed movie. Grey scale shows lack of movement; colour indicates movement. White asterisks mark motile cilia. **A**. 18S AB strain wild-type embryo with one motile cilium present on the medial wall (shown in inset). Scale bar: 20μm (applies to A-F). See Movie 1. **B**. 19S LWT wild-type embryo. Inset: presence of motile cilia next to anterior otolith and movement of the anterior otolith. See Movie 2. **C**. 22S LWT wild-type embryo. Insets: motile cilia present on the medial wall of the OV (two in the left hand inset, one in the right hand inset). See Movie 3. **D**. 23S LWT wild-type embryo. The posterior otolith is shown on two immotile tether cilia (grey); three motile cilia are nearby (coloured). See Movie 4. **E**. 26S AB wild-type embryo. Inset: motile cilia next to posterior otolith. See Movie 5. **F**. Different focal plane of the embryo shown in E. One motile cilium was present on the medial wall of the OV (inset) that rotated first one way and then the other. See Movie 6. **G**. 25hpf LWT wild-type embryo. Cilia away from the otolith have started to regress. The otolith sits on 2–3 tether cilia; two short, motile cilia remain directly underneath. See Movie 7. **H**. Very rarely an otolith precursor particle or small collection of otolith precursor particles is observed bound to a motile cilium (asterisk; 22S LWT wild-type embryo). Scale bar: 10μm (applies to G, H and insets in A-F). See Movie 8. **I**. Comparison of the number of motile cilia found per OV in AB and LWT wild-type strains.

As the OV continues to cavitate the otolith can be seen bound to between one and three (most frequently two) immotile tether cilia, with between one and four motile cilia

nearby (inset, Figure 3.3D, Movie 4). The neighbouring motile cilia may knock into the forming otolith as they rotate, making the otolith move (Figure 3.3C, E, Movies 3 and 5).

Motile cilia were also observed on the medial wall of the OV (Figure 3.3C, E, Movies 3 and 5) until at least 26S. However, motile cilia were never observed on the lateral wall of the OV (n=23 ears). Some cilia were recorded that either started or stopped moving during the brief (∼0.33s) recording time. In one case, a cilium on the medial wall of the OV was observed that rotated first one way and then the other (Movie 6). It is possible that these motile cilia correspond to the longer and thicker cilia seen on the medial wall of the OV when fixed embryos are labeled with anti-acetylated tubulin antibody (Figure 3.1A). However, determining if cilia were completely in the focal plane of the movie was not possible, just as for confocal data from the anti-acetylated tubulin antibody stained embryos. This meant that it was not possible to confirm if motile cilia were longer and thicker than non-motile cilia *in vivo* using the videomicroscopy data.

By 24–25hpf the first hair cells have a characteristic hair cell morphology: a rounded cell shape and a stereociliary bundle forming around the kinocilium (Tanimoto et al., 2011). These kinocilia tether the otolith, which at this stage is starting to biomineralise. The kinocilia have lengthened and the motile cilia near the otoliths have started to shrink but remain motile (Figure 3.3G, Movie 7). Motile cilia can not be seen anywhere else in the OV.

The total number of motile cilia in the OV was determined *in vivo* by recording a movie of the OV in which the focal plane was changed from the medial to the lateral wall (Example: Movie 9). The total number of motile cilia was then counted manually whilst watching the movie looped at 15fps. The mean number of motile cilia was found to be 9.8 (± s.e.m. of 1.4, n=4) in the OV of wild-type strain LWT embryos at 22–25S. However, the mean number of motile cilia in the OV of wild-type strain AB embryos at 22–25S was found to be significantly lower at 4.3 (± s.e.m. of 0.95, n=4) (2-tailed t-test, p=0.0166, t=3.292 d.f.=6) (Figure 3.3I). The beat frequency of motile cilia was estimated to be 28Hz (s.d. = 4.8) at 19–24S and 33Hz (s.d. = 5.9) at 24–25hpf, corroborating previously published data (Yu et al., 2011; Wu et al., 2011; Colantonio et al., 2009).

3.2.3 Tether cilia are immotile in the absence of otolith binding

Very rarely (in two cases out of 78 wild-type or phenotypically wild-type sibling OVs observed) an otolith precursor particle was seen bound to the tip of a motile cilium (Figure 3.3H, Movie 8). This suggested that a transient motile stage for tether cilia could be possible. Tethering of otolith precursor particles on the tips of the tether cilia may trigger a change in ciliary motility, potentially by acting through a signalling pathway or by mechanical hindrance of ciliary movement. This was investigated by observing ciliary motility in the *keinstein* (*kei*) mutant, which fails to form otoliths (Whitfield et al., 1996). The mutation in *kei* is currently uncloned.

Although *kei* mutants lack otoliths, hair cells, cilia, and tether cilia were all present

(Figure 3.4). Otolith precursor particles were present but appeared smaller than normal. Ciliary motility in *kei* mutant embryos was unaffected; motile cilia were present at the OV poles and both before and after 24hpf *kei* mutant tether cilia were present and immotile (Figure 3.4E and F, Movies 10 and 11). This suggests that tether cilia are immotile, regardless of otolith precursor particle binding.

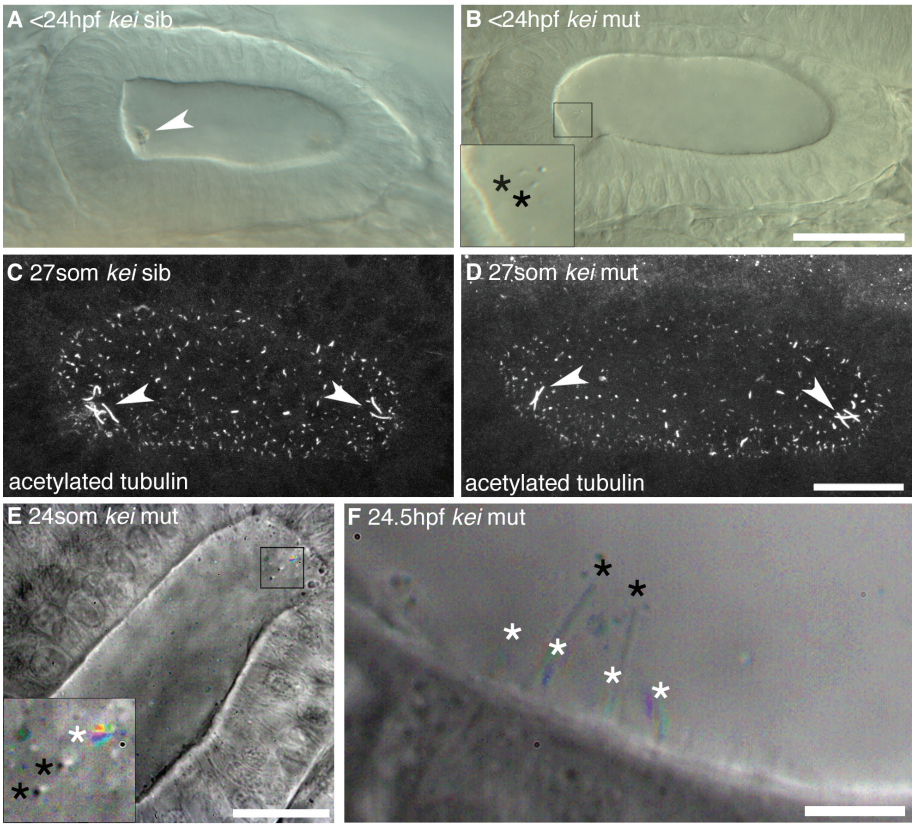

Figure 3.4: Tether cilia are immotile even in the absence of otoliths. A. DIC picture of lateral view of <24hpf *kei* sib embryo; anterior to left. The anterior otolith is visible (arrowhead). **B**. DIC picture of lateral view of <24hpf *kei* mutant embryo showing anterior tether cilia (inset, marked by black asterisks). There is no otolith bound; however, smaller than normal otolith precursor particles are present. Scale bar: 40μm, applies to A, B. **C**. Confocal stack through OV of 27S *kei* sibling embryo, stained with anti-acetylated tubulin antibody (lateral view, anterior to left). Arrowheads indicate kinocilia. **D**. Confocal stack through OV of 27S *kei* mutant, stained with anti-acetylated tubulin antibody. Cilia appear normal; arrowheads indicate kinocilia. Lateral view. Scale bar: 20μm, applies to C, D. **E.** Time-to-colour merge of 24S *kei* mutant. Inset shows immotile kinocilia (black asterisks), next to a motile non-tether cilium (white asterisk). Scale bar: 20μm. See Movie 10. **F**. Time-to-colour merge of 24.5hpf *kei* mutant OV. Two long kinocilia (black asterisks) are surrounded by four shorter motile cilia (white asterisks). Scale bar: 6μm. See Movie 11.

3.3 Discussion

My findings have confirmed previously published data (Riley et al., 1997): the OV is ciliated from cavitation and the cilia are denser at the anterior and posterior poles of the

OV where the otoliths tether. The increased density of cilia is due to the smaller apical surfaces of cells at the poles of the OV. I have also shown that only a subset of this denser patch of cilia are tether cilia on the first hair cells by examining the *pou4f3:mGFP* transgenic line that fluorescently labels hair cells and their cilia. By looking at dorsal views of the OV I have found that the medial wall of the OV is epithelialised before the lateral wall. The pattern of epithelialisation shows a similarity to otic placode invagination in chicken and mouse embryos. As the otic placode invaginates, forming the otic cup, what will be the medial wall of the otic vesicle moves into the embryo. The lateral wall is not formed until the cup pinches off from the surrounding ectoderm, forming the otic vesicle (Fritzsch et al., 1998). Although the zebrafish OV is formed by cavitation as opposed to invagination (Haddon and Lewis, 1996), it appears that the pattern of the medial wall of the OV being defined first is the same.

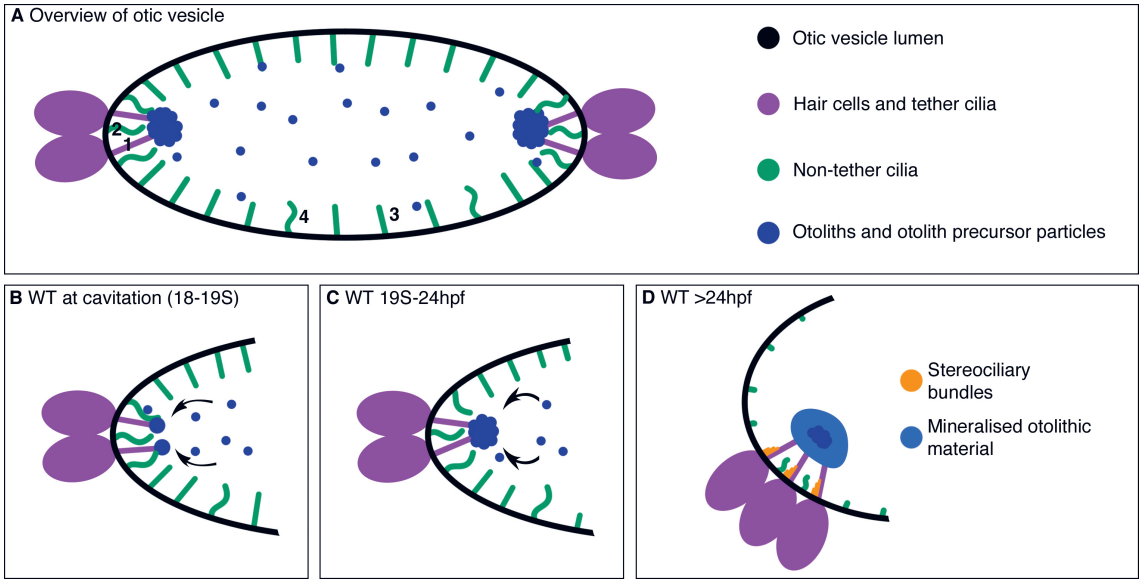

Figure 3.5: Model for otolith nucleation and tethering in the wild-type zebrafish otic vesicle. A. Cartoon overview of the OV between 19 and 24 hpf. At least three classes of cilia are present: tether cilia (1), motile cilia at the poles (2) and non-polar cilia lining the rest of the OV lumen (3), some of which are motile (4). **B-D**. Stage series showing proposed mechanism of otolith nucleation in wild-type embryos.

This study of otic cilia and ciliary motility has led to a new model of the role of cilia in otolith formation (Figure 3.5). I have found that there are at least three, possibly four, classes of cilia in the OV. The tether cilia, kinocilia of the first forming hair cells, are capable of binding otolith precursor particles and are immotile. Near these kinocilia are motile cilia; their proposed function is to produce fluid flow that helps to give the developing otolith its 'mushroom cap' shape (Wu et al., 2011). In Chapter 4 the function of motile cilia is investigated further by studying an immotile cilia mutant, *lrrc50* (Section 4.2.5). In addition to the motile cilia at the poles and near the forming otoliths, isolated motile cilia are present on the medial wall of the OV. These motile cilia do not appear to generate a directional flow of fluid within the OV as they are too few and too far apart. Riley et al.

(1997) reported Brownian motion of otolith precursor particles away from the poles of the OV, this has been confirmed more recently by Wu et al. (2011). I propose the function of the isolated motile cilia on the medial wall of the OV to be to prevent ectopic aggregation of the dense and sticky otolith precursor particles away from the kinocilia. Such ectopic aggregation would form a third, untethered otolith (see Chapter 4, Sections 4.2.1 to 4.2.5 for examples of this). It is unclear if these non-polar motile cilia on the medial wall of the OV belong to the same class of cilia as polar motile cilia, or are a cilia class of their own. Further research is required to investigate gene expression and signaling pathways required for specification of both motile cilia types. The vast majority of OV cilia are immotile; 92–98% of OV cilia are immotile if data from confocal microscopy of fixed specimens and *in vivo* videomicroscopy are combined. These immotile cilia are likely to have a sensory or signalling function, Chapter 5 describes the affect of ciliary disruption on ear morphogenesis and patterning.

Occasionally cilia were seen that stopped, started, or changed direction during video recording. I was unable to track cilia in a single OV for a long period of time using high-speed videomicroscopy due to the large file sizes generated. Also, the mounting technique used meant that embryos would asphyxiate if left mounted for too long, making use of a long term time-lapse strategy difficult. The possibility that cilia may be transiently motile and able to turn motility off and on is intriguing, and the cellular pathways that could regulate such activity even more so. Cilia are capable of changing motility in response to the environment: in animals that use cilia for locomotion these cilia respond to changes in the environment, allowing the animal to steer towards attractive stimuli or away from repulsive stimuli. For example, larvae of the marine annelid *Platynereis dumerilii* display phototaxis; two eyespots sense light, and alter the beat frequency of nearby motile cilia to change the swimming direction of the larva, bringing it towards the light source. This change in ciliary motility depends on acetylcholine-mediated neurotransmission to the larva's ciliated cells from neurons associated with the photosensitive eyespots of the larva (Jékely et al., 2008). Vertebrate motile cilia have also been shown to change beat frequency in response to stimuli. Tracheal cilia adapt their beat frequency in response to mechanical and nervous stimuli (Satir and Sleigh, 1990).

The rotary motion of the motile cilia in the OV is reminiscent of the way that motile cilia in the embryonic mouse node rotate. Mouse nodal cilia, unusually for motile cilia, have a 9+0 microtubule axoneme (Nonaka et al., 1998), though cilia in Kupffer's vesicle, the equivalent laterality organ of the zebrafish, have a 9+2 microtubule axoneme (Kramer-Zucker et al., 2005). The motile ependymal cilia of the zebrafish floor plate have a 9+0 axoneme, and also appear to rotate as opposed to beat (Kramer-Zucker et al., 2005). Zebrafish nodal and floor-plate cells are, like the cells lining the OV lumen, monociliated (Kramer-Zucker et al., 2005). These similarities suggest that OV motile cilia may have either a motile 9+2 or 9+0 microtubule axoneme. Unfortunately, we have so far been unable to visualise axoneme structure within the OV using electron microscopy. However,

a recent study undertook TEM on the supernumerary immotile kinocilia of the zebrafish *mindbomb* mutant (see Sections 1.3.4 and 4.2.7 for details of the *mindbomb* mutant phenotype) to confirm that zebrafish kinocilia have a 9+2 axoneme (Yu et al., 2011), as had been found for Burbot kinocilia (Flock and Duvall, 1965).

The significant difference in motile cilia number in the OVs of embryos of wild-type strains AB and LWT is interesting and suggests that though motile cilia are required in the OV, there is not a great selective pressure on the exact number of motile cilia present in the OV in evolutionary terms. There may be an optimum range for number of motile cilia in the OV. Too few motile cilia and otoliths would not form in the correct shape (Wu et al., 2011) and ectopic untethered otoliths may form (Sections 4.2.1 to 4.2.5). Too many motile cilia and otolith precursor particles may have difficulty tethering at the correct points in the OV. When *foxj1b*, a transcription factor required for differentiation of motile cilia (Yu et al., 2008), is over-expressed in *Tg(Hs::foxj1b)* embryos, ectopic motile cilia form in the OV; irregularly shaped otoliths form and aggregations of otolith precursor particles are seen (Yu et al., 2011). Although the total number of OV cilia between individual embryos was highly variable (Figure 3.1C), there was no significant difference in the total number of OV cilia between the AB and LWT wild-type strains (Figure 3.1D).

After describing the cilia in the OV of wild-type embryos, and confirming that the otolith is tethered by immotile kinocilia on the first forming hair cells, the next logical step was to investigate mechanisms of otolith tethering in more detail. Chapter 4 describes the roles of cilia, ciliary motility, hair cells and embryonic movement in otolith development.

Chapter 4

Mechanisms of Otolith Tethering in the Zebrafish Embryo

4.1 Introduction

The developing otolith is tethered by the kinocilia of the first hair cells, also known as the tether cilia (Riley et al., 1997; Tanimoto et al., 2011) (see Chapter 3). If development of the first hair cells is prevented, by injection of a morpholino against the *atoh1b* transcription factor, otoliths fail to tether and a single untethered otolith is formed (Millimaki et al., 2007). These first hair cells are hypothesised to produce an uncharacterised 'otolith precursor binding factor' required for tethering otolith precursor particles (Riley et al., 1997; Millimaki et al., 2007; Yu et al., 2011). The single otolith formed by *atoh1b*MO injection is eventually tethered by hair cells that develop in a later, *atoh1a* dependent wave (Millimaki et al., 2007).

It is also known that cilia mutants have defects in otolith formation. This has been directly addressed in some studies, where zebrafish mutants with defects in cilia motility were reported to form abnormal and ectopic otoliths. For example, injection of a morpholino against *gas8*, a component of the dynein regulatory complex, leads to defects in otolith shape and number due to disruption of ciliary motility (Colantonio et al., 2009). Similar otolith defects are seen if a morpholino against *foxj1b*, a forkhead box transcription factor required for motile ciliogenesis, is injected into zebafish embryos (Yu et al., 2011). Other studies have reported otolith defects in zebrafish cilia mutants, even though otolith formation was not the focus of the study (Panizzi et al., 2007; Neugebauer et al., 2009; Serluca et al., 2009; Wilkinson et al., 2009; Gao et al., 2010).

The kinocilia of the first hair cells is where the otolith precursor particles normally tether, and thus it is proposed any otolith precursor binding factor must normally localize to these tether cilia (Riley et al., 1997; Yu et al., 2011) (Chapter 3).

In this chapter the roles of hair cells and cilia in tethering the otoliths are investigated in more detail. The role of cilia is investigated by looking at a phenotypic series of cilia

mutants. These are: a mutant that completely lacks cilia, MZ*ovl* (maternal-zygotic *ovl* mutant) (Huang and Schier, 2009); two alleles of a mutant with a reduced number of cilia, igu^{ts294e} and igu^{tm79a} (Brand et al., 1996; Sekimizu et al., 2004; Wolff et al., 2004); a mutant that initially forms cilia which are then lost by 3dpf, *ovl* (here referred to as Z*ovl*, specifying zygotic *ovl* mutation) (Tsujikawa and Malicki, 2004); and a mutant that lacks ciliary motility, *lrrc50* (van Rooijen et al., 2008) (see Table 2.1 for details of mutant lines).

The role of hair cells was investigated by looking at a mutant with ectopic hair cell formation, *mib* (Table 2.1) (Jiang et al., 1996; Haddon et al., 1998; Itoh et al., 2003), and by preventing formation of the first hair cells that normally tether the otolith by injecting *atoh1b* morpholino (Millimaki et al., 2007) (see Section 2.6 for details of morpholinos used).

The role of hair cells in the absence of cilia was investigated by producing supernumerary hair cells in an MZ*ovl* mutant using the *Su(H)1+2* morpholino (Sieger et al., 2003; Echeverri and Oates, 2007), and by preventing formation of the first hair cells in MZ*ovl* by injecting *atoh1b* morpholino (morpholino injections into MZ*ovl* were undertaken by Peng Huang).

Otolith precursor particles are denser than the surrounding OV fluid and will aggregate if trapped in one part of the OV lumen by laser tweezers (Riley et al., 1997). It was possible that movement of the zebrafish embryo, thereby changing the orientation of the OV with respect to gravity, may be involved in otolith formation. The role of embryonic movement in otolith formation was investigated by Riley et al. (1997). Riley and colleagues found that immobilising wild-type embryos in either a head-up or head-down orientation had no effect on otolith formation. However, immobilising *monolith* mutant embryos, which only form one otolith, could bias which end of the OV the single otolith formed at. The mutation causing the phenotype of *monolith* mutants is currently uncloned. Kate Hammond observed that the paralysed mutant, *sloth* (*hsp90aa1.1*, Table 2.1), had a higher occurrence of otolith abnormalities than wild-type embryos (K. Hammond, unpublished observations). This suggested that perhaps movement did play a role in normal embryonic otolith formation, and is investigated in Section 4.2.11.

In this chapter I confirm the importance for cilia in otolith tethering, and present evidence that hair cells are absolutely essential for tethering the otolith, whereas otoliths can still tether in the absence of cilia. I also demonstrate that movement of the embryo during development plays a minor role in otolith formation.

4.2 Results

4.2.1 The effect of a complete loss of cilia (MZ*ovl*) on otolith formation

The maternal zygotic *ovl* (MZ*ovl*, a mutation in *ift88*, see Section 1.2.3) mutant completely lacks cilia in all tissues (Huang and Schier, 2009), including the otic vesicle (Figure 4.1B (compare with the M*ovl* ear in Figure 4.1A), and Huang and Schier (2009) Figure 1N).

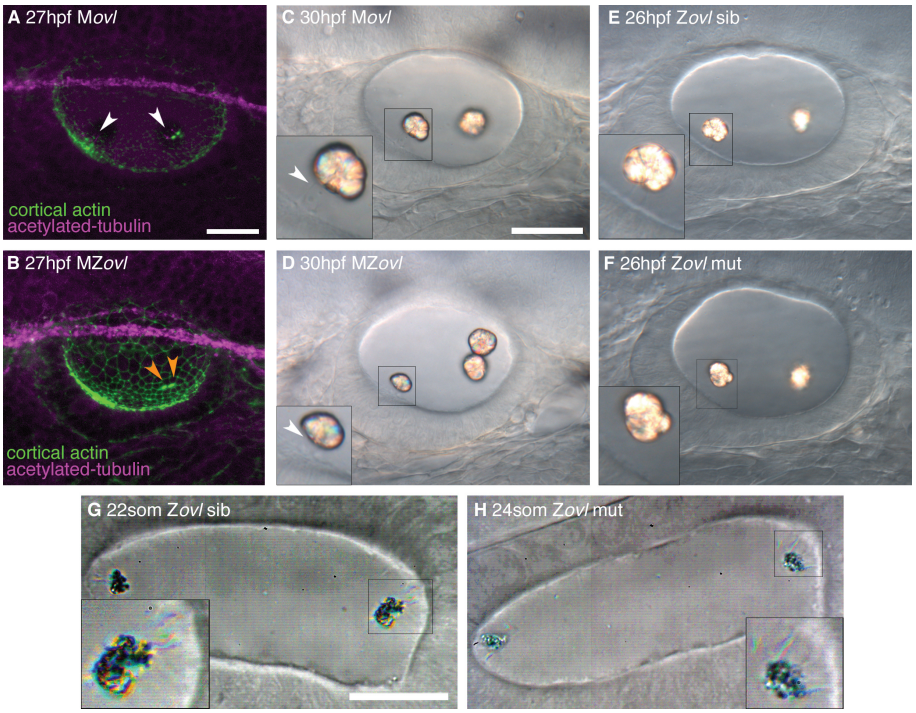

Figure 4.1: Formation of otoliths in the absence of cilia (*ovl*). A. Confocal projection of 27hpf M*ovl* ear stained with anti-acetylated tubulin antibody and FITC-phalloidin. Tether cilia are indicated by white arrowheads. Scale bar: 25μm, applies to A, B. **B**. Confocal projection of 27hpf MZ*ovl* ear; tether cilia are absent, but the stereociliary bundles still form (orange arrowheads). **C**. DIC image of 30hpf M*ovl* ear; inset shows anterior otolith on tether cilia (arrowhead). Scale bar: 30μm, applies to C–F. **D**. DIC image of 30hpf MZ*ovl* ear; imperfect otoliths form tethered in the correct location. Inset shows anterior otolith tethered directly to stereociliary bundles (arrowhead). **E**. DIC image of 26hpf Z*ovl* sibling ear; inset shows anterior otolith on tether cilia. **F**. DIC image of 26hpf Z*ovl* mutant embryo. Inset shows abnormally shaped otolith on tether cilia. **G**. Time-to colour merge of 22S Z*ovl* sibling ear; inset shows motile cilia near the anterior otolith (coloured). Scale bar: 20μm, applies to I, J. Movie 12. **H**. Time-to-colour merge of 24S Z*ovl* mutant; inset shows that motile cilia and tether cilia are still present in the mutant ear, due to maternal provision of *ift88* transcripts. Movie 13.

To our surprise, the MZ*ovl* mutant was still capable of tethering otoliths in the correct positions within the otic vesicle, above the anterior and posterior maculae (Figure 4.1D). However, otolith formation in these mutants is an imperfect process, as with the other cilia mutants studied. Only 14% of ears scored had a normal otolith phenotype; the majority (69%) of ears had a single anterior otolith and a posterior otolith consisting of a fusion of two otoliths (Figure 4.1D, Figure 4.2A).

Examination of MZ*ovl* mutant OVs revealed that otolithic material was tethering directly to the apical surface, and later the stereociliary bundles, of the first hair cells (Figure 4.1D, also see Figure 4.10B for a younger MZ*ovl* OV). This suggests that the otolith precursor binding factor, predicted to be normally localised to the tips of the tether cilia on the first hair cells, is localised to the apical surface of the hair cells in the absence of cilia.

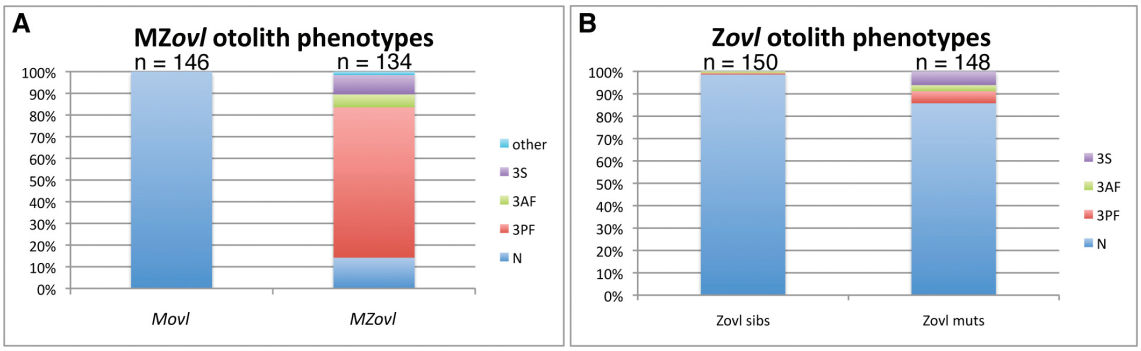

Figure 4.2: Otolith defects in embryos lacking cilia A. Graph of otolith defects in MZ*ovl* embryos. N, normal ear phenotype (two otoliths in correct positions); 3PF, three otoliths, with the two posterior otoliths fused; 3AF, three otoliths, with the two anterior otoliths fused; 3S, three separate otoliths, with one untethered otolith; other, other otolith defects. Scoring of M*ovl* and MZ*ovl* embryos kindly undertaken by Peng Huang. **B**. Graph of otolith defects in Z*ovl* embryos.

4.2.2 The effect of a zygotic loss of *ift88* on otolith formation (Z*ovl*)

The zygotic *ovl* mutant (Z*ovl*) (Tsujikawa and Malicki, 2004) is capable of producing cilia in the OV before 24hpf due to provision of maternal *ift88* mRNA transcripts (Tsujikawa and Malicki, 2004; Huang and Schier, 2009). Z*ovl* mutants were much less severely affected than MZ*ovl* mutants. Kinocilia were present on the first hair cells, allowing otolith tethering to take place as normal (Figure 4.1F). However, otoliths are sometimes abnormally shaped, without the flat bottom seen by 24hpf in wild-types. When Z*ovl* otolith phenotypes were scored at 30–32hpf, most (86%) Z*ovl* ears had normal otolith positioning with one anterior and one posterior otolith (Figure 4.2B).

High-speed videomicroscopy of Z*ovl* sibling and mutant embryos before 24hpf revealed that it was not possible to identify the genotype of the Z*ovl* mutants based upon the appearance of the cilia in the OV. Z*ovl* sibling embryos were from the same batch as Z*ovl* mutant embryos and may have had either a wild-type or heterozygous mutant *ovl* genotype. As the *ovl* mutation is recessive there is no phenotypic difference between wild-type and heterozygous *ovl* genotypes. Maternal contribution of *ift88* mRNA in Z*ovl* mutants was sufficient to produce tether cilia, motile cilia and immotile cilia in the OV, and these were indistinguishable between all embryos in a batch (Figure 4.1G, H, Movies 12, 13). Embryos were phenotyped by dismounting and growing on after the videomicroscopy for 1 day. At this stage a curly-down tail phenotype, typical of the majority of cilia mutant lines (Supatto and Vermot, 2011), was easily observed in Z*ovl* mutants. My observation of cilia in the Z*ovl* mutant OV before 24hpf corroborates Tsujikawa and Malicki's observation that cilia are present in Z*ovl* mutant OVs at 40hpf (Tsujikawa and Malicki, 2004).

4.2.3 The effect of a partial loss of cilia (*iguana*) on otolith formation

The *iguana* (*dzip1*) (Table 2.1) mutant was studied to assess the effect of a partial loss of cilia on otolith formation. Two alleles of the *igu* mutation were available: igu^{ts294e} and

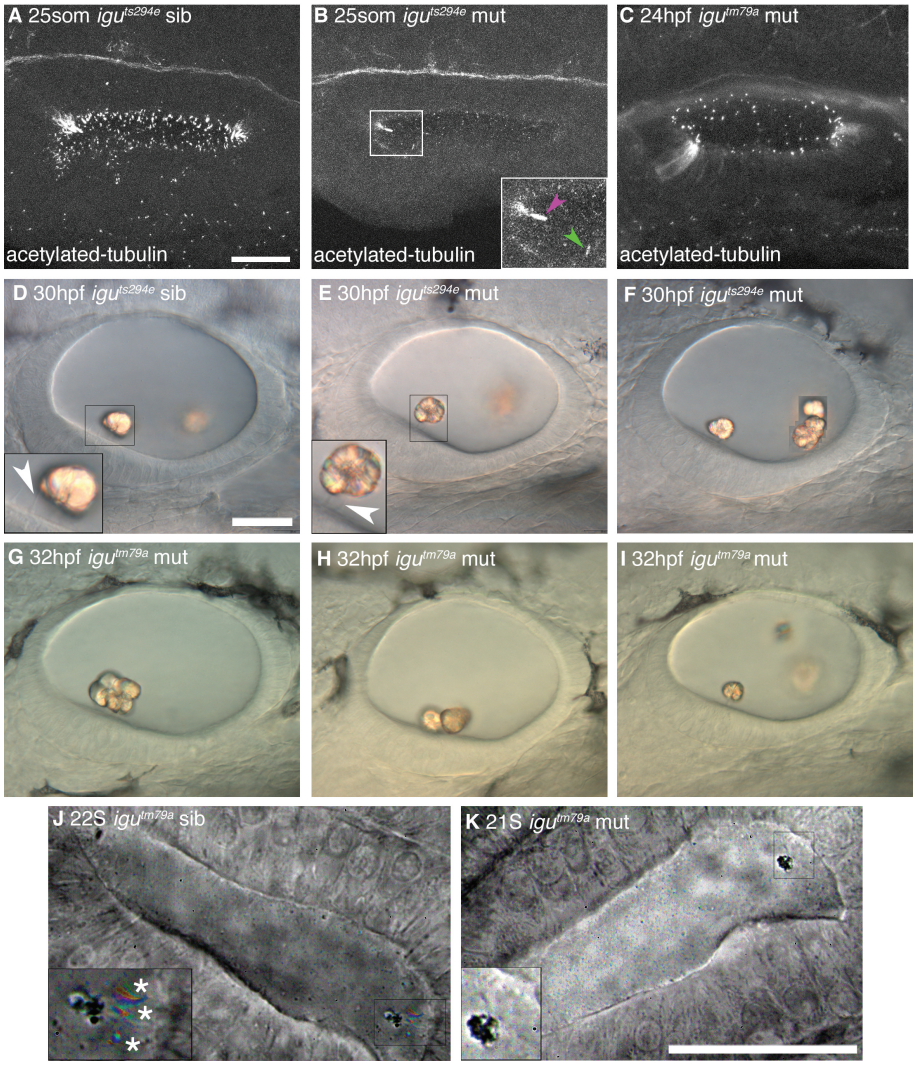

Figure 4.3: Formation of otoliths in embryos lacking cilia (*iguana*). A. Confocal projection of 25S stage igu^{ts294e} sibling embryo stained with anti-acetylated tubulin antibody. Dorsal view with anterior to left. Scale bar: 25μm, applies to A–C. **B**. Confocal projection of 25S igu^{ts294e} mutant embryo stained with anti-acetylated tubulin antibody. Dorsal view. Inset shows the presence of both an anterior tether cilium (magenta arrowhead) and non-tether cilium (green arrowhead). **C**. Confocal projection of 24hpf igu^{tm79a} mutant embryo stained with anti-acetylated tubulin antibody. Lateral view. **D**. DIC image of 30hpf igu^{ts294e} sibling embryo; inset shows anterior otolith on tether cilia (arrowhead). Scale bar: 20μm, applies to E–I. **E**. DIC image of 30hpf igu^{ts294e} mutant embryos with a normal otolith phenotype, inset shows anterior otolith on tether cilia (arrowhead). **F**. DIC image of 30hpf igu^{ts294e} mutant OV with a 3PF otolith phenotype. Posterior otoliths have been pasted in from an image of a different focal plane so that they appear in focus. **G**. DIC image of 32hpf igu^{tm79a} mutant OV with a 1A otolith phenotype. **H**. DIC image of a 32hpf igu^{tm79a} mutant OV with a 1 fused anterior otolith phenotype; the fused otolith is bound directly to the apical surface of the hair cells. **I**. DIC image of a 32hpf igu^{tm79a} mutant OV with 3 separate otoliths. **J**. Time-to-colour merge of 22S igu^{tm79a} sibling; inset shows three motile cilia near the otolith (asterisks). Movie 14. **K**. Time-to-colour merge of 21S igu^{tm79a} mutant embryo OV with no cilia visible; inset shows anterior otolith with no movement apparent. Movie 15. Scale bar: 40μm, applies to J, K.

igu^{tm79a}. The *igu*^{ts294e} mutants had strikingly fewer cilia present in the otic vesicle than *igu*^{tm79a} mutants, which in turn had fewer OV cilia than phenotypically wild-type siblings (Figure 4.3A–C) (Huang and Schier, 2009). Both alleles are characterized by nonsense mutations resulting in a premature stop codon and forming truncated *dzip1* protein products. *dzip1* encodes a protein 876 amino acids long. The *igu*^{ts294e} mutant allele is the stronger than *igu*^{tm79a}, with a point mutation causing a stop codon at amino acid 371. The *igu*^{tm79a} mutant allele has a point mutation causing a premature stop codon at amino acid 454 (Sekimizu et al., 2004; Wolff et al., 2004). Both of these zebrafish mutant alleles include the N-terminal dzip1-like domain, which shows 51% identity with the dzip1-like domain in human *DZIP1*. Both alleles are lacking C-terminal coiled-coil/PEST domains. The PEST domains may serve as a signal for rapid protein turnover (Sekimizu et al., 2004); however, their function is not known. It is not clear as to why the two mutant alleles vary so much in their ability to form cilia. The extra amino acids coded for in *igu*^{tm79a} *dzip1* may give the truncated Dzip1 protein an increased functionality. Alternatively, the longer *dzip1* coding sequence in *igu*^{tm79a} may be less affected by nonsense-mediated mRNA decay than the shorter *igu*^{ts294e} coding sequence. There is also the possibility that differences in wild-type background between the two alleles could play a role. Difference in wild-type background could also explain the difference between my observation of *igu*^{ts294e}, which I have found capable of forming a small number of cilia, and the report by Yu and colleagues that *igu*^{ts294e} completely lacks cilia (Yu et al., 2011).

The number of cilia at the anterior and posterior poles of 26hpf *igu*^{tm79a} mutant embryos was significantly lower in both the anterior and posterior maculae when compared to both *igu*^{tm79a} sibling embryos and wild-type (AB strain) embryos (Figure 4.4A).

Otolith formation did occur in both *igu* mutant alleles, but was disrupted, as in MZ*ovl* and Z*ovl* mutant embryos. A significant proportion of *igu* mutant ears developed with a normal otolith phenotype at 30–32hpf: 27% of *igu*^{ts294e} mutant embryos and 58% of *igu*^{tm79a} mutant embryos (Figure 4.4B, C). Though many *igu* mutants had a normal otolith phenotype, there was also a large range of abnormal otolith phenotypes, detailed in Figure 4.3D–I. High-speed videomicroscopy of *igu*^{tm79a} mutant embryos also showed a paucity of cilia compared to phenotypically wild-type sibling embryos (Figure 4.3J and K, Movies 14 and 15).

Studying the MZ*ovl*, *igu*^{ts294e} and *igu*^{tm79a} mutants provided a spectrum of cilia loss. The more cilia that were missing, the greater the proportion of ears with abnormal otoliths at 30–32hpf (Figures 4.2A and 4.4B, C). MZ*ovl* mutants with no cilia had the greatest proportion of ears with abnormal otoliths (86%). The stronger *igu*^{ts294e} allele with only some kinocilia and a few non-tether cilia (Figure 4.3 B) had the next greatest proportion of ears with abnormal otoliths (73%), while the weaker *igu*^{tm79a} mutant allele had only 42% of ears with abnormal otoliths. Z*ovl* mutants had the mildest otolith phenotype with 86% of ears forming normal otoliths. It has been reported that the number and morphology of fixed cilia in Z*ovl* mutant OVs is normal at 40hpf (Tsujikawa and Malicki, 2004). I

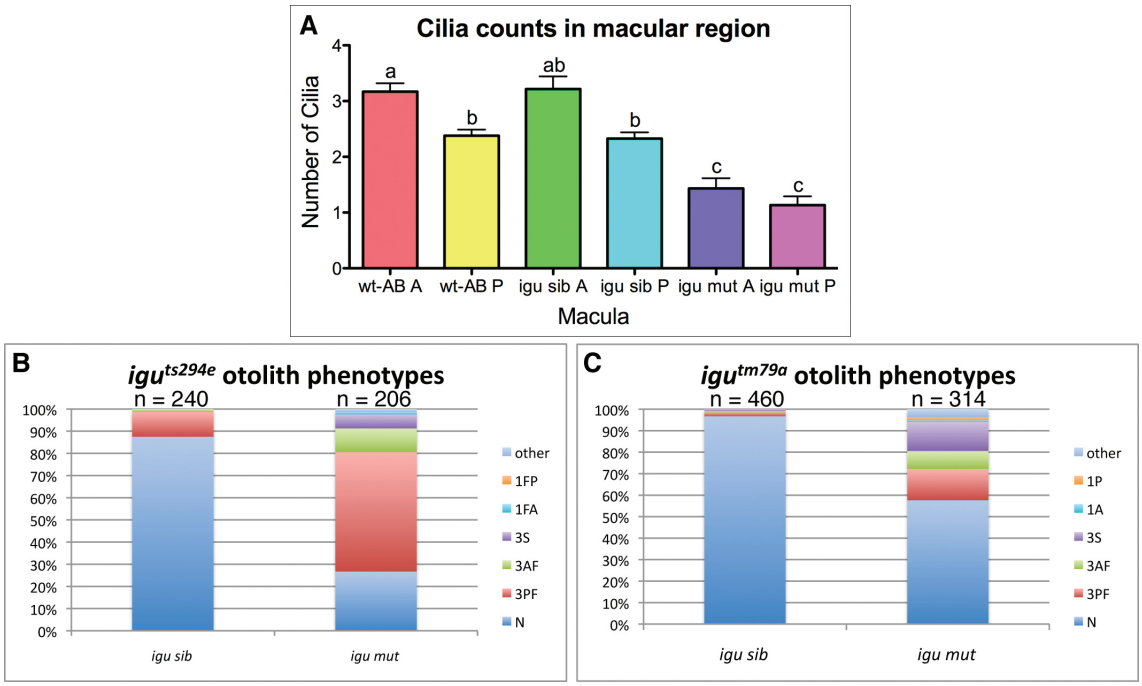

Figure 4.4: Cilia and otolith defects in embryos lacking cilia (*iguana*). A. Statistical analysis of the number of tether cilia in the anterior and posterior maculae of 26hpf wild-type (AB), igu^{tm79a} siblings and igu^{tm79a} mutant embryos. The median number of cilia in each sensory patch differs significantly (Kruskal-Wallis test, H=87.20, df=5, p<0.0001; bars labelled with the same letter do not have significantly different medians (Dunn's Multiple Comparison Test)). igu^{tm79a} mutant embryos have significantly fewer tether cilia in their maculae than siblings or wild-types, but do not lack cilia altogether. **B**. Graph of otolith defects in igu^{ts294e}. Phenotype labels as for Figure 4.2, with addition of 1FA, 1 fused anterior otolith; 1FP, 1fused posterior otolith. **C**. Graph of otolith defects in igu^{tm79a}.

observed tether cilia, motile cilia and non-motile cilia in 20-22hpf Z*ovl* mutant OVs using high-speed videomicroscopy (Figure 4.1H, Movie 13). Therefore as the cilia defect appears mild in Z*ovl* mutants before 3dpf (at 3dpf sensory cilia are lost (Tsujikawa and Malicki, 2004)) it is logical that these mutants should have the least severe defect in the initial stages of otolith formation.

4.2.4 Otolith defects in embryos lacking cilia are unlikely to be due to misexpression of genes required for otolith formation

To confirm that otolith defects seen in the mutants lacking cilia (MZ*ovl* and *igu*) were not due to misexpression of genes required for otolith formation (potentially caused by aberrant developmental signalling due to the lack of cilia) *in situ* hybridisations were done to look for expression of two otolith components: *starmaker* (*stm*) (Söllner et al., 2003) and *otolith matrix protein* (*otomp*) (Murayama et al., 2005) (see Table 1.1, page 26, for details of *stm* and *otomp* function). I found that despite the lack of cilia in MZ*ovl* and *igu* mutant embryos, these genes required for otolith formation were expressed normally (Figure 4.5).

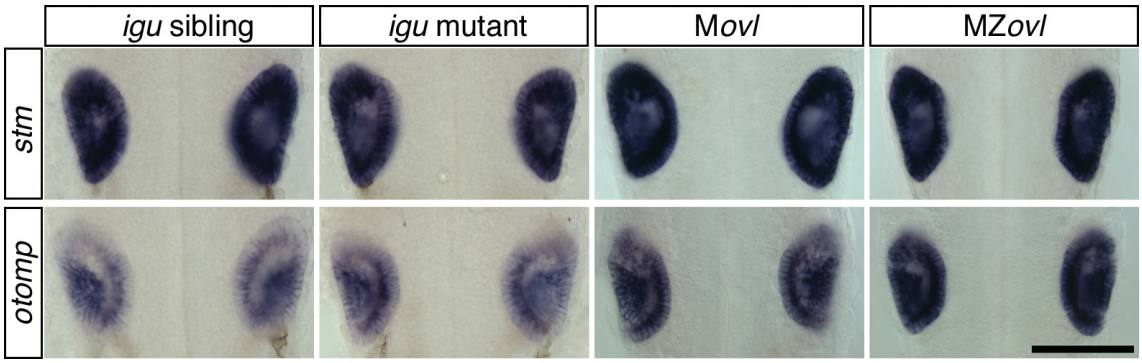

Figure 4.5: Expression of genes required for otolith development is not affected in cilia mutants. There was no difference in expression of *stm* and *otomp* between igu^{tm79a} mutants and siblings and MZ*ovl* and sibling M*ovl* embryos at 26hpf. Dorsal views with anterior to top, both OVs are pictured in each panel. Scale bar: 100μm. *In situ* RNA probes for *stm* and *otomp* were a gift from Leila Abbas.

4.2.5 The effect of a loss of ciliary motility (*lrrc50*) on otolith formation

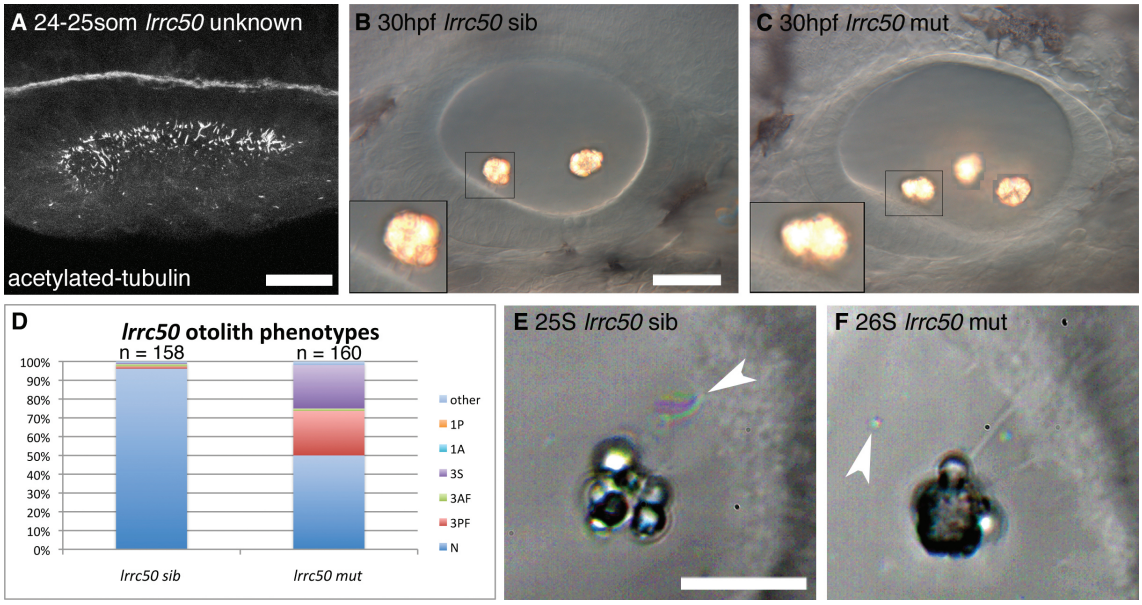

Figure 4.6: Formation of otoliths in embryos lacking ciliary motility (*lrrc50*). A. Confocal projection of 24–25S stage *lrrc50* embryo OV. It was not possible to distinguish *lrrc50* mutant from sibling embryos in fixed specimens stained with anti-acetylated tubulin antibody. Dorsal view with anterior to left. Scale bar: 25μm. **B**. DIC image of 30hpf *lrrc50* sibling OV. Posterior otolith has been pasted in from a different focal plane. Inset shows anterior otolith bound to tether cilia. Scale bar: 20μm, applies to B, C. **C**. DIC image of 30hpf *lrrc50* mutant OV with three otoliths; anterior, posterior and one untethered. The two most posterior otoliths have been pasted in from a different focal plane. Inset shows anterior otolith. **D**. Graph of *lrrc50* otolith phenotypes. **E**. Time-to-colour merge of 25S *lrrc50* sibling; a motile cilium is present near the anterior otolith (arrowhead). Movie 16. Scale bar: 10μm, applies to E, F. **F**. Time-to-colour merge of 25S *lrrc50* mutant; the only motile objects in the OV are otolith precursor particles (arrowhead). Movie 17.

The *lrrc50* (*dnaaf1*) mutant line (Sullivan-Brown et al., 2008; van Rooijen et al., 2008) (see Table 2.1 for further information) was used to investigate the effect of losing ciliary

motility on otolith formation. The cilia in fixed *lrrc50* mutant embryos stained with anti-acetylated tubulin antibody looked no different to phenotypically wild-type sibling OV cilia. It was not possible to determine mutant from sibling embryos by the morphology of fixed otic vesicle cilia at 24–25S (Figure 4.6A).

Otoliths of *lrrc50* mutant embryos still formed bound to the tether cilia of the anterior and posterior poles (Figure 4.6C). However, a large proportion (50%) of ears developed an ectopic otolith. Most commonly this third otolith would remain untethered in the OV or fuse to the tethered posterior otolith (Figure 4.6D).

Lack of ciliary motility in *lrrc50* mutant embryo OVs was confirmed by high-speed videomicroscopy (Figure 4.6E–F, Movies 16 and 17). Although no cilia were motile, otolith precursor particles still moved due to Brownian motion (arrowhead, Figure 4.6F).

Fluid flow caused by motile cilia is therefore likely to be involved in normal otolith formation. *dnaaf1* is not thought to have any function beyond its requirement for motile ciliogenesis and is expressed in all tissues with motile cilia, not just the OV (Sullivan-Brown et al., 2008; van Rooijen et al., 2008).

4.2.6 The effects of otolith tethering and ciliary flow on the visible length of kinocilia

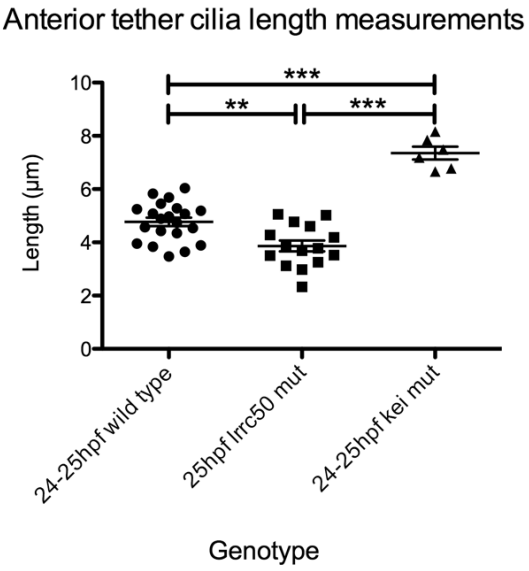

Figure 4.7: Anterior tether cilia visible length varies between wild-type, *lrrc50* mutants and *kei* mutants. The measurable length of the anterior tether cilia in *kei* mutants was significantly longer than in wild-type embryos and *lrrc50* mutants ($p<0.001$). *lrrc50* mutant cilia were significantly shorter than wild type cilia ($p<0.01$). (One-way ANOVA; $F=48.28$, d.f.=2,39, bars show mean ± s.e.m.). The visible length of the cilia was measured, so *kei* cilia may appear longer as the ciliary tip is not buried within the otolith.

The length of the anterior tether cilia (kinocilia) between the apical hair cell surface and the outside of the otolith was measured from high-speed movie stills of 24–25hpf wild-

type, *lrrc50* mutant and *kei* mutant embryos (see Section 3.2.3 for more information on *kei* mutant embryos). A graph comparing kinocilia lengths between mutants and wild-types is shown in Figure 4.7.

The visible length of kinocilia in *lrrc50* mutant embryos was significantly shorter than in wild-type embryos. This supports published data that ciliary flow normally shapes the otolith, giving it a flat bottom and preventing mineralisation close to the hair cell surface (Wu et al., 2011); in this study ciliary flow was disrupted by laser ablation of ciliary motility, as a result otoliths were seen to develop a more rounded shape, mineralising closer to the hair cell surface. I have observed that in *lrrc50* mutants, mineralisation also appears to occur closer to the hair cell surface, obscuring more of the ciliary axoneme and so making the visible ciliary length shorter. However, I did not make any measurements of otolithic shape or roundness.

There is a possibility that the visible length of kinocilia in *lrrc50* mutants could be shorter because the total kinocilia length is shorter, or that shorter kinociliary length is combined with mineralisation of the otolith closer to the hair cell surface in the absence of ciliary flow. I saw no obvious length difference in cilia between fixed *lrrc50* mutant and sibling embryos at 24–25S, and fixed OV cilia of these embryos appear wild-type (compare Figure 4.6A with Figure 3.1A). However shorter cilia in some tissues of *lrrc50* mutant embryos have been reported: van Rooijen et al. (2008) found that ciliary length was not strongly affected in the *lrrc50* mutant Kupffer's Vesicle, but that there was a significant reduction in the length of *lrrc50* mutant kinocilia in the 7dpf lateral line (van Rooijen et al., 2008). Sullivan-Brown et al. (2008) reported that *lrrc50* mutant embryos had cilia of normal length in the pronephric duct at 26–30hpf (Sullivan-Brown et al., 2008).

In *kei* mutant embryos the visible length of kinocilia was longer than in wild-type embryos (See Figure 3.4). This is unlikely to indicate a ciliary length defect; rather, it suggests that normally the tips of the kinocilia are buried in the forming otolith, and so are not visible. This has also been suggested by immunofluorescent stains on wild-type embryos for anti-acetylated tubulin antibody, marking the kinocilia, and anti-starmaker antibody, marking the otoliths (Yu et al., 2011).

4.2.7 The effect of ectopic hair cells and tether cilia on otolith tethering (*mindbomb*)

We looked at otolith formation in the *mindbomb* (*mib*) mutant embryo (Jiang et al., 1996) to determine the consequence of having ectopic hair cells (Haddon et al., 1998) on the first stages of otolith formation. The *mib* mutation occurs in the gene for an E3 ubiquitin ligase required for activity of the Notch-Delta signalling pathway (Itoh et al., 2003). In the *mib* mutant, failure in Notch-mediated lateral inhibition leads to the formation of ectopic hair cells in the OV (Haddon et al., 1998), including the formation of the first hair cells and their tether cilia (Haddon et al., 1998, 1999) (Figure 4.8B, D, E). We observed that all tether cilia, including supernumerary tether cilia, were capable of binding otolith

precursor particles (Figure 4.8F, See Movie 18).

High-speed videomicroscopy analysis also revealed that the cell type that produces motile cilia was not lost (Movie 18). As it has already been reported that *mib* mutant embryos lack supporting cells in the otic vesicle (Haddon et al., 1999), this observation suggests that either some supporting cells remain on the periphery of the sensory patch, or that motile cilia are not exclusively on supporting cells in the developing otic vesicle.

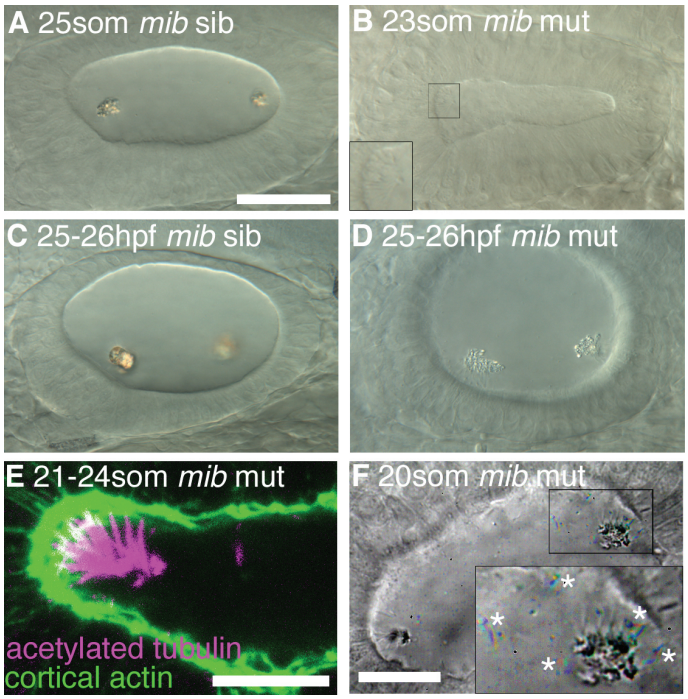

Figure 4.8: Formation of otoliths in the presence of ectopic hair cells and tether cilia (*mib*). A. DIC image of 25S *mib* sibling OV. Lateral view with anterior to left. Scale bar: 40μm, applies to A–D. **B**. DIC image of 23S *mib* mutant OV; inset shows ectopic anterior tether cilia. **C**. DIC image of 25–26hpf *mib* sibling OV. **D**. DIC image of 25–26hpf *mib* mutant OV. **E**. Confocal stack of 21–24S *mib* mutant stained with anti-acetylated tubulin antibody and FITC-phalloidin showing anterior tether cilia. Scale bar: 10μm. **F**. Time-to-colour merge of 20S *mib* mutant; all the ectopic tether cilia bind otolithic material, and motile cilia are still present (inset, asterisks). Dorsolateral view with anterior to right. Scale bar: 20μm. See Movie 18.

4.2.8 The effect of hair cell loss on otolith tethering (*atoh1b* morpholino injection)

As otoliths were always observed to tether to the cilia of the first hair cells, and not to cilia on other cell types, I tested whether otoliths would bind to an alternative site in the otic vesicle if the first hair cells were absent. Formation of the first hair cells was prevented by injection of a start-site specific morpholino (MO) against *atoh1b* (Millimaki et al., 2007). Morphant embryos failed to form the first hair cells; no anti-acetylated tubulin antibody stained hair cells or kinocilia could be seen in fixed embryos (Figure 4.9E, cf. Figure 3.1A), and hair cells with kinocilia were not observed during high-speed videomicroscopy (Fig-

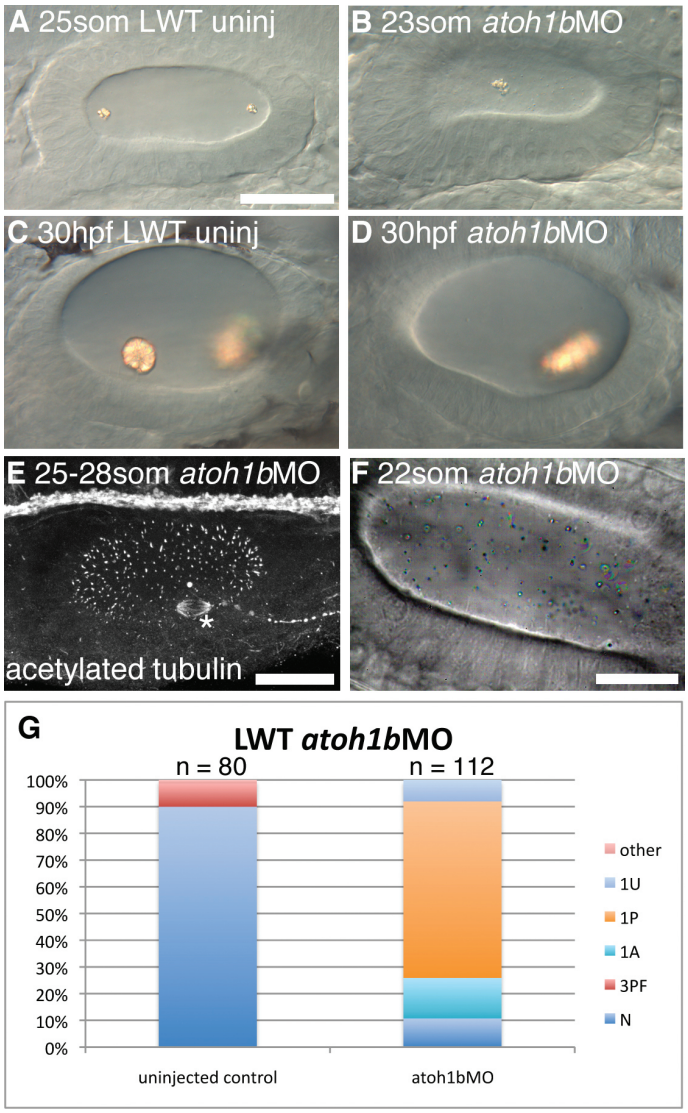

Figure 4.9: Otolith formation in the absence of hair cells (*atoh1b* morphants). A. DIC image of 25S wild-type (LWT strain) uninjected control embryo. Lateral view with anterior to left. Scale bar: 40μm, applies to A–D. **B**. DIC image of 23S wild-type (LWT strain) embryo injected with *atoh1b* morpholino. Hair cells and tether cilia are not formed and a single untethered otolith has formed in the OV. **C**. 30hpf LWT uninjected control embryo. **D**. 30hpf LWT injected with *atoh1b* morpholino; the single otolith has tethered to hair cell kinocilia that develop after initial otolith formation. **E**. Confocal projection of anti-acetylated tubulin antibody stained *atoh1b* morphant OV; hair cells and kinocilia are absent, but non-hair cell cilia are still present. The mitotic spindle of a dividing cell is present (asterisk). Scale bar: 25μm. (cf. Figure 3.1A). **F**. Time-to-colour merge of 22S *atoh1b* morphant OV; there is a build up of otolith precursor particles. Hair cells, tether cilia and otoliths are absent. Motile cilia are still present. Dorsolateral view with anterior to right. Scale bar: 20μm. See Movie 19. (cf. Figure 3.3D, Movie 4). **G**. Graph of otolith phenotypes seen in LWT *atoh1b*MO injected embryos. N = normal OV with 1 anterior and 1 posterior otolith; 3PF = 3 otoliths, posterior fused; 1A = 1 anterior otolith; 1P = 1 posterior otolith; 1U = 1 untethered otolith; other = other otolith defect.

ure 4.9F, cf. Figure 3.3D). Other aspects of ear development appeared to proceed normally; the OV still had an ovoid shape with anterior and posterior poles (Figure 4.9B), and non-

tether cilia were still present in the OV (Figure 4.9E). It has already been reported that *atoh1b*MO-injected embryos have no hair cells and have only formed a single untethered otolith at 24hpf (Millimaki et al., 2007).

I examined *atoh1b* morphant embryos using high-speed videomicroscopy before 24hpf to confirm that otolith precursor particles failed to tether anywhere within the otic vesicle before 24hpf. A build up of otolith precursor particles was observed before a single untethered otolith had formed, and both motile cilia and non-motile cilia were still present in the OV (Figure 4.9F, Movie 19).

By 24hpf, otolith precursor particles had aggregated into a single untethered otolith. Later in development a second wave of hair cell generation that is dependent on *atoh1a* expression takes place (Millimaki et al., 2007). The hair cells formed in this second wave were capable of tethering the already-formed otolith (Figure 4.9D). Normally the single otolith tethered to the hair cells of the posterior macula. In embryos scored at approximately 30hpf, 66% of ears had a single otolith tethered at the posterior macula; 15% had a single otolith tethered at the anterior macula; 8% had a single untethered otolith; and 11% had normal otoliths (most likely due to incorrect injection of *atoh1b* morpholino: tether cell loss was not confirmed in these embryos during the initial period of otolith nucleation at 19–21S) (Figure 4.9G). This presumably reflects an increased likelihood of the untethered otolith being in the posterior part in the ear when the hair cells of the second wave are forming. The bias in otolith position may be caused by the shape of the otic vesicle and movement of the embryo at this stage.

4.2.9 The effect of loss of cilia and gain of hair cells on otolith tethering (MZ*ovl* injected with *Su(H)1+2* morpholino)

In order to test the ability of supernumerary hair cells to tether otolith precursor particles to their apical surface in the absence of cilia, the *Su(H)1+2* morpholino was injected into MZ*ovl* embryos (experiment done by Peng Huang). The ectopic hair cells could all tether otolith precursor particles to their apical surface (Figure 4.10D).

4.2.10 The effect of loss of both cilia and hair cells on otolith tethering (MZ*ovl* injected with *atoh1b* morpholino)

To test if otolith formation in the absence of both cilia and hair cells was any different to otolith formation in the absence of hair cells only, *atoh1b*MO was injected into MZ*ovl* embryos (experiment done by Peng Huang). There was no difference in the formation of a single untethered otolith between M*ovl* *atoh1b* morphants and MZ*ovl* *atoh1b* morphants (Figure 4.10E, F), suggesting that fluid flow produced by cilia did not have an effect on the eventual aggregation of untethered otolith precursor particles. It was difficult to compare *atoh1b* morpholino-injected MZ*ovl* embryos with M*ovl* siblings as the morpholino also had non-specific effects that caused variable developmental delay. This means that loss of

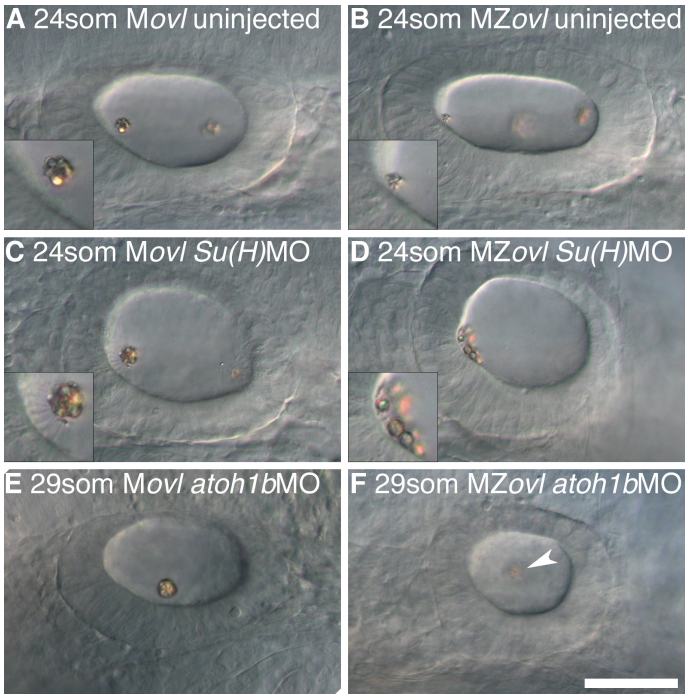

Figure 4.10: The effect of ectopic hair cells and hair cell absence in the absence of cilia. All panels show left ear with anterior to left. Data acquired by Peng Huang **A**. 24S uninjected M*ovl* OV; inset shows anterior otolith on tether cilia. **B**. 24S uninjected MZ*ovl* OV; inset shows small anterior otolith tethered to apical surface of hair cell membrane. **C**. 26S OV of M*ovl* embryo injected with *Su(H)*MO; inset shows otolith bound to several ectopic tether cilia. **D**. 24S OV of MZ*ovl* embryo injected with *Su(H)*MO; inset shows otolith precursor particles tethered to the apical surface of the ectopic hair cells. **E**. 29S OV of M*ovl* injected with *atoh1b*MO; one untethered otolith is present in the ear. **F**. 29S OV of MZ*ovl* embryo injected with *atoh1b*MO; one untethered otolith (out of focal plane) is present in the ear, arrowhead. Scale bar: 40μm; applies to all panels.

ciliary flow may have had an undetected effect on the timing of aggregation of the single untethered otolith in MZ*ovl atoh1b* morphants. However, no striking difference was seen in timing of otolith precursor aggregation between the two morphant genotypes, so it seems that presence/absence of ciliary flow does not have a major effect on aggregation of an untethered otolith.

4.2.11 The role of embryonic movement in otolith tethering

The hypothesis that orientation of the developing embryo may play a role in otolith formation was first proposed by Riley and colleagues (Riley et al., 1997). They investigated this by immobilising embryos either head up or head down in agarose prior to otolith formation and then scoring the phenotype 6 hours later. They reported that immobilising the embryo in either orientation had no effect on otolith formation in wild-type embryos. However, it could bias the position of formation of the single otolith in the *monolith* (*mnl*) mutant. The uncloned *mnl* mutation is a dominant semi-lethal mutation that is not fully penetrant; mutant embryos have abnormal otolith formation, typically only forming a posterior otolith (Riley and Grunwald, 1996). Formation of the posterior otolith in *mnl* does

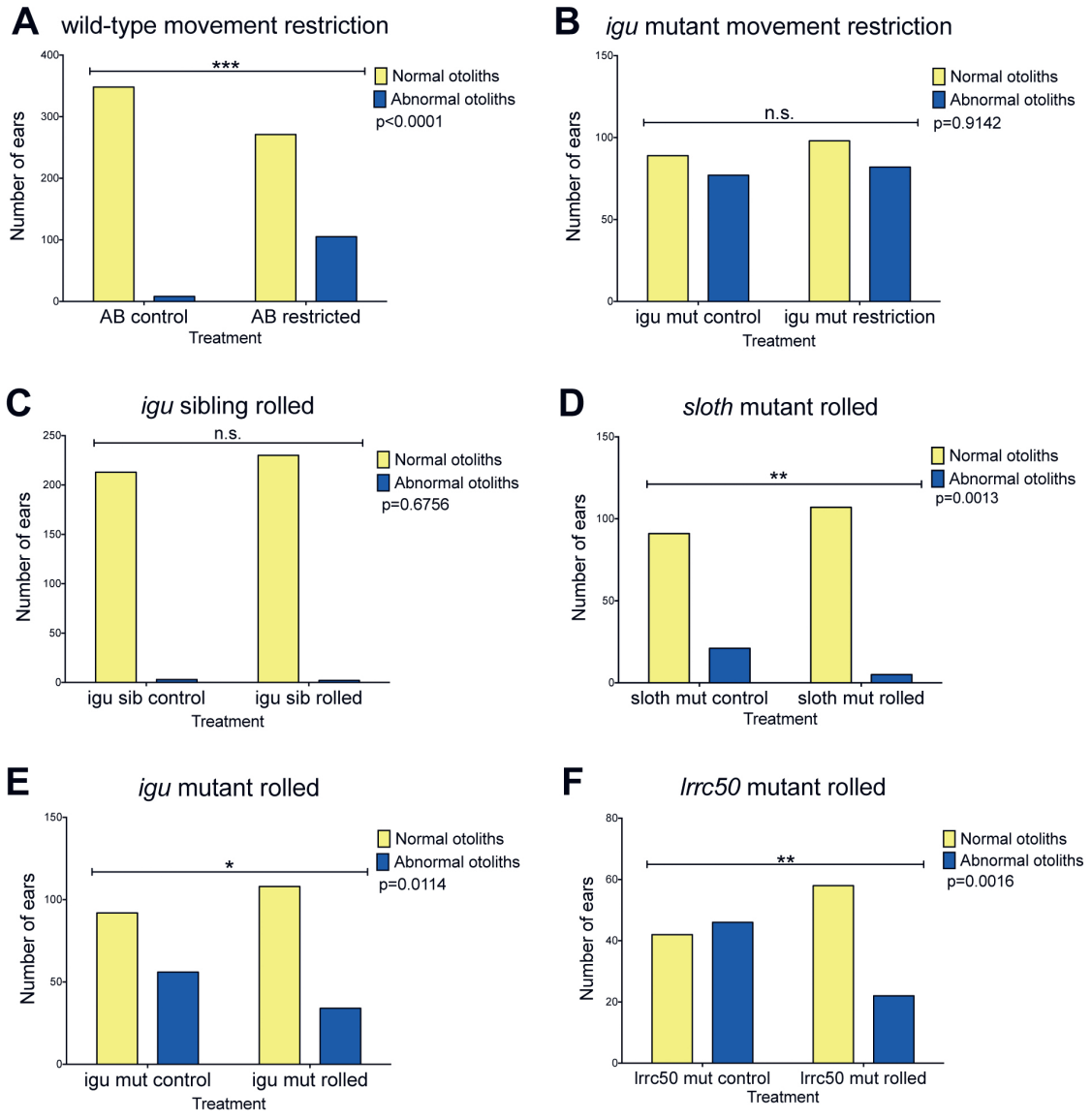

Figure 4.11: Embryonic movement contributes to correct otolith formation. A. Effect of restricting movement of wild-type embryos (strain AB) for 24h from the 15–18S stage. **B**. Restricting the movement of igu^{tm79a} embryos has no significant effect on otolith formation. **C**. Forced motion (rolling) of phenotypically wild-type igu^{tm79a} sibling embryos has no effect on otolith formation. **D-F**. Rolling *sloth*, igu^{tm79a} and *lrrc50* mutant embryos partially rescues their otolith defects. P values obtained by Fisher's exact test; n.s., not significant.

not commence at 18hpf, as in wild-type embryos, but instead does not start until approximately 22hpf (Riley et al., 1997). *mnl* mutants immobilised head-down had a significantly higher proportion of ears which formed anterior otoliths (Riley et al., 1997).

Kate Hammond noted that paralysed *sloth* (*hsp90aa1.1*) mutant embryos (See Table 2.1) have a higher proportion of ears with an abnormal otolith phenotype than wild-type embryos (unpublished observation). Zebrafish embryos that have ciliary defects nearly all have a 'curly-down' tail phenotype, which stops the embryos from moving normally.

Instead of swimming dorsal side uppermost, they pinwheel on the bottom of the petri dish with either the left or right side up. This fixed posture and abnormal movement may be a contributing factor in the formation of abnormal otoliths in the cilia mutants.

In order to investigate whether embryonic movement is required for normal otolith formation, AB strain wild-type embryos were dechorionated and had their movement restricted by being put into 3% methyl cellulose in the bottom of a petri dish at the 15–18 somite stage, before the onset of embryonic movement. The otolith phenotypes of ears were scored approximately 28 hours later. The proportion of ears with abnormal otoliths was significantly increased in the movement-restricted embryos when compared with controls left to develop as normal (Figure 4.11A) (28% of ears scored were abnormal, n=376 ears). The most common abnormal ear phenotype was due to the formation of a third otolith, which either remained untethered in the OV lumen or fused with either anterior or posterior otolith.

Restricting movement in igu^{tm79a} mutants in this way did not lead to a significant change in the proportion of ears with abnormal otoliths (Figure 4.11B). This may have been because the loss of cilia has a much greater effect to perturb otolith formation than the loss of embryonic movement, or because of the *igu* mutant embryos fail to move normally from 18–46hpf due to their curved body axis.

Attempts at restricting movement were also made by anaesthetising embryos in tricaine. Tricaine was added to the embryo medium before muscle twitching started at 18hpf and incubation was continued for 28 hours. Embryos that had been anaesthetised for this time showed a high level of apoptotic cells, identifiable by their rounded morphology, when examined with a compound microscope (data not shown). I decided that this was not a useful way to restrict embryonic movement as the high level of apoptosis may have had non-specific effects on otolith formation. Another method tried in order to immobilise embryos was to mount them in low-melting point agarose of concentrations between 0.5% and 1% for 24–28 hours. The immobilised embryos showed growth defects, particularly in the tail, but also had abnormal ear morphology. In an attempt to solve this problem embryos were mounted in agarose and then the tails were freed, leaving only the head embedded. However, in this case ear morphology was still noticeably affected (data not shown). I decided not to pursue agarose embedding as a method of preventing embryonic movement.

Aberrant otolith formation could be partially rescued by forcing motion in embryos. To force motion, embryos were grown in a 50ml tube on a roller-mixer at approximately 26.5°C from 2–3hpf until 30–32hpf. Embryos grown on the roller-mixer at 26.5°C developed at the same rate as embryos incubated in a petri dish at 28.5°C. This may have been due to better aeration of the growth medium on the roller-mixer. Forced motion had no effect on the proportion of ears with abnormal otoliths in phenotypically wild-type igu^{tm79a} sibling embryos (Figure 4.11C), or phenotypically wild-type *lrrc50* and *sloth* sibling embryos (data not shown). However, a significant partial rescue effect was seen in mutant *sloth*,

igu^{tm79a} and *lrrc50* embryos, where there was a significant decrease in the proportion of ears with abnormal otoliths (Figure 4.11D–F). The forced motion constantly changes the orientation of the otic vesicle with respect to gravity, which may prevent the dense otolith precursor particles from settling at the lowest point of the OV and aggregating to form an ectopic untethered otolith.

Forced motion was not a great enough intervention to rescue otolith defects fully in any of the mutant lines (though the proportion of abnormal ears in rolled *sloth* mutants was close to the proportion of abnormal ears in unrolled wild-types). Though movement of the embryo is playing a role in normal otolith formation it appears that cilia and ciliary flow are playing a greater role in ensuring otolith formation occurs normally.

4.2.12 Cilia and ciliary motility are normal in the *sloth* mutant

To confirm that the abnormal otoliths seen in *sloth* mutant embryos were not caused by a previously unnoticed ciliary defect, *sloth* mutant OV cilia were observed by anti-acetylated tubulin antibody stain in fixed embryos (Figure 4.12B). Ciliary motility was also observed to be normal *in vivo* by high-speed videomicroscopy (Figure 4.12D, Movie 21). No defects were seen in either the fixed cilia or in movement of cilia *in vivo*.

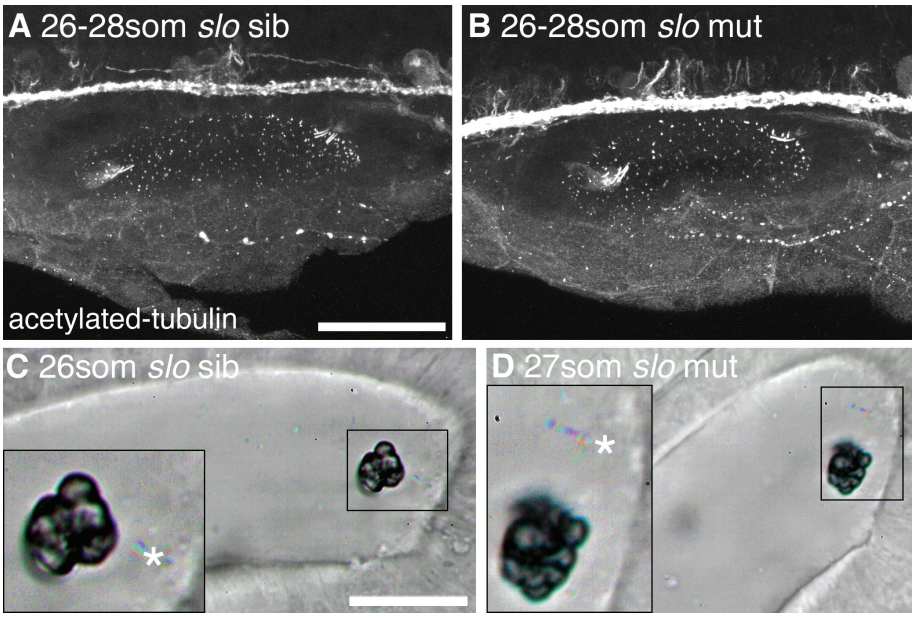

Figure 4.12: Cilia are normal in *sloth* mutant embryos though otolith defects are present. A. Confocal projection of anti-acetylated-tubulin antibody stain on 26–28S *slo* sibling OV. Dorsal view with anterior to left; Scale bar: 40μm, applies to A, B. **B**. Confocal projection of anti-acetylated tubulin antibody stain on 26–28S *slo* mutant OV. Cilia appear normal. **C**. Time-to-colour merge of 26S *slo* sibling OV. Inset shows anterior otolith with one motile cilium nearby (asterisk). Dorsolateral view with anterior to right; Scale bar: 20μm, applies to C, D. Movie 20. **D**. Time-to-colour merge of 27S *slo* mutant OV. Inset shows anterior otolith with nearby motile cilium (asterisk). Ciliary motility was normal. Movie 21.

4.2.13 Normal development can rescue otolith defects in mutants lacking cilia (*igu*^{ts294e}) or ciliary motility (*lrrc50*)

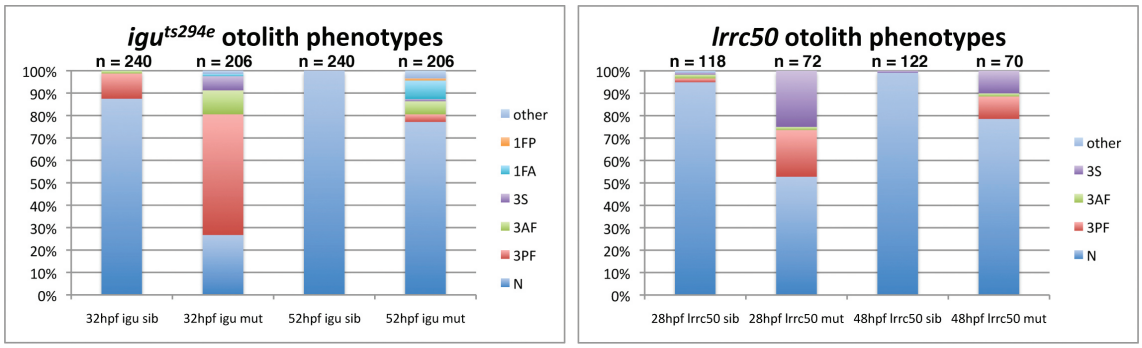

Figure 4.13: Age-related rescue of otolith defects in *igu*^{ts294e} and *lrrc50* embryos. Both sibling and mutant *igu*^{ts294e} and *lrrc50* embryos showed a rescue of the number of ears with abnormal otoliths with increasing age.

Observation of 2dpf *lrrc50* and *igu*^{ts294e} mutant embryos showed that the number of ears with abnormal otoliths decreased when compared to 1dpf mutant embryos (Figure 4.13). This suggests that as otolith growth and mineralisation continues during embryonic development, otolith defects can be rescued. The mechanisms for this may involve further movement of the embryo, resulting in untethered otoliths becoming stuck to tethered otoliths. Continued biomineralisation of otoliths by $CaCO_3$ may make a previously fused otolith (with a figure of eight shape) into a single, rounded otolith.

The rescue of otolithic defects in cilia mutants by continued embryonic development may explain wild-type rescue of otolithic defects. A small proportion (∼2%) of wild-type embryonic OVs left to develop under control conditions form otolith defects, most often a third otolith that would remain untethered or have fused to the anterior or posterior otolith by 30–32hpf (for example see wild-type controls in Figure 4.11A). However, it is very rare for a wild-type embryo older than 2dpf to have otolith defects (unscored observation). This suggests that continued otolith growth can correct early defects in otolith formation.

4.3 Discussion

In this chapter, I have investigated the roles of cilia, hair cells and embryonic movement in otolith tethering and growth in the zebrafish embryo. A review article dealing with the formation of otoliths and otoconia splits this process into six steps: 1) Forming a normal otic vesicle, 2) Forming normal macular compartments (sensory patches) and normal nonsensory epithelium, 3) Establishing the ionic environment, 4) Correct production and export of otolith matrix proteins, 5) Assembly and attachment of matrix proteins in the correct places in the inner ear, and 6) Locally increasing calcium and carbonate concentrations to initiate growth of the otolith/otoconia (Hughes et al., 2006). For a more detailed discussion of otolith formation, see Section 1.3.5.

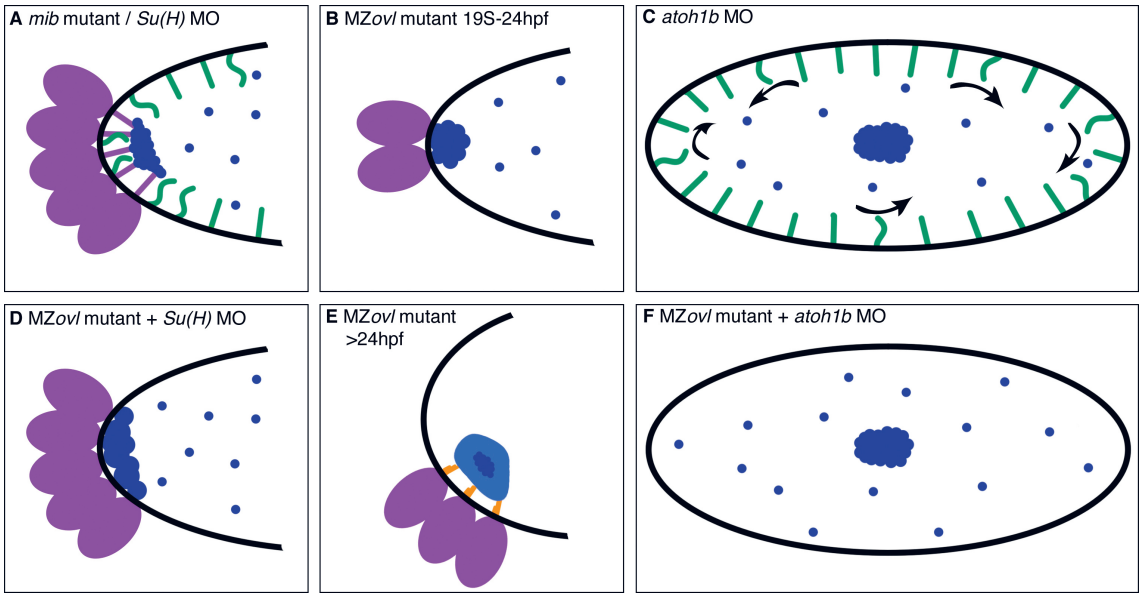

Figure 4.14: Model for otolith nucleation and tethering in the zebrafish otic vesicle in the absence of cilia and/or with ectopic/absent hair cells. A. In the ears of *mib* mutants or *Su(H) 1+2* morphants, ectopic hair cell tether cilia initially nucleate a flatter otolith. **B**. In MZ*ovl* mutant embryos, which lack all cilia, hair cells still produce the otolith precursor-binding factor; otolith precursor particles attach directly to the hair cell apical surface. **C**. In the absence of hair cells (*atoh1b*MO), otolith precursor particles have no tethering point, and settle to the lowest point in the OV, forming a single untethered otolith. **D**. In MZ*ovl* mutants injected with *Su(H) 1+2* morpholino, the otolith precursor particles tether to the apical membranes of all the ectopic hair cells. **E**. In MZ*ovl* mutants, hair cells are still able to produce stereocilia as normal and the otolith can become pushed away from the apical membrane by the stereociliary bundles. **F**. An untethered otolith still forms in MZ*ovl* mutants injected with *atoh1b* morpholino.

4.3.1 Ciliary flow helps to prevent the formation of untethered otoliths

My findings regarding the cilia mutants are related to the fifth step above; the assembly and attachment of otolith matrix proteins in the correct places in the inner ear. Embryos that completely lack cilia (MZ*ovl*), have a reduced number of cilia (*igu*), or lack ciliary flow (*lrrc50*) are still able to form an ovoid otic vesicle with an anterior and posterior pole containing hair cells. Otoliths do still form in the cilia mutant ear, indicating that otolithic components are correctly made and secreted. The otoliths biomineralise correctly and show normal early growth, suggesting that regulation of calcium and carbonate ions within the OV is normal. However, these cilia mutants frequently fail to nucleate two correctly tethered otoliths above the anterior and posterior maculae within the OV. Instead, a third untethered otolith is often formed. This either remained untethered when cilia mutants were scored at 30–32hpf or had fused with either the tethered anterior or posterior otolith (Sections 4.2.1–4.2.5). The third otolith is likely formed due to the loss of ciliary flow within the OV, as it is seen in both the cases where cilia are absent (MZ*ovl* and *igu*) and when cilia are present but not-motile (*lrrc50*). Ciliary flow should keep the dense and sticky otolith precursor particles moving within the OV, by preventing them sinking to the

lowest point in the OV where they can aggregate to form an ectopic, untethered otolith.

It was surprising to find that cilia are not absolutely required for otolith tethering by examining the MZ*ovl* mutant, which completely lacks cilia (work done in collaboration with Dr. Peng Huang and Professor Alexander Schier at Harvard University), given that previous work had shown that otoliths always tether to the tips of the kinocilia of the first hair cells (Riley et al., 1997; Colantonio et al., 2009; Tanimoto et al., 2011). The otoliths of MZ*ovl* mutant embryos are able to tether directly to the apical surface of the hair cells before 24hpf (see Figure 4.10B). After stereociliary bundles have formed, the otolith then appears to be tethered by the stereocilia (Figure 4.1F). The finding that otoliths tether in the absence of cilia supports the hypothesis that the first hair cells nucleate otolith formation by producing an otolith precursor binding factor (Riley et al., 1997). Normally this otolith precursor binding factor (or factors) is localised to the tips of the kinocilia, making them able to tether otolith precursor particles within the OV. If the kinocilia are absent, as in MZ*ovl*, the otolith precursor binding factor is instead localised to the apical surface of the hair cells. This means that otolith precursor particles now tether directly to the hair cells' apical surface, and the otoliths form here (Figure 4.14B). This is shown most dramatically in MZ*ovl* embryos injected with *Su(H)1+2* morpholino (Section 4.2.9): all the ectopic hair cells are capable of tethering otolith precursor particles directly to their apical surface (Figure 4.10D).

The ability of the stereociliary bundles to tether the otolith once they have formed on the hair cells is interesting. The factor or factors that normally bind the otolith at the tips of the kinocilia also appear to be able to localise to the tips of the stereocilia. Other proteins localise to both the kinocilium and the stereociliary bundles in zebrafish, for example Harmonin (Ush1c), which plays a role in shaping the stereociliary bundle and ensuring correct hair cell number during development (Phillips et al., 2011).

The Z*ovl* mutant had the lowest proportion of ears with abnormal otoliths (14%) in comparison to the other mutants lacking cilia that were studied. When Z*ovl* mutant embryos were observed before 24hpf using high-speed videomicroscopy there were so many cilia in the OV that it was not possible to determine mutant from sibling embryos based on cilia phenotype; motile, immotile and tether cilia were observed in Z*ovl* mutant OVs. Another study has reported a normal number of cilia in the Z*ovl* mutant OV at 40hpf (Tsujikawa and Malicki, 2004). As the Maternal Zygotic *ovl* mutant completely lacks cilia (Huang and Schier, 2009), this suggests that maternal provision of *ift88* mRNA is at such a level that a normal or near-normal number of cilia are produced in the Z*ovl* mutant OV during early development. It appears that in most cases there is a large enough number of cilia in the Z*ovl* mutant OV before 24hpf for otolith formation to proceed normally.

In *igu* mutants the greater proportion of ears with abnormal otoliths, combined with the difficulty seeing cilia *in vivo* using high-speed videomicroscopy, suggests that maternal provision of *dzip1* transcripts may be lower than maternal provision of *ift88* transcripts. One study has shown that there is a maternal provision of *dzip1* mRNA by *in situ* hy-

bridisation on 16 cell embryos (Wolff et al., 2004). However, another study reported that *dzip1* mRNA expression was not detected until 12hpf, after the onset of zygotic gene expression (Sekimizu et al., 2004). It would be interesting to produce a maternal zygotic *dzip1* mutation to see if it had a different cilia phenotype to the MZ*ovl* mutant. It has been reported that the *igu* mutation prevents immotile ciliogenesis, whilst motile ciliogenesis can still occur (Tay et al., 2010; Glazer et al., 2010; Kim et al., 2010). A maternal zygotic *iguana* mutation would prove or disprove this hypothesis. My study of the zygotic *iguana* mutants has shown that the cilia phenotype is variable, and even in the stronger igu^{ts294e} allele some immotile cilia may still be formed (Figure 4.3B). A start-site blocking *igu* morpholino would be able to knock down expression of maternal transcripts as well as zygotic transcripts. However, morpholinos are also prone to causing non-specific off target effects and so are not as thorough a test as a maternal zygotic mutant. Start-site blocking morpholinos against igu have already been used; Wolff and colleagues designed and trialled 3 different *igu* start-site morpholinos and reported that none of them were effective (Wolff et al., 2004). If an MZ*igu* mutant did only have motile cilia, it would allow the study of the effect of removing just the immotile cilia from the OV, something that I have not been able to test.

My findings with *ovl*, *igu* and *lrrc50* clarify the importance of cilia and ciliary flow for otolith tethering and positioning. Since otoliths are always tethered by the hair cell tether cilia, the next investigation was to manipulate hair cell number to clarify the role of hair cells in otolith formation.

4.3.2 The first hair cells produce a factor or factors essential for otolith tethering

I investigated the requirement of hair cells for tethering the otolith by observing the *mindbomb* mutant, where all the ectopic hair cells formed tether cilia that nucleated otolithic material (Section 4.2.7). The converse experiment, in which the first hair cells were prevented from forming by injection of *atoh1b* morpholino (Millimaki et al., 2007), showed that otolith precursor particles could not tether to an alternative point within the OV if hair cells were absent (Section 4.2.8).

Hair cells were confirmed to be tethering otolith precursor particles in the absence of cilia by examining MZ*ovl* mutants injected with *Su(H)1+2*MO to form ectopic hair cells, and MZ*ovl* mutants injected with *atoh1b*MO to prevent hair cell formation. Just as in embryos with cilia, supernumerary hair cells were all capable of tethering otolithic material, and otolithic material could not tether if hair cells were absent (Figure 4.14D and F).

The existence of an otolith precursor binding factor or factors was first hypothesised by Riley and colleagues (Riley et al., 1997). Further evidence to support the hypothesis that hair cells were producing otolith precursor particle binding factors was supplied by Yu and colleagues, when they reported that otoliths can tether directly on the apical membrane

in *igu*^{ts294e} mutants that lack kinocilia (Yu et al., 2011). However, the otolith precursor binding factor(s) has not been identified.

Zebrafish mutants that only form one otolith are good candidates for otolith precursor binding factor components. These mutants would initially be unable to tether otolith precursor particles, like *atoh1b* morphants, and as in *atoh1b* morphants the otolith precursor particles would aggregate to form a single, untethered otolith. This single otolith may or may not be able to tether to one of the sensory maculae later in development by a secondary mechanism, as occurs in *atoh1b* morphants once *atoh1a* dependant hair cell differentiation has taken place (Millimaki et al., 2007). There are several uncloned zebrafish mutant lines with a single otolith that are homozygous viable or semi-viable: *einstein*, *stein und bein*, *menhir* (Whitfield et al., 1996), and *monolith* (Riley and Grunwald, 1996). Cloning these mutants would prove a useful start to understanding the process of otolith precursor particle tethering. The fact that there are several zebrafish mutants with only one otolith hints that there is likely to be more than one otolith precursor binding factor, and that otolith precursor particle binding may be a multi-stage process. This process would likely require correct production and assembly of otolith precursor binding factors within the hair cells and then transport to the kinocilium tip. Likewise, corresponding factors would need to be made and transported to the otolith precursor particles to allow them to stick to each other and to recognise the kinociliary tips as binding sites within the OV.

A component required for otolith precursor particle tethering has already been identified. *hsp90b1* (*GP96*) morphant embryos are initially unable to tether otolith precursor particles, despite the presence of hair cells and kinocilia, instead forming a single otolithic mass, which is later tethered (Sumanas et al., 2003). Hsp90b1 is a chaperone protein localised to endoplasmic reticulum, suggesting that it is required for correct folding and secretion of an otolith precursor particle binding factor (Sumanas et al., 2003).

The hair cell localised otolith precursor particle binding factor may be localised to the kinociliary tip via the basal body of the kinocilium. The basal body still correctly docks to the hair cell apical surface in MZ*ovl* mutants (Huang and Schier, 2009), and so if otolith precursor particle binding factors reached the basal body as normal they may be localised to this cellular location with no cilium to be trafficked up.

4.3.3 Embryonic movement plays a minor role in normal otolith formation

I found that embryonic movement plays a minor role in otolith formation. Embryonic movement also appears to be involved in the fifth step of otolith formation proposed in Hughes et al. (2006), the correct localisation of otolithic components.

My findings are different from those reported in Riley et al. (1997). This may be because I restricted embryonic movement for longer, and perhaps from an earlier stage (Riley et al. (1997) report that embryos were immobilised prior to otolith formation for 6h,

though they do not put an exact stage from which embryos were immobilised). Embryos that had movement restricted by use of 3% methyl cellulose tended to lie on their sides in the methyl cellulose, whilst Riley and colleagues immobilised embryos in either a head up or down position using agarose. There is a concentration of motile cilia at both the anterior and posterior pole of the OV (Chapter 3); these motile cilia prevent otolith precursor particles from settling at the poles of the OV, even if a pole is the lowest part of the OV. However, there are very few motile cilia on the medial wall of the OV, and none on the lateral wall of the OV (Chapter 3). Otolith precursor particles that sink and settle on either the lateral wall of the OV, or on areas of the medial wall away from motile cilia may experience no motile cilia-induced fluid flow, and so collect and aggregate in these regions if not made to fall back into the middle of the OV by movement of the embryo.

Other tests of environmental effects on otolith formation have been done by changing the gravitational forces that embryos are subject to during development. Zebrafish have been grown in simulated micro-gravity using wall-vessel rotation apparatus in order to test the stimulus dependence of vestibular system development (Moorman et al., 1999; Li et al., 2010). When zebrafish embryos are grown in this way from ∼3hpf to 96hpf their posterior otoliths are smaller than normal and compensatory eye-movement in response to tilting is reduced compared to control embryos allowed to develop under normal gravity conditions (Moorman et al., 1999). The second study reported a different effect of wall-vessel rotation on zebrafish vestibular system development (Li et al., 2010); embryos developed larger otoliths when developing under simulated micro-gravity from 10hpf until 3–6dpf. However, longer development until 9–12dpf in simulated micro-gravity led to otoliths that were not significantly different in size to control embryos that had developed under normal gravity conditions. It appears that although early otolith development is dependent on gravity stimulus, continued development leads to otoliths of a normal size regardless of gravity environment. However, Li et al. (2010) did not test functionality of the vestibular system of zebrafish that had developed in simulated micro-gravity. This leaves a possibility that development of vestibular function depends on appropriate stimulus, as does the functional developments of other sensory systems.

4.4 Conclusion

I find that hair cells are absolutely essential for tethering the forming otoliths, while cilia are dispensable in this role. However, ciliary flow is important for shaping the forming otoliths and preventing formation of a third otolith caused by aggregation of otolith precursor particles away from the hair cells. Movement of embryos during development also helps to prevent aggregation of otolith precursors away from the hair cells.

Looking beyond the zebrafish, only two human ciliopathies are reported to have deafness as a symptom, these are Alström Syndrome (Marshall et al., 2007) and Bardet-Biedl Syndrome (Billingsley et al., 2010) (see Section 1.2.5 for further details). There are no

human ciliopathies that have vestibular defects reported as a symptom. A mouse model of Bardet-Biedl syndrome has been shown to have hearing loss (Ross et al., 2005), as has a mouse model of Alström syndrome (Jagger et al., 2011), but neither study reported any vestibular defect in these mouse mutant models.

The OV also contains a large number of immotile cilia (92–98% of all cilia in the OV) which are likely to have a function in normal OV development. As immotile cilia are required for transduction of several developmental signalling pathways (Eggenschwiler and Anderson, 2007) (see Section 1.2.4), they are likely to be involved in relaying signals required for normal ear development and morphogenesis. The effect of complete loss of cilia, lack of cilia and loss of ciliary motility on patterning the anterior and posterior maculae and on morphogenesis of the OV up to 5dpf is investigated in the next chapter.

Chapter 5

The Role of Cilia in Inner Ear Patterning and Morphogenesis

5.1 Introduction

Hair cell maturation consists of several steps and is discussed in Section 1.3.4. Hair cells have a cell polarity, such that the single kinocilium is at the edge of the apical hair cell domain with the stereociliary bundle behind it. The hair cell kinocilium is assumed to be important for polarising the apical surface of the hair cell and its stereociliary bundle during maturation (Tilney et al., 1992; Denman-Johnson and Forge, 1999). However, the mechanism by which the stereociliary bundle is polarised is not yet known (Deans, 2013). As hair cells in the developing mouse cochlea which lack cilia, due to a conditional knock out of *Ift88*, occasionally form non-polarised circular bundles (Jones et al., 2008) we sought to test whether a deficiency in cilia could also disrupt stereociliary bundle morphology in zebrafish hair cells.

As well as the apical surface of each hair cell being polarised the zebrafish anterior (utricular) and posterior (saccular) sensory patches also have a stereotyped polarity pattern (Haddon et al., 1999; Whitfield et al., 2002). Maculae of cilia mutants were studied at 4dpf to see if cilia were required for both individual hair cell polarity and the formation of hair cell polarity across the sensory maculae.

Every cell lining the embryonic zebrafish OV is mono-ciliated from cavitation (Riley et al., 1997; Borovina et al., 2010), also see Section 3.2.1. However, only a small subset of these cilia are motile; the vast majority are immotile (Section 3.3). As most cilia in the zebrafish OV are immotile and not producing fluid flow, I studied ear morphology in cilia mutants at 4 and 5dpf in order to ascertain what function the immotile cilia might have. As cilia are known to be required for Hh signalling in the zebrafish (Huang and Schier, 2009; Tay et al., 2010; Kim et al., 2010), I anticipated an effect on ear morphology similar to that seen in zebrafish Hh signalling pathway mutants (Hammond et al., 2010).

The MZ*ovl*, Z*ovl*, igu^{tm79a} and *lrrc50* mutants were studied to provide a series of ciliary

phenotypes, as described in Chapter 4.

5.2 Results

5.2.1 Sensory patch polarity is not affected in mutants completely lacking cilia (MZ*ovl*)

Anterior and posterior maculae of MZ*ovl* mutants were examined at 4dpf in order to determine if hair cells could still form the normal stereotyped polarity pattern (Haddon et al., 1999; Whitfield et al., 2002). M*ovl* sibling embryos were used as a phenotypically wild-type control. Although there were fewer stereociliary bundles in MZ*ovl* maculae compared to M*ovl* maculae (see Section 5.2.5), the stereociliary bundles that formed did appear to polarise correctly. Both anterior and posterior maculae of MZ*ovl* embryos had the correct

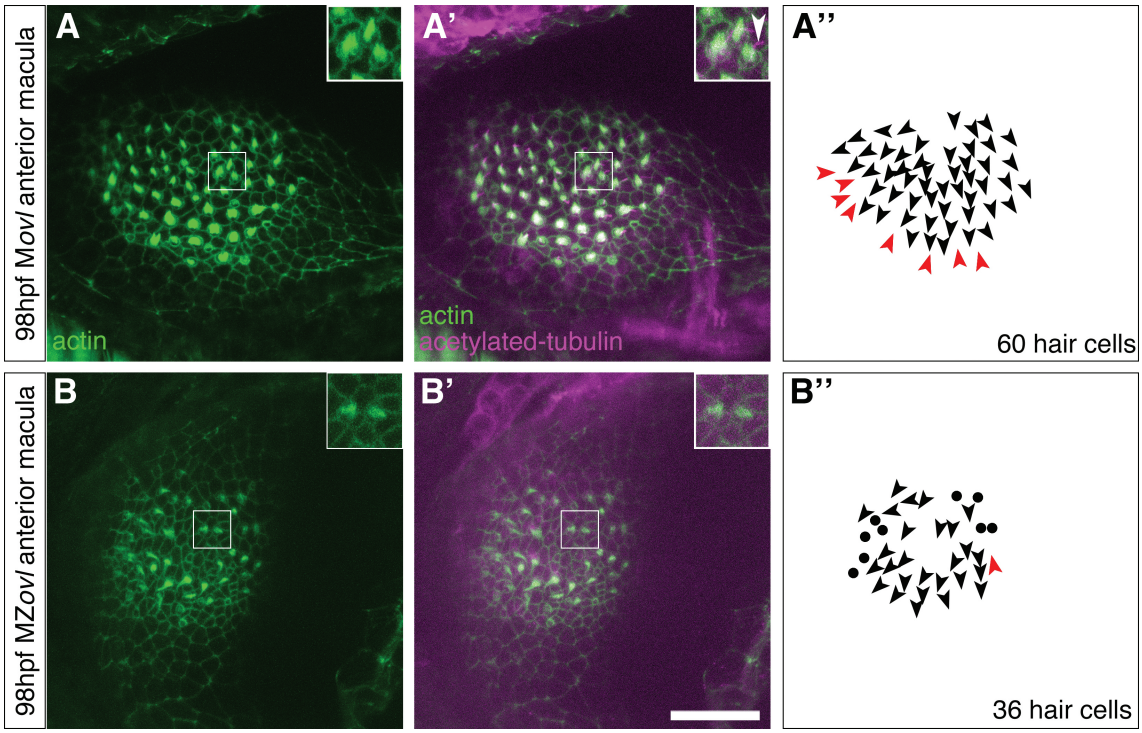

Figure 5.1: Stereociliary bundle polarity in 4dpf M*ovl* and MZ*ovl* anterior maculae. **A** and **A'**. Confocal projection of 98hpf M*ovl* anterior macula of left ear stained with FITC-phalloidin (green) and anti-acetylated tubulin antibody (magenta). Dorsal view with anterior to left. Inset shows detail of stereociliary bundles (A) and kinocilia associated with stereociliary bundles (A', arrowhead). **A"**. Arrowheads indicate polarity of hair cells in the macula; arrows point from stereociliary bundle to the associated kinocilium. Red arrowheads indicate the zone of polarity reversal. **B** and **B'**. Confocal projection of 98hpf MZ*ovl* anterior macula of left ear as in A. No kinocilia were detected (inset in B'). Scale bar: 20μm, applies to all panels. **B"**. Arrowheads indicate polarity of hair cells in macula; arrows point from the stereociliary bundle to the gap where a kinocilium would normally be present. Dots indicate position of hair cells where polarity could not be determined. One hair cell with reversed polarity is seen (red arrowhead). Loss of the zone of polarity reversal was variable between different embryos analysed.

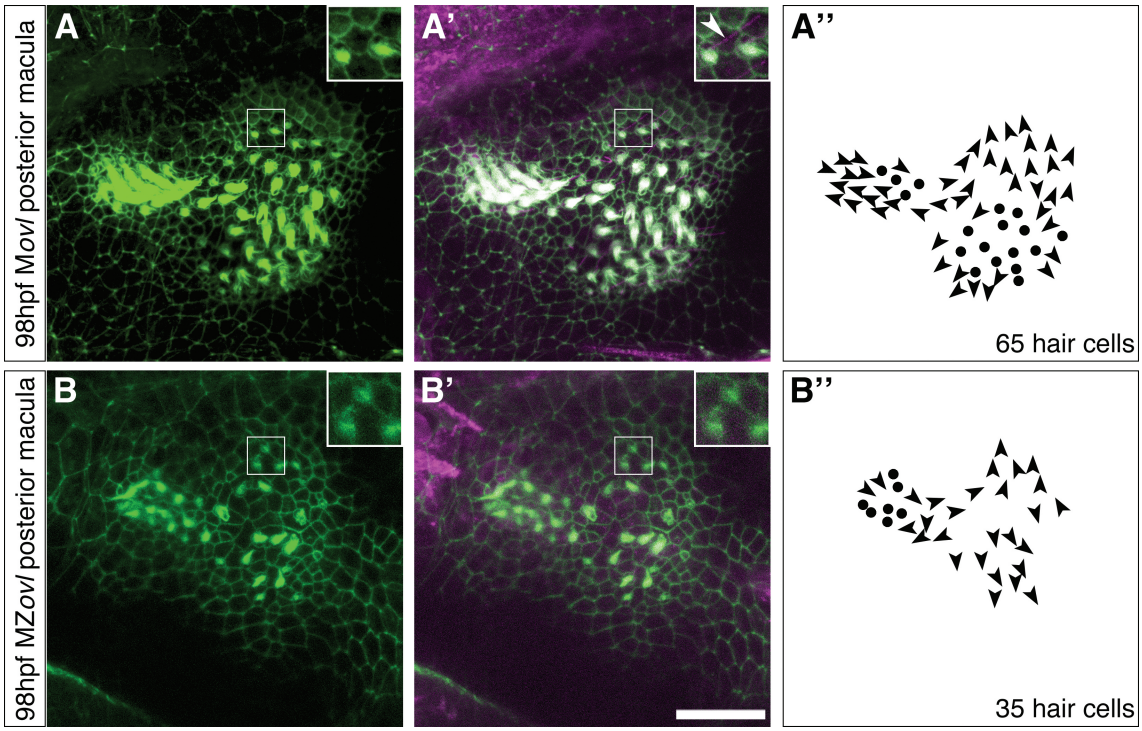

Figure 5.2: Stereociliary bundle polarity in 4dpf M*ovl* and MZ*ovl* posterior maculae. **A** and **A'**. Confocal projection of 98hpf M*ovl* posterior macula of left ear, stained as in Figure 5.1. Lateral view with anterior to left. Kinocilia are present (arrowhead, inset in A'). **A"**. Polarity pattern of M*ovl* posterior macula. **B** and **B'**. Confocal projection of 98hpf MZ*ovl* posterior macula of right ear. Image has been flipped horizontally to allow comparison with A. Kinocilia were not detected (inset, B'). Scale bar: 20μm, applies to all panels. **B"**. Polarity pattern of MZ*ovl* posterior macula.

shape; a rounded fan-like anterior macula (utricle) and a table tennis bat-like posterior macula (saccule).

MZ*ovl* maculae completely lacked kinocilia, making it more difficult to determine hair cell polarity than in M*ovl* maculae. However, the gap for the kinocilium could still be seen in the stereociliary bundle and cuticular plate on MZ*ovl* mutant hair cells (Figures 5.1B' and 5.2B', also see Figure 5.11). This suggests that formation of the gap for the kinocilium does not depend on the growth of the kinocilium. Formation of the gap in the cuticular plate may depend on the docking of the basal body to the apical surface of the hair cell instead. The basal body is still correctly localised in the MZ*ovl* mutant (Huang and Schier, 2009).

All hair cells where polarity could be determined in MZ*ovl* anterior maculae had the expected polarity when compared with hair cells in a similar position in the anterior maculae of M*ovl* (n=6 MZ*ovl* anterior maculae; n=4 M*ovl* anterior maculae). The anterior maculae showed the fan-like spreading-out of hair cell orientation (Figure 5.1B"). The presence of hair cells with reversed polarity at the lateral edge of the anterior macula was variable: 3 of 4 MZ*ovl* anterior maculae analysed had at least one reversed polarity hair cell at the lateral edge (see red arrowhead in Figure 5.1B" for an example). However, no

MZ*ovl* utricle had a full band of reversed polarity hair cells as seen in M*ovl* embryos at this stage. It is not possible to determine if the observed lack of reversed polarity hair cells was due to a defect in polarity signalling caused by lack of cilia, or due to the reduced number of hair cells in MZ*ovl* maculae (see Section 5.2.5).

Similarly, hair cells in MZ*ovl* posterior maculae had a comparable polarity to hair cells in M*ovl* posterior maculae (n=9 MZ*ovl* anterior maculae; n=2 M*ovl* posterior maculae). Hair cells showed anti-parallel polarity in the anterior region of the macula, and were polarised dorsally and ventrally away from the centre of the posterior part of the maculae (Figure 5.2A", B").

The total number of stereociliary bundles in the maculae of MZ*ovl* was noticeably less than in M*ovl* maculae (see Section 5.2.5). This may have been caused by either developmental delay, lack of hair cell differentiation, lack of stereociliary bundle formation, hair cell death, or a combination of these. Hair cell death has already been reported after 3dpf in Z*ovl* mutants (Tsujikawa and Malicki, 2004), so it seems likely that this is also happening in the MZ*ovl* mutants.

Some purple anti-acetylated tubulin staining is seen in MZ*ovl* embryos because hair cells bodies and neural cell types are also marked by the anti-acetylated tubulin antibody.

5.2.2 Sensory patch polarity is not affected in mutants with a severe loss of cilia (Z*ovl*)

The anterior and posterior maculae of Z*ovl* sibling and mutant embryos were examined at 4dpf for polarity. Z*ovl* sibling embryos acted as a phenotypically wild-type control for Z*ovl* mutant embryos. There appeared to be fewer stereociliary bundles in Z*ovl* mutant anterior and posterior maculae when compared to siblings (see Section 5.2.5). Stereociliary bundles in Z*ovl* mutant maculae appeared to polarise correctly when compared to siblings (Figures 5.3 and 5.4).

Z*ovl* mutant anterior and posterior maculae had the correct overall shape compared to siblings (n=2 Z*ovl* mutant anterior maculae and one Z*ovl* mutant posterior macula; n=2 Z*ovl* sibling anterior maculae (left and right maculae from a single embryo) and 3 Z*ovl* sibling posterior maculae (from 2 embryos)). However, stereociliary bundles appeared to be reduced in the centre of anterior maculae, and the centre of the posterior portion of the posterior maculae. This suggests that the hair cell death that occurs from 3dpf in Z*ovl* mutant maculae (Tsujikawa and Malicki, 2004) may affect hair cells at the centre of the macula first.

The zone of polarity reversal was still present in anterior maculae of Z*ovl* mutant embryos (red arrows, Figure 5.3B"). In the Z*ovl* mutant posterior macula examined, the antiparallel polarity in the anterior region was still seen, and dorsal and ventral polarity was still seen spreading out from the centre of the posterior half of the posterior macula (Figure 5.4B").

One of the two Z*ovl* mutant anterior maculae examined had one kinocilium present on

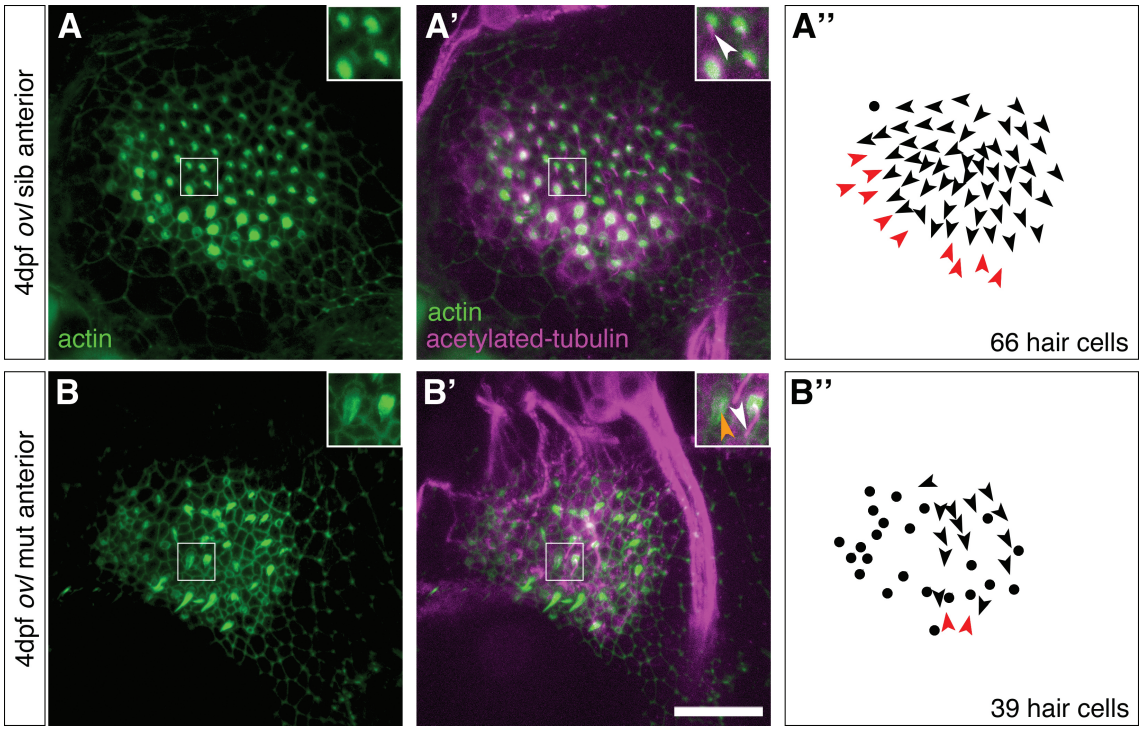

Figure 5.3: Stereociliary bundle polarity in 4dpf Z*ovl* anterior maculae. A and **A'**. Confocal projection of 4dpf Z*ovl* sibling anterior macula of left ear stained with FITC-phalloidin (green) and anti-acetylated tubulin antibody (magenta). Dorsal view with anterior to left. Insets show detail of stereociliary bundles (A) and kinocilia (arrowhead) associated with stereociliary bundles (A'). **A"**. Polarity pattern of Z*ovl* sibling anterior macula. Red arrowheads indicate the zone of polarity reversal. **B** and **B'**. Confocal projection of 4dpf Z*ovl* mutant anterior macula of left ear as in A; kinocilia were present on a few hair cell bundles (inset in B'; white arrowhead shows hair cell bundle with kinocilium present, orange arrowhead shows hair cell bundle lacking a kinocilium). Scale bar: 20μm, applies to all panels. **B"**. Polarity pattern of Z*ovl* mutant anterior macula: the zone of polarity reversal was present (red arrowheads).

a hair cell in the centre of the macula, while the other anterior macula had five kinocilia present on hair cells in the centre of the macula (Figure 5.3B'). Cilia are initially present on all or nearly all cells making up the OV epithelium (Tsujikawa and Malicki, 2004) (also see Section 4.2.2). The presence of cilia on the central hair cells of the epithelium may indicate that these are hair cells that formed early, when ciliogenesis could still occur due to presence of maternal *ovl* transcripts. Alternatively, it may be that hair cells at the centre of the maculae are the last to lose their kinocilia during the hair cell death seen in Z*ovl* mutants (Tsujikawa and Malicki, 2004). However, this contradicts my hypothesis that the central region of Z*ovl* mutant maculae are depleted of hair cells because this is where hair cell death is occurring first. The Z*ovl* mutant posterior macula examined had no kinocilia. As only a single Z*ovl* mutant maculae was examined, further investigation is needed to characterise development of maculae and hair cell polarity in mutants that fail in ciliogenesis after maternal *ift88* mRNA is depleted.

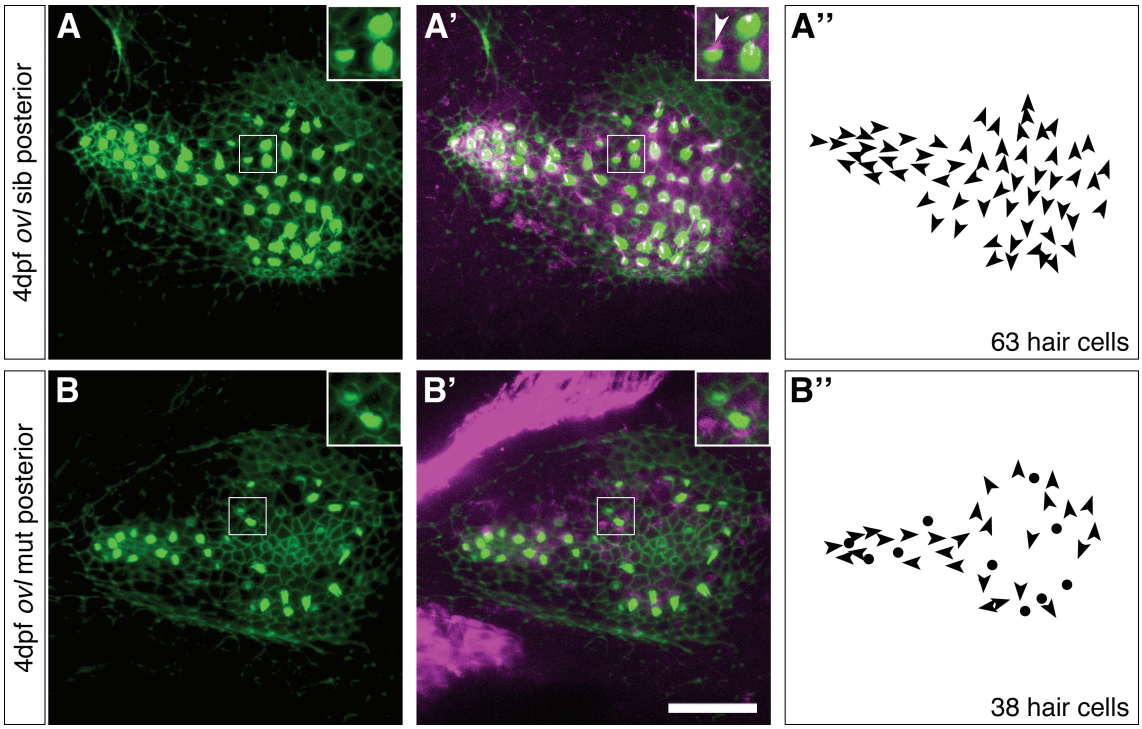

Figure 5.4: Stereociliary bundle polarity in 4dpf Z*ovl* posterior maculae. A and **A'**. Confocal projection of 4dpf Z*ovl* sibling posterior macula of right ear, stained as in Figure 5.3. Image has been flipped horizontally to allow comparison with posterior maculae in Figures 5.2–5.8. Lateral view with anterior to left. Kinocilia (arrowhead) were present (inset, A'). **A"**. Polarity pattern of Z*ovl* sibling posterior macula. **B** and **B'**. Confocal projection of 4dpf Z*ovl* posterior macula of right ear. Image has been flipped horizontally to allow comparison with posterior maculae in Figures 5.2–5.8. Kinocilia were not present (inset, B'). Scale bar: 20μm, applies to all panels. **B"**. Polarity pattern of Z*ovl* mutant posterior macula.

5.2.3 Sensory patch polarity is not affected in mutants with a reduced number of cilia (*iguana*)

The anterior and posterior maculae of igu^{tm79a} mutant and sibling embryos were examined at 4dpf for polarity. igu^{tm79a} sibling embryos acted as a phenotypically wild-type control for igu^{tm79a} mutant embryos. The anterior and posterior maculae of igu^{tm79a} mutant embryos had the same overall shape as those of sibling embryos. The number of stereociliary bundles in *igu* mutant anterior maculae was unaffected, but stereociliary bundle number in *igu* mutant posterior maculae was reduced compared to sibling embryos (Figures 5.5 and 5.6, also see Section 5.2.5).

Anterior maculae of *igu* mutant embryos appeared the same as the phenotypically wild-type *igu* sibling embryos. Kinocilia were present on all mature hair cells with an associated stereociliary bundle (Figure 5.5B'). The zone of polarity reversal at the lateral edge of the anterior macula was present in *igu* mutants (Figure 5.5B") (n=8 *igu* mutant anterior maculae, 9 *igu* sibling anterior maculae).

Posterior maculae of *igu* mutants had hair cell kinocilia associated with stereociliary bundles and a normal polarity pattern (Figure 5.6B' and B"). However, the number of

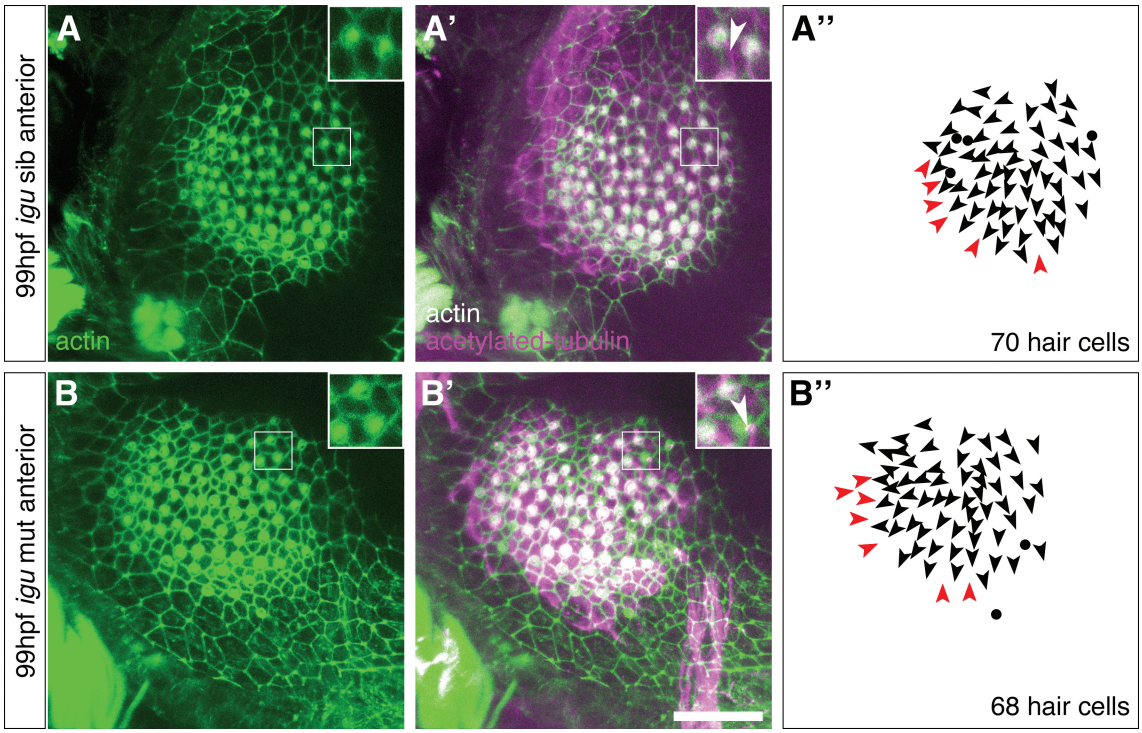

Figure 5.5: Stereociliary bundle polarity in 4dpf *igu*^{tm79a} anterior maculae. A and **A'**. Confocal projection of 99hpf *igu*^{tm79a} sibling anterior macula of right ear stained with FITC-phalloidin (green) and anti-acetylated tubulin antibody (magenta). Image has been flipped vertically to allow comparison with B–B". Dorsal view with anterior to left. Inset shows detail of stereociliary bundles (A) and kinocilia (arrowhead) associated with stereociliary bundles (A'). **A"**. Polarity pattern of *igu*^{tm79a} sibling anterior macula. Red arrowheads indicate the zone of polarity reversal. **B** and **B'**. Confocal projection of 99hpf *igu*^{tm79a} mutant anterior macula of left ear as in A; kinocilia were present (arrowhead in inset, B'). Scale bar: 20μm, applies to all panels. **B"**. Polarity pattern of *igu*^{tm79a} mutant anterior macula. The zone of polarity reversal in still present (red arrowheads).

stereociliary bundles in *igu* mutant posterior maculae was reduced compared to siblings (Section 5.2.5) (n=6 *igu* mutant posterior maculae, 3 *igu* sibling posterior maculae).

5.2.4 Sensory patch polarity is not affected in mutants lacking ciliary motility (*lrrc50*)

The anterior and posterior maculae of *lrrc50* mutant and sibling embryos were examined at 4dpf for polarity. The *lrrc50* sibling embryos acted as a phenotypically wild-type control for *lrrc50* mutant embryos. The anterior and posterior maculae of *lrrc50* mutant embryos had the same overall shape as those of sibling embryos. The number of stereociliary bundles in *lrrc50* mutant anterior maculae was unaffected, but stereociliary bundle number in *lrrc50* mutant posterior maculae was reduced compared to sibling embryos (Figures 5.7 and 5.8, also see Section 5.2.5).

Anterior maculae of *lrrc50* mutant embryos appeared the same as the phenotypically wild-type *lrrc50* sibling embryos. Kinocilia were present on all mature hair cells with

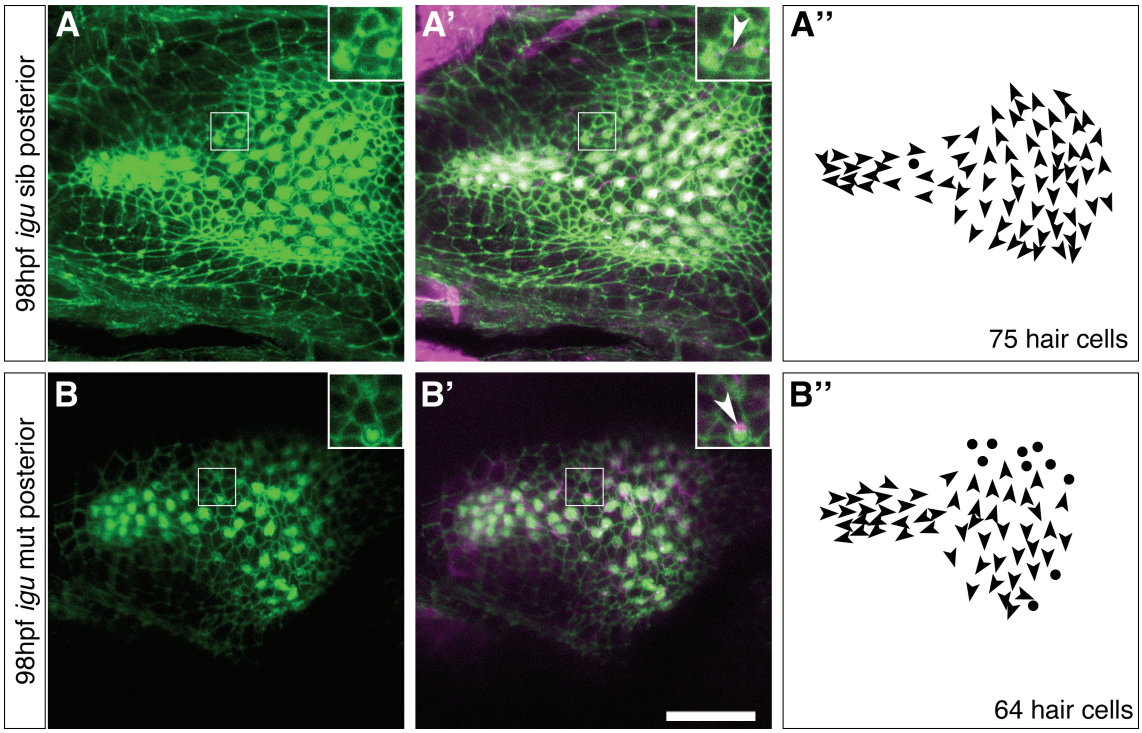

Figure 5.6: Stereociliary bundle polarity in 4dpf *igu*^{tm79a} posterior maculae. A and **A'**. Confocal projection of 98hpf *igu*^{tm79a} sibling posterior macula of right ear, stained as in Figure 5.5. Image has been flipped horizontally to allow comparison with B–B". Lateral view with anterior to left. Kinocilia were present (arrowhead in inset, A'). **A"**. Polarity pattern of *igu*^{tm79a} sibling posterior macula. **B** and **B'**. Confocal projection of 98hpf *igu*^{tm79a} posterior macula of left ear. Kinocilia were present (arrowhead in inset, B'). Scale bar: 20μm, applies to all panels. **B"**. Polarity pattern of *igu*^{tm79a} mutant posterior macula.

an associated stereociliary bundle (Figure 5.7B'). The zone of polarity reversal at the lateral edge of the anterior macula was present in *lrrc50* mutants (Figure 5.7B") (n=4 *lrrc50* mutant anterior maculae from 2 embryos, 2 *lrrc50* sibling anterior maculae from 2 embryos).

Posterior maculae of *lrrc50* mutants had hair cell kinocilia associated with stereociliary bundles and a normal polarity pattern (Figure 5.8B' and B"). However, the number of stereociliary bundles in *lrrc50* mutant posterior maculae was reduced compared to siblings (Section 5.2.5) (n=3 *lrrc50* mutant posterior maculae from 2 embryos, 3 *lrrc50* sibling posterior maculae from 3 embryos).

A lack of ciliary motility does not lead to sensory patch polarity defects at 4dpf.

5.2.5 Hair cell number is reduced in the posterior maculae of all ciliary mutants, and reduced in both the anterior and posterior macula of zygotic or maternal zygotic *ovl* mutants

The stereociliary bundles were counted in the confocal stacks taken of M*ovl*, MZ*ovl*, Z*ovl*, *igu*^{tm79a} and *lrrc50* anterior and posterior maculae at 4dpf (Figure 5.9). The stereociliary

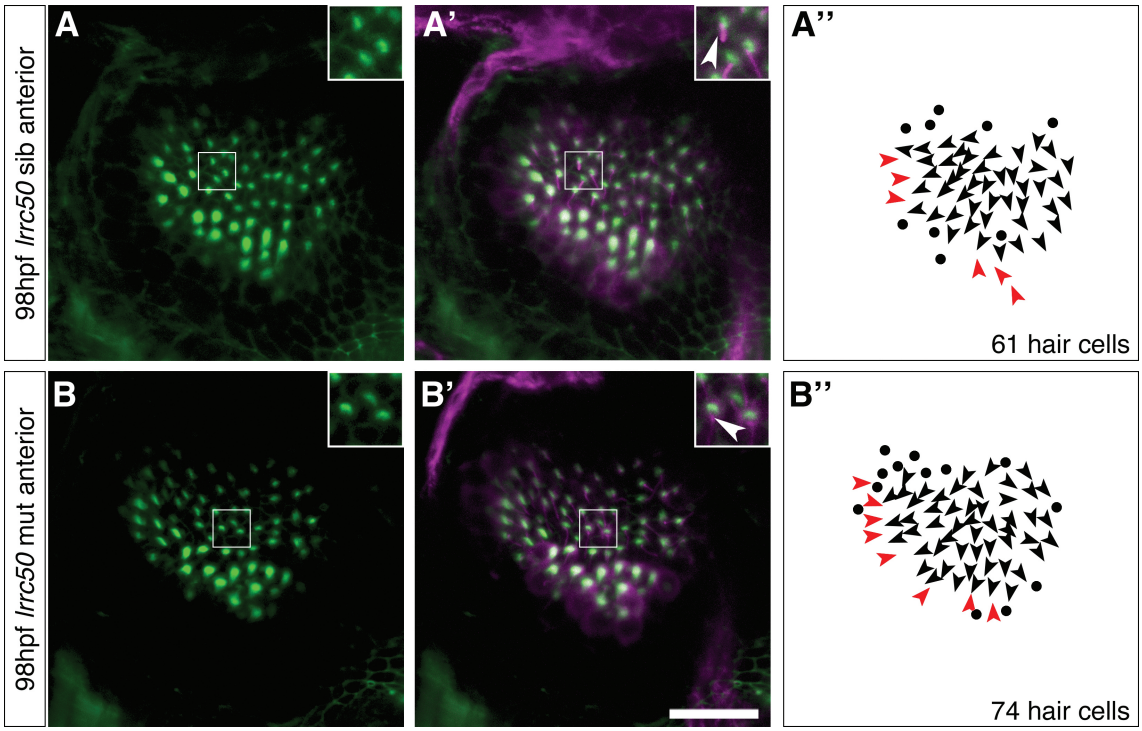

Figure 5.7: Stereociliary bundle polarity in 4dpf *lrrc50* anterior maculae. A and **A'**. Confocal projection of 98hpf **lrrc50** sibling anterior macula of left ear stained with FITC-phalloidin (green) and anti-acetylated tubulin antibody (magenta). Dorsal view with anterior to left. Inset shows detail of stereociliary bundles (A) and kinocilia (arrowhead) associated with stereociliary bundles (A'). **A"**. Polarity pattern of *lrrc50* sibling anterior macula. Red arrowheads indicate the zone of polarity reversal. **B** and **B'**. Confocal projection of 98hpf *lrrc50* mutant anterior macula of left ear as in A; kinocilia were present (arrowhead in inset, B'). Scale bar: 20μm, applies to all panels. **B"**. Polarity pattern of *lrrc50* mutant anterior macula. The zone of polarity reversal is still present (red arrowheads).

bundle count for a macula should be an accurate representation of the number of hair cells in that macula as no anti-acetylated tubulin-stained cell bodies were seen in sensory maculae that did not have an associated stereociliary bundle.

The number of hair cells in both MZ*ovl* anterior and posterior maculae was significantly decreased compared to phenotypically wild-type M*ovl* maculae (Figure 5.9A, B). There is also likely to be a significant decrease in the number of hair cells in the anterior and posterior maculae of Z*ovl* mutants compared to Z*ovl* sibling embryos. However, the number of maculae analysed for this was not high enough to be able to perform a two-tailed t-test (Figure 5.9C, D). There was no difference in the number of hair cells present in igu^{tm79a} mutant anterior maculae when compared to siblings (Figure 5.9C). However, the number of hair cells in igu^{tm79a} mutant posterior maculae was significantly lower than in siblings (Figure 5.9), though the number of hair cells in an *igu* mutant posterior maculae showed a high variability. There was no difference in the number of hair cells in *lrrc50* mutant anterior maculae when compared to siblings (Figure 5.9G). There was a significant reduction in the number of hair cells in *lrrc50* mutant posterior maculae when compared

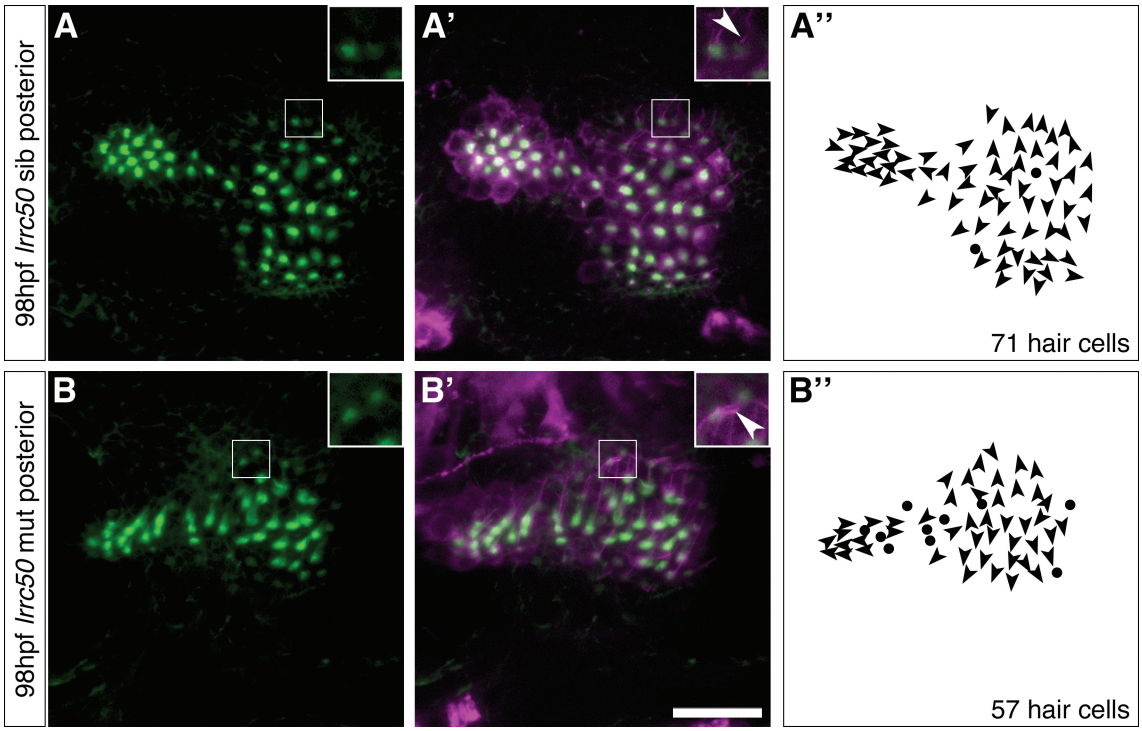

Figure 5.8: Stereociliary bundle polarity in 4dpf *lrrc50* posterior maculae. A and **A'**. Confocal projection of 98hpf *lrrc50* sibling posterior macula of left ear, stained as in Figure 5.7. Lateral view with anterior to left. Kinocilia were present (arrowhead in inset, A'). **A"**. Polarity pattern of *lrrc50* sibling posterior macula. **B** and **B'**. Confocal projection of 98hpf *lrrc50* posterior macula of right ear. Image has been flipped horizontally to allow comparison with A–A". Kinocilia were present (arrowhead in inset, B'). Scale bar: 20μm, applies to all panels. **B"**. Polarity pattern of *lrrc50* mutant posterior macula.

to siblings (Figure 5.9H), though the reduction in hair cell number in *lrrc50* mutants was less severe than that seen in MZ*ovl* and Z*ovl* mutants.

The reduction of hair cell number at 4dpf in both maternal zygotic or zygotic *ovl* mutants may be caused by hair cell death, as reported to have occurred by 5dpf in both anterior and posterior maculae of Z*ovl* mutants (Tsujikawa and Malicki, 2004). Tsujikawa and Malicki (2004) reported that hair cell death occurred after first the loss of the hair cell kinocilium, and then the loss of the hair cell stereociliary bundle.

The reduction of hair cells in only the posterior maculae of igu^{tm79a} and *lrrc50* embryos is interesting. This may be because the anterior macula develops before the posterior macula in zebrafish (Riley et al., 1997); alternatively, it may be because the anterior and posterior maculae experience different signalling environments due to differing levels of Hh, FGF, BMP, Wnt and RA throughout the OV (See Introduction Section 1.3) (Hammond et al., 2003; Riley and Phillips, 2003; Whitfield and Hammond, 2007; Hammond and Whitfield, 2011; Radosevic et al., 2011). Both *igu* and *lrrc50* mutants have kinocilia on all hair cells (Figures 5.5 – 5.8). This may mean that hair cell survival is unaffected; lack of cilia on non-sensory cells may lead to a lack of hair cell differentiation in these mutants, though more evidence would be required to support this. Apoptotic staining,

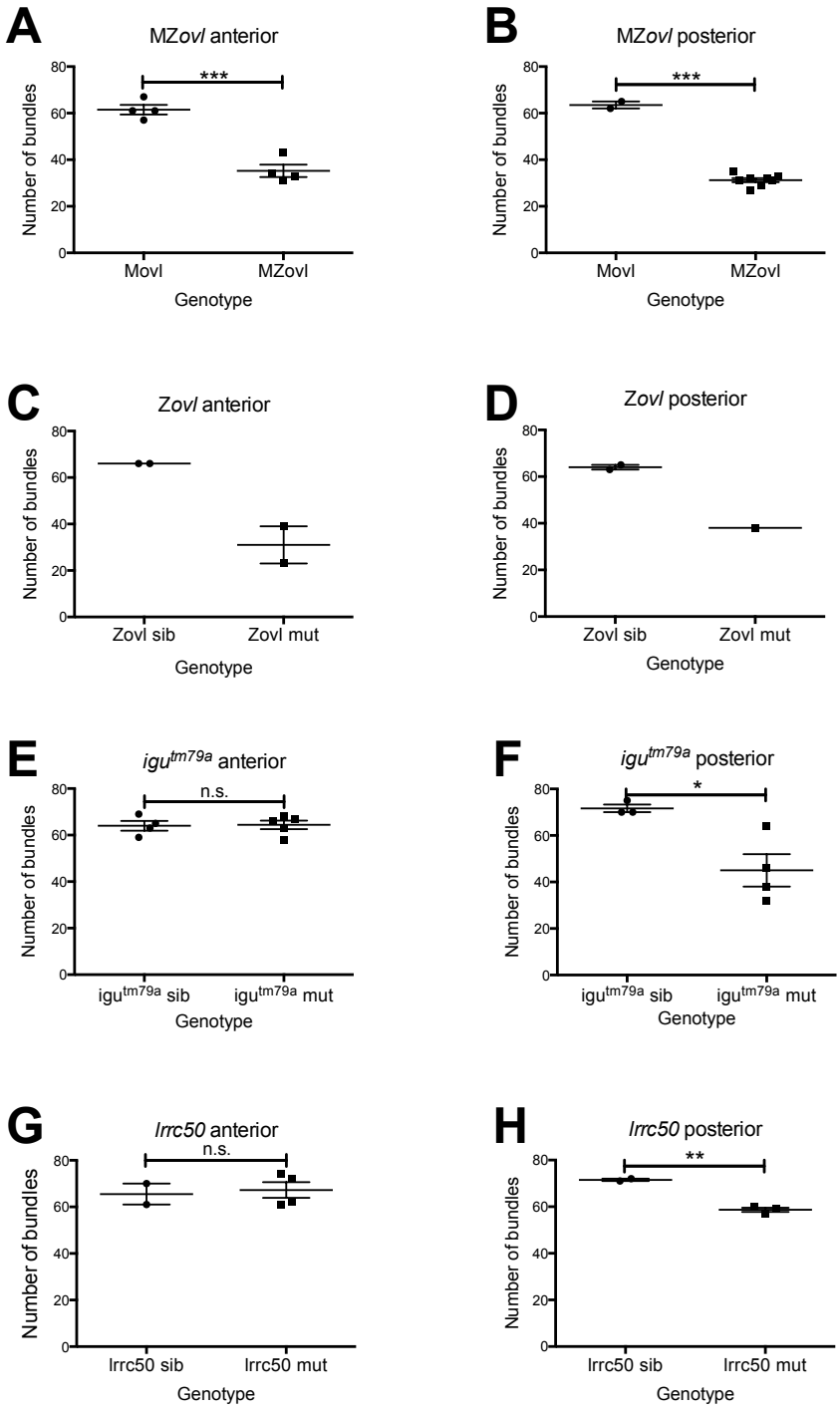

Figure 5.9: Effect of cilia disruption on number of stereociliary bundles in anterior and posterior maculae at 4dpf.

such as a TUNEL stain, would reveal if hair cell death was occurring in these mutants, while BrdU staining could reveal if there was a lack of cell proliferation in the region of mutant maculae.

Figure 5.9: Effect of cilia disruption on number of stereociliary bundles in anterior and posterior maculae at 4dpf. All graphs have all maculae analysed plotted and show mean ± SEM. **A**. Number of stereociliary bundles present in M*ovl* and MZ*ovl* anterior maculae. The number of stereociliary bundles was significantly lower in MZ*ovl* than in M*ovl*. Two-tailed t-test, p=0.0002, t=7.805, df=6. **B**. Number of stereociliary bundles present in M*ovl* and MZ*ovl* posterior maculae. The number of stereociliary bundles was significantly lower in MZ*ovl* than in M*ovl*. Two-tailed t-test, p <0.0001, t=17.01, df=8. **C**. Number of stereociliary bundles present in Z*ovl* sibling and mutant anterior maculae. The number of bundles in the mutant maculae appear lower; however, it was not possible to calculate a p value using a two-tailed t-test because both Z*ovl* sibling anterior maculae analysed had the same number of stereociliary bundles, so the variance of the sample could not be calculated. **D**. Number of stereociliary bundles present in Z*ovl* sibling posterior maculae. The number of bundles in mutant maculae appear lower; however, it was not possible to calculate a p value using a two-tailed t-test because n=1 for the Z*ovl* mutant posterior macula. **E**. Number of stereociliary bundles present in igu^{tm79a} sibling and mutant anterior maculae. There was no significant difference between the number of stereociliary bundles in mutant and sibling embryos. Two-tailed t-test, p=0.8882, t=0.1457, df=7. **F**. Number of stereociliary bundles present in igu^{tm79a} sibling and mutant posterior maculae. The number of stereociliary bundles was significantly lower in igu^{tm79a} mutant posterior maculae compared to siblings. Two-tailed t-test, p=0.0241, t=3.196, df=5. **G**. Number of stereociliary bundles present in *lrrc50* sibling and mutant anterior maculae. There was no significant difference between the number of stereociliary bundles in mutant and sibling embryos. Two-tailed t-test, p=0.7754, t=0.3053, df=4. **H**. Number of stereociliary bundles present in *lrrc50* sibling and mutant posterior maculae. The number of stereociliary bundles was significantly lower in *lrrc50* mutant posterior maculae compared to siblings. Two-tailed t-test, p=0.0017, t=10.71, df=3.

5.2.6 The establishment of sensory patch polarity is not dependent on ciliary flow

There is a possibility that ciliary flow may help to polarise the first hair cells in the developing anterior and posterior maculae (an idea suggested by Masashi Tanimoto, personal communication). To see if this was the case I examined 27hpf *lrrc50* mutant and sibling embryos to determine the polarity of the first hair cells formed in the anterior and posterior maculae. It had already been reported that hair cells at this stage have formed stereociliary bundles (Tanimoto et al., 2011) and stereociliary bundles are visible in my high-speed movies of 24–25hpf embryos (see Figure 3.3G for an example).

Polarity patterns were made by examining confocal stacks through 27hpf *lrrc50* mutant and sibling anterior and posterior maculae (Figure 5.10). Though the exact positioning and number of hair cells was variable at this stage, there was no obvious defect in the polarity of these hair cells in *lrrc50* mutant embryos when compared to siblings. Two anterior and two posterior maculae were examined from both *lrrc50* mutant and sibling embryos.

Observation with high-speed videomicroscopy confirmed that cilia where immotile in *lrrc50* mutant embryos both before 24hpf and at 24–25hpf (see Section 4.2.5).

The independence of hair cell polarity establishment from ciliary flow suggests that the hair cell polarity is established by either a mechanism intrinsic to the hair cell, or more likely, by a mechanism that depends on communication between the hair cell and

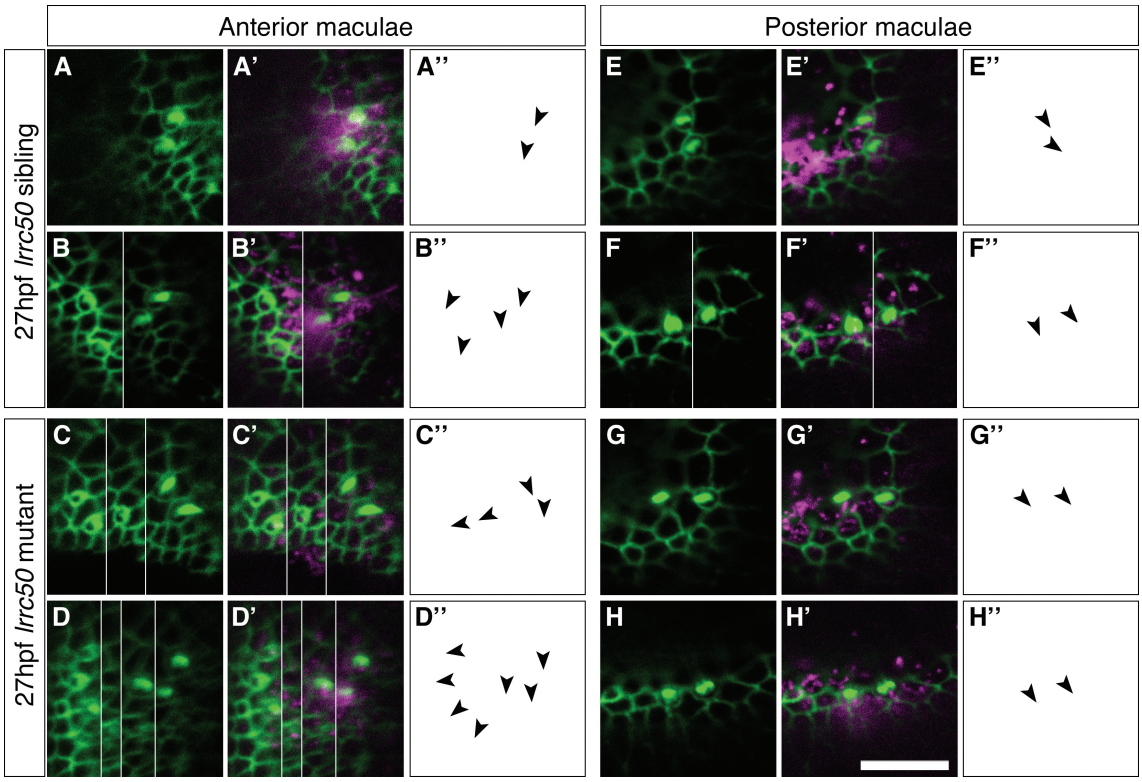

Figure 5.10: Early stereociliary bundle polarity appears unaffected in the absence of ciliary motility (27hpf *lrrc50* mutant embryos). A–A" and **B–B"**. Confocal slices and polarity patterns for 27hpf *lrrc50* sibling anterior maculae stained with FITC-phalloidin (green) and anti-acetylated tubulin (magenta). Dorsal views with anterior to left. Panels A–A" show anterior macula of right ear that has been flipped vertically to allow comparison with other panels. **C–C"** and **D–D"**. Confocal slices and polarity patterns for 27hpf *lrrc50* mutant anterior maculae. Dorsal views with anterior to left. **E–E"** and **F–F"**. Confocal slices and polarity patterns for 27hpf *lrrc50* sibling posterior maculae. Lateral views with anterior to left. **G–G"** and **H–H"**. Confocal slices and polarity patterns for 27hpf *lrrc50* mutant posterior maculae. Lateral views with anterior to left. Scale bar: 10μm, applies to all panels. Vertical white lines in panels B, B', C, C', D, D', F and F' indicate where confocal slices of different z-postions have been interposed in order to show the polarity of all hair cells in the maculae.

surrounding cells. This is discussed further in Section 5.3.

5.2.7 The hair cell cuticular plate is nearly normal in mutants lacking cilia or ciliary motility

A preliminary study was done to see if there might be an effect on the morphology of the cuticular plate (see Section 1.3.4 for a description of hair cell anatomy) in mutant embryos lacking or with defective cilia (Figure 5.11). As mutants completely lacking cilia are capable of forming correctly polarised hair cells within the sensory patch (Section 5.2.1), this means that a polarised stereociliary bundle is capable of forming in the absence of a kinocilium. The alternative to a polarised stereociliary bundle is an unpolarised bundle where the gap for the kinocilium is absent or within the bundle instead of on the edge; for example, unpolarised bundles are seen in the cochlea of conditional *Ift88* knock out mice (Jones

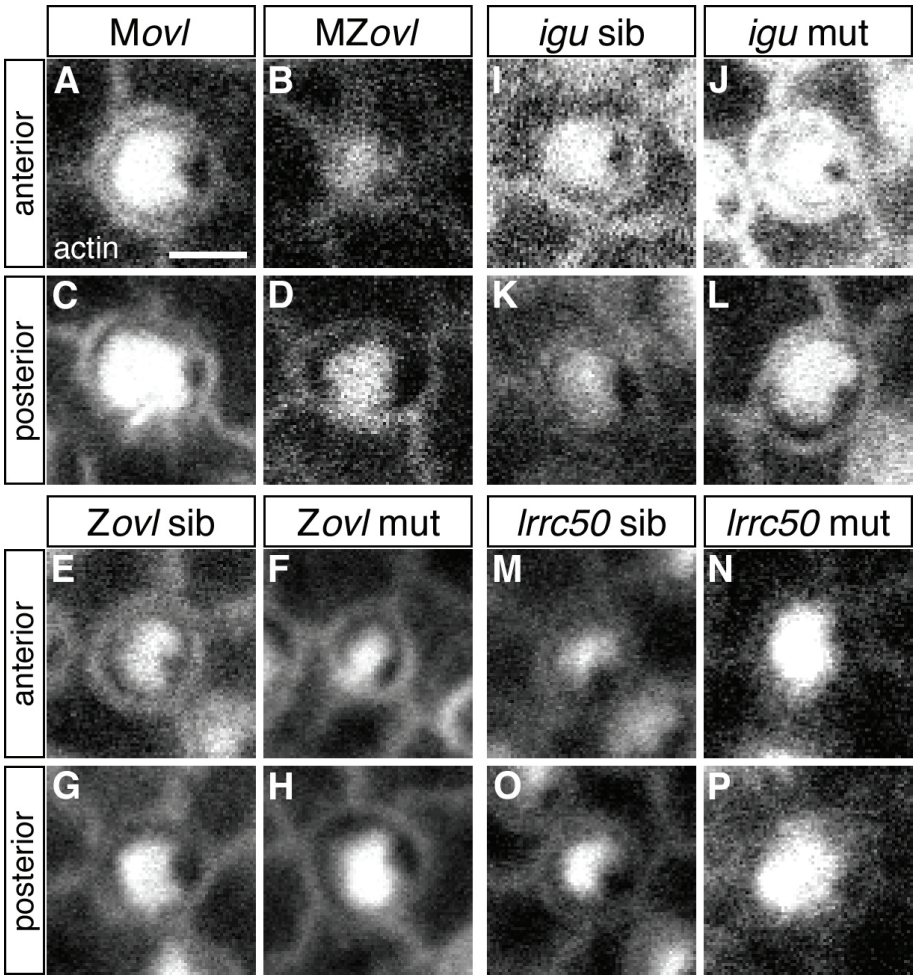

Figure 5.11: Cuticular plate morphology in hair cells lacking cilia or with no ciliary motility. All panels show a single confocal slice of a FITC-phalloidin stained cuticular plate. Bundles were from anterior or posterior maculae, as indicated. Panels have been rotated such that all panels show a comparable polarity, with the gap for the kinocilium to the right hand side. Scale bar: 2μm, applies to all panels. **A**–**D**. Cuticular plate morphology appears less well defined in MZ*ovl* (complete lack of cilia) compared to M*ovl*. **E**–**H**. The gap for the kinocilium appears to be less well defined in Z*ovl* mutant hair cells (lack of the kinocilium was confirmed by looking at the anti-tubulin stain for the confocal slice) than in Z*ovl* sibling hair cells. **I**–**L**. There is no apparent difference in plate morphology between igu^{tm79a} mutant and sibling hair cells, which all have a kinocilium. **M**–**P**. There may be a difference in plate morphology between *lrrc50* mutant and sibling embryos. The data are poor and so it was not possible to determine if there was an affect on the formation of the gap for the kinocilium.

et al., 2008).

Examination of stereociliary bundles lacking an associated kinocilium suggests that although the stereociliary bundle is polarised, the gap for the kinocilium is less well defined at the level of the cuticular plate than in sibling embryos where a kinocilium was present (Figure 5.11A–H).

If a kinocilium was present, as in igu^{tm79a} mutant embryos, then the cuticular plate had a kinociliary gap that was as well defined in the mutant as the sibling embryo (Figure 5.11I–

L).

Preliminary data for *lrrc50* mutant embryos were inconclusive (Figure 5.11M–P). It appears that *lrrc50* mutant cuticular plates may form a less well defined gap for kinocilia. However, preliminary confocal data for this mutant were poor quality. As *igu* mutant hair cells with a kinocilium form a well defined gap for the kinocilium, it would be surprising to find that *lrrc50* mutant hair cells, which all have a kinocilium, were unable to form as well defined a gap for the kinocilium as sibling hair cells.

The polarity of the cuticular plate and associated stereociliary bundle in zebrafish could be determined by positioning of the basal body as opposed to the kinocilium. As the basal body is capable of docking to the hair cell apical surface in MZ*ovl* mutants (Huang and Schier, 2009) this suggests that the mechanism of polarising the stereociliary bundle is dependent on correct polarity of the basal body at the hair cell apical surface. However, formation of the kinocilium appears to be required for the cuticular plate to form a well-defined gap for the kinocilium.

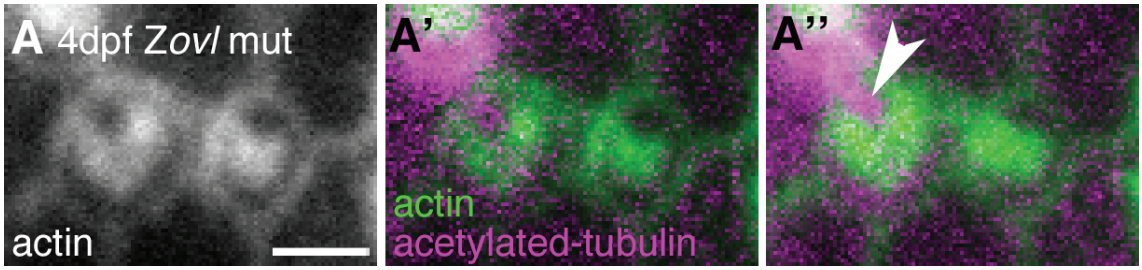

Figure 5.12: Within macula comparison of stereociliary bundle morphology with and without a kinocilium. A. Single confocal slice showing two stereociliary bundles from the anterior macula of a 4dpf Z*ovl* mutant embryo stained with FITC-phalloidin. The hair cell on the left had a kinocilium; the hair cell on the right did not. Scale bar: 2μm, applies to all panels. **A'**. The same confocal slice as in A, also showing the anti-acetylated tubulin antibody stain (magenta). **A"**. Maximum confocal projection through the two stereociliary bundles. The kinocilium of the left bundle is indicated by an arrowhead. The stereociliary bundle appears more defined when a kinocilium is present. However, it is not certain that both stereociliary bundles are at the same stage of development.

The Z*ovl* mutant anterior macula pictured in Figure 5.3B provided an opportunity to compare the morphology of hair cells with and without a kinocilium within a single macula (Figure 5.12). The two hair cells adjacent to one another showed that the hair cell with a kinocilium had a more defined gap for the kinocilium in the cuticular plate (Figure 5.12A) than the hair cell that lacked a kinocilium. As a fixed sample was examined it is not possible to say if the hair cell lacking a kinocilium had lost its kinocilium in the process of degeneration, as described in Tsujikawa and Malicki (2004), or if the hair cell without a kinocilium was less mature than the hair cell with a kinocilium, and so did not have as well-developed a cuticular plate and stereociliary bundle.

It would be interesting to do a more in-depth study of hair cell development in Z*ovl* mutants to see if hair cells differentiate without forming a kinocilium, as presumably occurs in MZ*ovl* embryos.

5.2.8 The number of hair cells in the posterior macula of a mutant completely lacking cilia is reduced from 48hpf

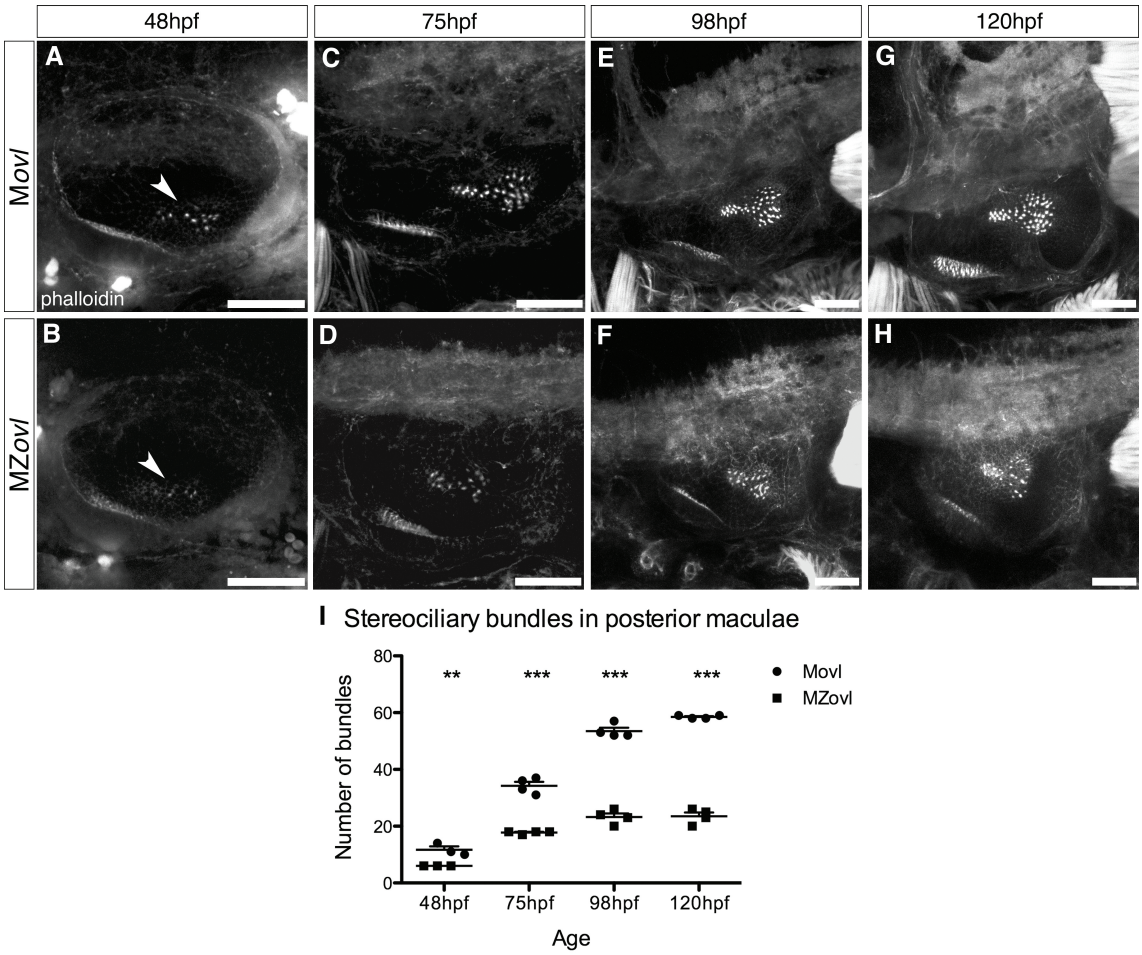

Figure 5.13: Embryos lacking cilia (MZ*ovl*) show defects in stereociliary bundle formation in the posterior macula from 48hpf. A–H. FITC phalloidin-stained otic vesicles of M*ovl* and MZ*ovl* embryos at stages from 48–120hpf. All are maximum confocal projections through the posterior macula of the left OV; lateral views with anterior to the left. Scale bars: 50μm. The posterior macula is indicated with an arrowhead in A and B. MZ*ovl* posterior maculae are slightly misshapen compared to M*ovl* posterior maculae. **I**. Graph comparing number of stereociliary bundles in posterior maculae of M*ovl* and MZ*ovl* from 48–120hpf. Two-way ANOVA analysis showed that the effect of age, genotype and the interaction between the two were all highly significant on the number of stereociliary bundles in the posterior macula, with $p<0.0001$. Stars indicate the effect of genotype in the mean number of stereociliary bundles for each age (** = $p<0.01$, *** = $p<0.001$). For 48hpf, n=3 for each genotype. For all other ages analysed, n=4 for each genotype.

Whole-mount phalloidin stained MZ*ovl* and M*ovl* embryos were examined by confocal microscopy at 48, 75, 98 and 120hpf to observe the development of the posterior macula within the OV (Figure 5.13). The MZ*ovl* posterior macula developed in the normal location in the ear (M*ovl* embryos acted as phenotypically wild-type controls), but appeared slightly misshapen in comparison to M*ovl* maculae. Specifically, MZ*ovl* posterior maculae appear shorter along the anterior-posterior axis than M*ovl* posterior maculae at 75, 98 and 120hpf.

I found a significant decrease in the number of stereociliary bundles making up the MZ*ovl* posterior maculae at every stage examined (Figure 5.13I). This is in contrast to the finding that the number of stereociliary bundles in the anterior macula of Z*ovl* mutant embryos is not significantly different to wild-type at 2dpf (Tsujikawa and Malicki, 2004). As I made no observation of hair cell number in the anterior maculae of MZ*ovl* over development, it is not possible for me to say if this difference in findings is due to a difference between development of the anterior and posterior maculae in *ovl* mutants, or if the failure of the MZ*ovl* mutant to form any cilia leads to an earlier phenotype than in the Z*ovl* mutant, which initially forms cilia (Tsujikawa and Malicki, 2004).

5.2.9 Mutants with a partial or complete loss of cilia have defects in the development of dorsolateral ear structures

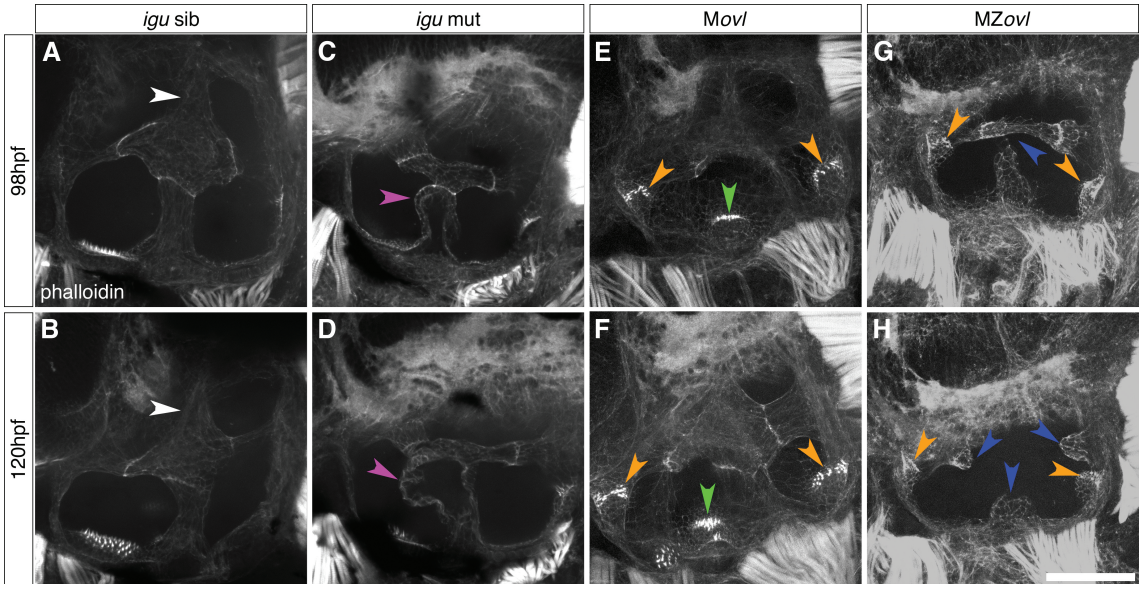

Figure 5.14: Mutants that have reduced cilia number (*iguana*) or lack cilia (MZ*ovl*) have abnormal inner ear morphogenesis. Panels A–D were provided by Kate Hammond. All panels show maximum confocal projections through the canal pillars of FITC-phalloidin stained left ears; lateral views with anterior to left. **A**, **B**. Canal projections of phenotypic wild-type 98hpf and 120hpf *igu* sibling embryo. White arrowheads indicate the dorsolateral septum. **C**, **D**. Canal projections and cristae of 98hpf and 120hpf *igu* mutant embryos. The dorsolateral septum has failed to form. Magenta arrowheads indicate an abnormal bulge where the ventral canal pillar meets the anterior and posterior projections. **E**, **F**. Canal projections of phenotypic wild-type 98hpf and 120hpf M*ovl* embryos. Green arrowheads indicate the lateral crista. Orange arrowheads indicate the anterior and posterior cristae. **G**, **H**. Canal projections and cristae of 98hpf and 120hpf MZ*ovl* embryos. Blue arrowheads indicate failure of canal projections to grow out or fuse normally (the phenotype was variable). Both the lateral crista and dorsolateral septum fail to form. The anterior and posterior cristae were still present (orange arrowheads). Scale bar in H: 100μm, applies to all panels.

Observation of 4 and 5dpf *igu* and MZ*ovl* semicircular canal projections and cristae stained with FITC-phalloidin revealed that these mutants have a loss of dorsolateral structures in the OV (data for *igu* embryos obtained by Kate Hammond).

igu mutants that have a reduced number of cilia (Section 4.2.3) fail to form the dorsolateral septum of the semicircular canals and show a defect in semicircular canal pillar fusion (Figure 5.14C, D). It has previously been reported that in approximately 30% of *igu* embryos the lateral crista is absent or reduced (Hammond et al., 2010).

Preliminary findings indicate that the defect in MZ*ovl* mutants that completely lack cilia appears to be even more severe (98hpf MZ*ovl* embryos, n = 3; 120hpf MZ*ovl* embryos, n = 3): in addition to loss of the dorsolateral septum there is a variable effect on growth and fusion of the semicircular canal pillars (blue arrowheads, Figure 5.14G, H) and the lateral crista is lost (Figure 5.14G, H). The anterior and posterior cristae were still present in MZ*ovl* embryos (orange arrowheads, Figure 5.14G, H), but morphology and hair cell number of mutant anterior and posterior cristae was not assessed.

These defects in inner ear morphogenesis in the reduction or absence of cilia may indicate that cilia-mediated signalling plays a role in shaping dorsolateral structures of the inner ear. Previous work shows that a gain of Hedgehog signalling leads to a loss of dorsolateral structures in the zebrafish OV (Hammond et al., 2010). As cilia are required for transduction of the hedgehog signalling pathway in zebrafish (Huang and Schier, 2009) it is logical that Hh signalling is mis-regulated in the reduction or absence of cilia seen in *igu* and MZ*ovl* mutants.

It should be noted that both *igu* and MZ*ovl* mutant embryos have several developmental defects, including abnormal neural patterning (Sekimizu et al., 2004; Huang and Schier, 2009). Signals from the hindbrain are required for otic placode specification (Whitfield, 2002; Abbas and Whitfield, 2010), so it follows that defects in patterning of the hindbrain may lead to defects in otic vesicle morphogenesis. The *igu* and MZ*ovl* mutants are also slightly developmentally delayed when compared to *igu* siblings and M*ovl* embryos. This suggests that ear morphogenesis may also be delayed in mutant embryos, though abnormal morphology such as the bulge seen on the ventral canal pillar in *igu* mutants (Figure 5.14C, D) suggests that the ear defects seen are not only due to developmental delay. Also, the structures absent at 98hpf in mutant embryos, but present in 98hpf sibling embryos (lateral crista and dorsolateral septum) are still absent at 120hpf in the mutant embryos, suggesting that their absence is not due to delayed development.

It is also possible that either or both of Dzip1 (the protein disrupted in *igu*) and Ift88 (the protein disrupted in *ovl*) have functions in ear development beyond their role in ciliogenesis. For example, Ift88 has been shown to be involved in mammalian cell cycle progression (Robert et al., 2007), mitotic spindle orientation in mouse and zebrafish (Delaval et al., 2011), and oriented cell division in gastrula and neurala stage zebrafish embryos (Borovina and Ciruna, 2013). Such possibilities must be ruled out before the ear defects seen in *igu* and MZ*ovl* mutants can be attributed solely to defects in ciliogenesis.

5.2.10 Polarity graphs may aid the comparison of macular polarity between different zebrafish lines

I investigated the possibility of using polarity graphs to aid comparison of different mutant and sibling maculae (Figure 5.15). I did not have enough complete or nearly complete polarity patterns for most of the genotypes analysed. In order to produce a polarity graph a polarity arrow pattern needed to be nearly complete so as not to bias the data shown in the polarity graph.

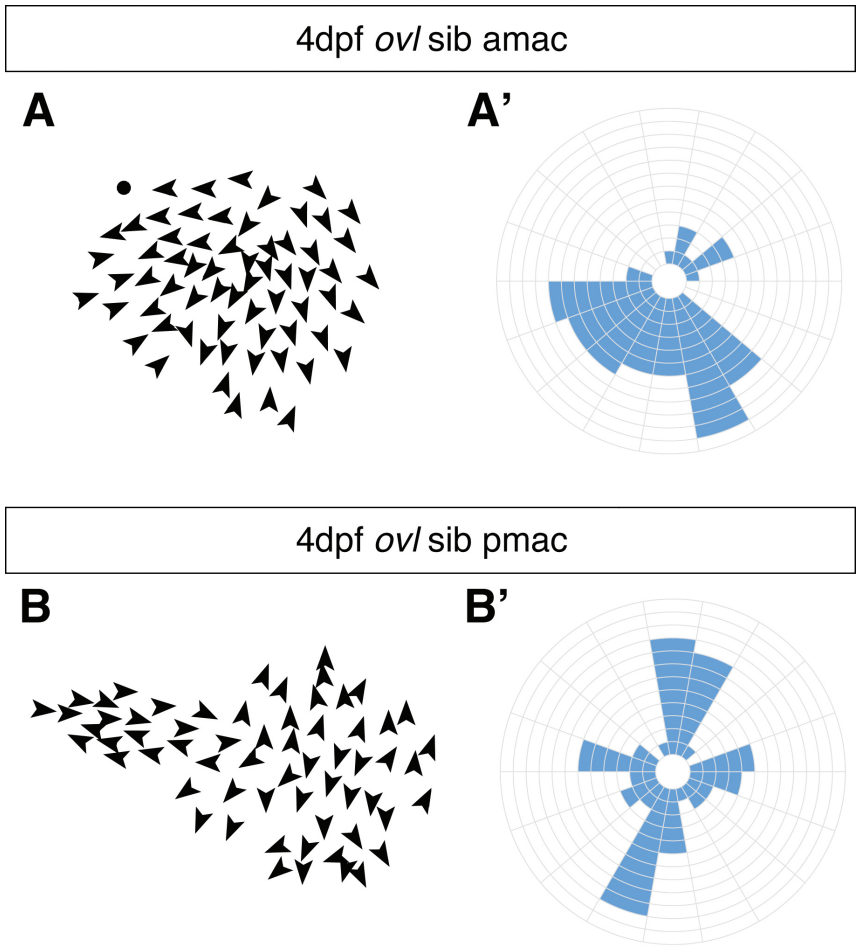

Figure 5.15: Polarity graphs of 4dpf ovl sibling maculae. Anterior and posterior maculae from Z*ovl* sibling embryos were selected to make example anterior and posterior polarity graphs due to their completeness. **A**. The same polarity pattern that appears in Figure 5.3A". **A'**. Polarity graph of the macula shown in A. Each filled in blue section represents one hair cell of that orientation in the polarity diagram. The main body of the fan of hair cells is represented by the blue bars at the bottom of the graph. The zone of polarity reversal at the lateral edge of the macula is represented by the blue bars at the top-right of the graph. The hair cell where polarity could not be determined (dot in A) is not included in the graph. **B**. The same polarity pattern that appears in Figure 5.4A". **B'**. Polarity graph of the macula shown in B. The bars to left and right represent the anti-parallel polarity hair cells at the anterior portion of the macula; the bars to top and bottom of the macula represent the dorsal and ventral polarised hair cells in the posterior portion of the macula.

The polarity graphs that I did produce (Figure 5.15) demonstrate the stereotyped pattern of polarity for both anterior and posterior maculae at 4dpf. This technique may prove useful for future investigations of zebrafish sensory maculae hair cell polarity as comparing these graphs by eye would be simpler than comparing arrow-based polarity patterns.

5.3 Discussion

I have investigated the effects of a complete lack of cilia (MZ*ovl*), a severe loss of cilia (Z*ovl*), a partial loss of cilia (igu^{tm79a}), and a loss of ciliary motility (*lrrc50*) on the formation of stereocilia and on sensory patch polarity in the 4dpf zebrafish OV. In addition, I have looked at the effect of a complete lack of cilia (MZ*ovl*) or a partial loss of cilia (igu^{tm79a}) on morphogenesis of the zebrafish inner ear.

I have found that hair cells can form near-normal stereociliary bundles in the absence of a kinocilium. All stereociliary bundles that were imaged at the correct angle by confocal microscopy had a recognisable polarity, with a gap for the kinocilium present in the cuticular plate (Section 5.2.7). I never saw a stereociliary bundle or cuticular plate with a kinocilium, or gap for a kinocilium, in the middle. This is in contrast to the finding that approximately 10% of mouse cochlear outer hair cells mutant for *Ift88* form non-polarised circular bundles, some of which have centrioles in the centre, and form a 'donut' shape (Jones et al., 2008). This may be because teleost hair cells polarise earlier during development of the apical sensory structures. An electron microscopy study of the development of the saccule in the toadfish *Opsanus tau* did not find a stage where stereocilia are surrounding the hair cell kinocilium (Sokolowski and Popper, 1987), as is seen in early chick auditory (Tilney et al., 1992), and mouse vestibular (Denman-Johnson and Forge, 1999) hair cells. Scanning electron micrographs of zebrafish lateral line hair cells at various stages of maturity also show that stereocilia form on only one side of the kinocilium and that kinocilial-links and tip-links are present from very early stages (Kindt et al., 2012). There is no study of zebrafish utricular or saccular development that has been carried out with SEM at a high enough magnification to confirm the findings of Kindt and colleagues also hold true in the inner ear.

In all the cilia mutants I studied, the overall polarity of anterior and posterior maculae was preserved, though it was not possible to get data from a full macula with the *ovl* mutants, which lacked cilia, as it was more difficult to determine polarity of the hair cell in absence of a kinocilium. However, hair cells where polarity could be determined had the expected polarity for their position within the epithelium (Sections 5.2.1 and 5.2.2). This result is not surprising, as studies of the relationship between planar cell polarity (PCP) pathways and ciliogenesis have suggested that non-canonical Wnt signalling acts upstream of ciliogenesis in the zebrafish, with evidence that PCP pathways are required to correctly position the basal body on the apical surface of polarised tissue before ciliogenesis

occurs (Borovina et al., 2010; Caron et al., 2012). Therefore, polarity of the stereociliary bundle is likely to depend on correct positioning of the basal body in zebrafish, and not on positioning of the kinocilium. However, a study looking at stereociliary bundle morphology in the zebrafish lateral line using SEM reported that kinocilia were severely stunted (0.29μm length, compared to 14.42μm in wild-type), as opposed to completely absent, in Z*ovl* mutant embryos (Kindt et al., 2012). Electron microscopy has not been performed on the MZ*ovl* mutant and so it is possible that a severely stunted kinocilium can still form, and this could play a role in polarising the stereociliary bundle.

The signalling pathways that produce the overall polarity pattern of the vestibular epithelium in vertebrates are not yet known. A recent review (Deans, 2013) suggests two possibilities, both of which rely on classic PCP pathways acting across the vestibular epithelium, giving the tissue a unidirectional 'ground' polarity. A secondary mechanism may then enable this ground polarity to be interpreted differently by hair cells in different areas of the macula. For instance, hair cells on either side of the zone of polarity reversal in the zebrafish anterior macula will interpret this signal to produce oppositely polarised hair cell bundles. One possible model is that the secondary mechanism is due to a gradient of a second signalling pathway, such as Wnt. In *C. elegans* vulval development, cell divisions either side of the vulva are mirror symmetric due to the interaction of multiple Wnt pathways, allowing different interpretations of the 'ground' PCP signal across the vulva (Green et al., 2008). An alternative possibility is that hair cells on either side of a line of polarity reversal have different transcriptional profiles, and therefore respond to the ground polarity signal in different ways. The transcription factor *Emx2* has been shown to be required for reversal of polarity in the mouse vestibular epithelia (Holley et al., 2010). In zebrafish *emx2* is expressed in the OV from 1dpf (Thisse and Thisse, 2005) and may be a good candidate for investigation into polarity pattern establishment. An earlier theory for generation of hair cell polarity hypothesised that the extracellular matrix may contact hair cell kinocilia during growth, and pull them into the correct orientation (Cotanche and Corwin, 1991). However, this theory was discounted when observations of the mouse vestibular epithelium showed even growth of the otoconial membrane and orientation of hair cell bundles before the kinocilium was long enough to make contact with the otoconial membrane (Denman-Johnson and Forge, 1999).

The loss of dorsal and lateral ear structures in zebrafish mutants lacking cilia reflects the finding that zebrafish mutants without cilia fail to regulate Hh signalling correctly, losing very high-level response to Hh signal and increasing the domain of low-level Hh response (Huang and Schier, 2009). The effect of loss of cilia on OV morphogenesis is consistent with zebrafish mutants that fail to fully repress Hh signalling (Hammond et al., 2010), suggesting that it is an expansion of low-level Hh signalling within the OV causing the phenotype in *igu* and MZ*ovl* mutants. Strong repression of Hh signalling during zebrafish development leads to a double anterior OV, whilst stong up-regulation of Hh signalling leads to a double posterior OV (Hammond et al., 2003). Although cilia are com-

pletely absent in the zebrafish MZ*ovl* mutant (Huang and Schier, 2009), the loss of cilia does not cause a dramatic reduction in Hh signalling as seen in *Ift88* null mutant mice (Huangfu et al., 2003). Huang and Schier (2009) suggest that this phenotypic difference between the two species is due to differential expression of *gli1* in the mouse and zebrafish: mouse *Gli1* expression is fully dependant on Hh signalling (Bai et al., 2002), whereas zebrafish *gli1* is still expressed at a low level in the absence of any Hh signalling pathway activity (Karlstrom, 2003; Ninkovic et al., 2008).

5.4 Conclusion

In this chapter I confirm that the immotile cilia within the zebrafish OV play an important role in development and morphogenesis of the inner ear. Without a full complement of cilia, the zebrafish OV lacks hair cells in the saccule at 4dpf, and if the reduction in cilia is severe the utricle also lacks hair cells. Cilia are required for the normal morphogenesis of dorsolateral structures in the zebrafish inner ear, providing further evidence for their role in Hh signal transduction.

I also find that in the zebrafish hair cell polarity is determined independently of cilia or before ciliogenesis has occurred. This suggests that zebrafish hair cells develop in a slightly different way to hair cells in the mouse.

Chapter 6

Discussion

6.1 Overview of results

This thesis presents data on the role of cilia in the zebrafish otic vesicle (OV). A description of cilia and ciliary motility in the wild-type otic vesicle is given in Chapter 3. The role of cilia and hair cells in otolith tethering and development is more thoroughly investigated by mutant and morpholino approaches (Chapter 4). Finally, a study addressing the role of cilia in OV patterning and morphogenesis is presented (Chapter 5).

I find that the majority of cilia present in the zebrafish OV during early ear development (18–24hpf) are immotile. These immotile cilia presumably have a role in developmental signalling pathways, and this is investigated further in Chapter 5. Motile cilia are concentrated at the anterior and posterior poles of the OV, around the kinocilia, or tether cilia, of the first hair cells where the otoliths nucleate and grow. There are also a small number of motile cilia on the medial wall of the OV. I hypothesise that the role of these motile cilia is to prevent ectopic aggregation of otolith precursor particles to form a third otolith.

As the otoliths always nucleate on the tips of the kinocilia of the first hair cells I investigated if and how otoliths would tether if cilia were completely absent by using the maternal zygotic *ovl* mutant. Surprisingly, in the complete absence of cilia otoliths were still able to tether in the OV. Instead of tethering to the tips of kinocilia they instead tethered to the apical membranes of the first hair cells. I also investigated mutants with a partial loss of cilia (*iguana*), that normally had the kinocilia present, and mutants with a loss of ciliary motility (*lrrc50*). These experiments indicated that ciliary motility is required to prevent the formation of an ectopic untethered otolith in the OV.

As hair cells seemed to be the exclusive point of otolith tethering within the OV I manipulated hair cell number in the OV to see how otolith tethering and cilia were affected. I found that otolith precursor particles cannot tether in the absence of hair cells, and instead form a single untethered otolith within the OV (embryo injected with *atoh1b* morpholino). However, hair cells are not required for the formation of motile cilia within the OV. If ectopic hair cells were present (*mindbomb* mutant or *Su(H)1+2* morpholino

injection) all ectopic hair cells were capable of binding otolithic material. In the complete absence of cilia, otoliths still could not tether if hair cells were absent, and ectopic hair cells could all tether otolith precursor particles to their apical surface.

As the otolith precursor particles are denser than the surrounding OV fluid I investigated if movement of the embryo was required to prevent aggregation of otolith precursor particles in the lowest point of the OV. I found that restricting normal embryonic movement increased the proportion of ears with ectopic otoliths. I also found that it was possible to partially rescue the formation of an ectopic third otolith in mutants lacking cilia or without ciliary motility by forcing embryonic movement. The formation of otoliths is a mechanical as well as a genetic process, depending on physical factors as well as signalling pathways.

Investigating the role of cilia in OV growth after 24hpf revealed that cilia are required for normal OV morphogenesis and hair cell number in the utricle and saccule. Complete loss of cilia (MZ*ovl*) resulted in a loss of dorsolateral ear structures and a reduction in the number of hair cells in the utricle and saccule at 4 and 5dpf. A partial loss of cilia (*iguana*) resulted in a less severe loss of dorsolateral ear structures and a reduction of hair cell number in only the saccule. Ear structure was not investigated in mutants lacking ciliary motility (*lrrc50*) but a reduction in hair cell number in the saccule was seen. Cilia were not required for hair cell polarity in the sensory maculae. Even in the complete absence of cilia the hair cell stereociliary bundle was able to form the wild-type horseshoe shape and was correctly polarised based on its overall position within the macula.

In the next sections I discuss how best to continue this research and the context of my findings in the wider fields of ear and cilia development and disease.

6.2 Finding the otolith precursor binding factors

The observation that otoliths always tether to the hair cell kinocilia has led to the hypothesis that hair cells produce one or more otolith precursor binding factors (Riley et al., 1997; Yu et al., 2011; Stooke-Vaughan et al., 2012). The otolith precursor binding factor or factors will be capable of interacting with one or more of the proteins making up the otolith precursor particles, so sticking them to the tip of the hair cell kinocilium.

An interesting direction to continue this work in would be to try to characterise the otolith precursor binding factors. It would be expected that factors are required in both the hair cells and the otolith precursor particles themselves such that an adhesive interaction can take place.

Some components required for otolith tethering have already been characterised. For example *hsp90b1* (formerly *GP96*) is required for adhesion of otolith precursor particles to tether cilia (Sumanas et al., 2003). Embryos injected with a morpholino against *hsp90b1* successfully produce and secrete otolith precursor particles into the OV. However, the otolith precursor particles then fail to adhere to the hair cell tether cilia, instead aggre-

gating to form a single untethered otolith (Sumanas et al., 2003). The otolith phenotype appears similar to that of embryos injected with morpholino against *atoh1b*, although in *atoh1b* morphant embryos the failure to tether otolith precursor particles is due to the absence of the first hair cells and tether cilia (Section 4.2.8).

As mentioned in Section 4.3.2, there are uncloned zebrafish mutant lines that fail to correctly tether otolith precursor particles to the anterior and posterior tether cilia, instead forming a single otolith. Cloning these mutant lines would reveal further components required for tethering otolith precursor particles.

An example of an uncloned mutant zebrafish line that fails to tether otolith precursor particles is the *einstein* (*eis*) mutant line (Whitfield et al., 1996). The *eis* mutant has a similar phenotype to a *hsp90b1* morphant, in that otolith precursor particles are secreted into the OV but fail to tether to the kinocilia of the first hair cells, with the result that a single otolith is formed. The *eis* mutation must occur in a different gene to *hsp90b1*; *eis* has been rough-mapped to chromosome 7 (Geisler et al., 2007), whereas *hsp90b1* is located on chromosome 4 (Ensembl(Zv9):ENSDARG00000003570). Cloning *einstein* and other similar mutants should reveal other components of the otolith tethering pathway. It is unlikely that Hsp90b1 is the only otolith precursor binding factor as it is a chaperone protein. It is therefore more likely to be a component of the pathway required for localisation of an active otolith precursor binding factor to the tip of a tether cilium, as opposed to an otolith precursor binding factor that interacts with otolith precursor particles.

Another process necessary for otolith tethering is the proper secretion of otolith precursor particles into the OV. These otolith precursor particles must be able to adhere to each other and to the tips of the kinocilia of the first hair cells. An example of a zebrafish mutant that fails to properly secrete otolith precursor particles into the OV is the *otopetrin1* (*otop1*) mutant (*backstroke*). Otop1 is a transmembrane protein localised to the apical surface of cells making up the OV lumen and is required for secretion of key otolithic components. *otop1* mutants fail to secrete any otolith precursor particles into the OV. Immunofluorescent antibody staining for the Stm protein (see Table 1.1) in *otop1* mutants shows a mislocalisation to the cells surrounding the OV lumen instead of being localised within the OV lumen. The inability to secrete otolithic components into the OV leads to a complete failure of otolith formation in the *otop1* mutant (Söllner et al., 2004).

Another zebrafish mutant line that fails to form otoliths is *keinstein* (*kei*) (Whitfield et al., 1996; and see Section 3.2.3). In *kei* mutants otolith precursor particles are secreted into the OV; however, they appear smaller than normal and never adhere to each other or to the tether cilia. If examined carefully with DIC or brightfield illumination it is possible to see that there is a gelatinous looking substance localised to the tips of the kinocilia at approximately 24hpf in *kei* mutants. I have not pursued what this substance is but it may be an early stage of otolithic membrane formation, made visible due to the lack of otolith formation in this mutant. Cloning *kei* is likely to reveal a binding factor normally localised to the otolith precursor particles. This factor would then interact with factors

on the other otolith precursor particles, potentially by homodimerising, allowing them to adhere to each other. The gene coded for by *kei* may also be involved in the interaction between otolith precursor particles and the binding components on the tether cilia.

Some or all of the otolith precursor binding factors expressed by the hair cells may be components of the otolithic membrane, which forms between the sensory macula and the otolith, and is thought to play a role in adhesion of the otolith to the sensory macula. In order to be a component of the otolithic membrane it is necessary for an otolith precursor binding factor to be a secreted extracellular matrix protein.

Previous observation of teleost ears by TEM has suggested that the mechanism for otolith and otolithic membrane formation may involve the secretion of membrane bound vesicular structures from the apical surface of epithelial cells into the otic lumen (For example: Dunkelberger et al., 1980; Takagi and Takahashi, 1999). However, another study has reported that this observation is likely to be a fixation artefact (Ibsch et al., 2001), and so the mechanism of otolithic membrane production is currently unclear.

A recent study has shown that ciliary tips can act as a site for exocytosis in the unicellular alga *Chlamydomonas* (Wood et al., 2013). Flagella in *Chlamydomonas* are the only part of the cell that is not encased in a cell wall, and so the only site available for exocytosis of vesicles required for 'hatching' of *Chlamydomonas* daughter cells from the cell wall of the mother cell. Exocytosis has not yet been observed in any other cilia, so this may be a specialised adaptation in *Chlamydomonas*. However, discovery of this mechanism raises the intriguing possibility that exocytosis from the tips of the kinocilia in the zebrafish OV may be involved in establishment and maintenance of otolith tethering, or development of the otolithic membrane.

Another potential mechanism that may be involved in normal otolith and otolithic membrane development is autophagy. Mice deficient for a component of the autophagy pathway, Atg5, fail to correctly localise Otolin1, Otopetrin and Oc90 within the utricle, have otoconia which are large and reduced in number, or missing entirely, and have a severe balance phenotype (Mariño et al., 2010). A study in which *atg5* was knocked down by morpholino injection in zebrafish embryos reported some defects in development of the otic vesicle and otoliths but did not look at the effect in detail (Hu et al., 2011). Mariño et al. (2010) proposed that autophagy was required for the normal assembly and secretion of otoconial components in the mouse; it would be interesting to investigate the role of autophagy pathways in zebrafish ear development.

Experiments investigating *otolin1a* (see Table 1.1, page 26) function suggest that there are separate mechanisms of adhesion for the interaction between the otolith and tether cilia and the interaction between the otolith and otolithic membrane. Zebrafish *otolin1a* morphants maintain adhesion of the otolith to the kinocilia, but lose adhesion between the otolith and the sensory macula, resulting in a fused anterior and posterior otolith (Murayama et al., 2005). *otolin1a* is orthologous to *Otolin1*, a component of otoconia and the otoconial membrane in the mouse ear (Deans et al., 2010). The zebrafish *rolling*

stones mutant (Whitfield et al., 1996) also hints at more than one mechanism of otolith adhesion. In this mutant, otoliths initially tether and grow normally, but then the otoliths lose adhesion to the sensory maculae at 4–5dpf and become loose within the otic cavity.

There are a number of approaches available to clone the zebrafish otolith tethering mutant lines. One approach is to take previously published rough-map data for the sites of the mutations (Geisler et al., 2007), and use this information to search for candidates in the same region as the mutation. Most genes are annotated in the Ensembl zebrafish genome assembly, so searching for genes in the region of the mutation map site that are involved in ear development or extracellular matrix formation and interactions may provide candidate genes for otolith precursor binding factors (the Ensembl zebrafish genome is available at *http://www.ensembl.org/Danio_rerio/Info/Index* (Flicek et al., 2013)). A newer technique for cloning mutant lines is also being developed. This technique does not require a rough-map position but searches for areas of homozygosity in the entire genome of homozygous mutant embryos to reveal potential phenotype-causing mutations (Obholzer et al., 2012).

Once a mutation is found in a candidate gene it must be confirmed that it is the phenotype-causing mutation. This may be done in a variety of ways. Expression of the gene in the tissue of interest (the OV in the case of otolith precursor binding factors) should be confirmed by *in situ* hybridisation. If an antibody against the protein product of the gene is available it is possible to see if the protein is also localised within the tissue of interest. RNA expression and protein localisation can both be examined in the mutant to see if there is a reduction in gene expression due to improper transcription or nonsense mediated decay of mutant transcripts. Morpholino knockdown of the target gene in wild-type embryos can be used to verify that disruption of the gene function causes the mutant phenotype of interest. Another important test is to attempt rescue of the mutant phenotype by injection of either mRNA for the gene of interest, or injection of a BAC carrying the region of genome containing the gene of interest and associated promoter sequence. Generally, once expression, knock-down and rescue experiments have been carried out, it is possible to be confident that the mutation isolated by cloning is within the gene associated with the (for example, otolith) phenotype.

We have all the experimental tools required to clone and characterise the zebrafish otolith tethering mutants; it will be possible to clarify the processes of otolith nucleation and otolithic membrane formation in the very near future. Learning more about otolith formation in the zebrafish may also lead to new research avenues for understanding otoconia formation in mammals.

6.3 The role of cilia in zebrafish hair cell development

It appears that cilia are not required for hair cell specification and the formation of a stereocilary bundle in the zebrafish; however, the kinocilium does appear to have a role in hair cell maintenance. It had already been reported that zebrafish zygotic *ovl* mutants

initially produced a normal complement of sensory cells, including hair cells. However, the loss of hair cell kinocilia by 3dpf is followed by the loss of hair cells by 5dpf (Tsujikawa and Malicki, 2004). I have found that hair cells developing in the complete absence of a kinocilium (maternal zygotic *ovl* mutant (Huang and Schier, 2009)) still differentiate and form polarised stereociliary bundles. However, MZ*ovl* bundles and their associated cuticular plates may have slight defects (Section 5.2.7). Investigations into the requirement of the kinocilium for hair cell morphogenesis in the zebafish would be best continued by performing Scanning Electron Microscopy (SEM) on wild-type and MZ*ovl* zebrafish embryos with the aim of capturing a time series of hair cell development and maturation in the presence and absence of the kinocilium.

The kinocilium is required to establish within-cell polarity in mammalian hair cells (Jones et al., 2008), but my results suggest that this does not appear to be the case in the zebrafish. All hair cell bundles that were imaged at the correct angle in mutants without cilia had a recognisable polarity. Although I never saw any occurrences of a 'donut' shaped bundle, with the gap for the kinocilium in the middle, I cannot rule out the possibility that some bundles where I could not determine the polarity represented unpolarised bundles with no gap for a kinocilium and not bundles that were imaged at the wrong angle to determine polarity.

Kindt et al. (2012) show that Z*ovl* mutant kinocilia are severely stunted but not absent in 3dpf lateral line neuromasts. Therefore to be sure that there is never a kinocilium present on MZ*ovl* mutant hair cells, SEM should be used to verify the negative anti-acetylated tubulin antibody stain in the inner ear. SEM would also allow a more detailed analysis of bundle polarity in the ear.

MZ*ovl* mutants completely lacking cilia had reduced hair cell number in both the utricle and saccule. Mutants with a less severe loss of cilia or with a loss of ciliary motility had a reduced number of hair cells in the saccule only. Why this happens and what signalling pathway is involved is not clear. It has been shown that sensory cells in zebrafish Z*ovl* (zygotic *ift88*) mutants initially form cilia, but the cilia then degenerate. Degeneration of sensory cell cilia is then followed by sensory cell loss (Tsujikawa and Malicki, 2004). Tsujikawa and Malicki (2004) found that degenerating hair cells were marked by TUNEL staining, indicating that cell death was mediated by the apoptotic pathway. Although it is known that loss of cilia leads to hair cell degeneration, it has not yet been tested if ciliary loss also affects hair cell proliferation. This could be tested by performing proliferation assays in mutants lacking cilia such as MZ*ovl* and *igu*.

There has been a study into hair cell development and functional maturation in *ovl* mutant zebrafish. Kindt et al. (2012) showed that *ovl* mutant embryos form lateral line hair cells that develop normally and have normal polarity. However, hair cells lacking kinocilia fail to develop mechanotransduction in the same way as wild-type hair cells. Wild-type hair cells show an initial stage of 'reversed' functional polarity, where the hair cell depolarises in response to deflections of the kinocilium towards the stereociliary bundle. This

polarity later develops, via a bidirectional response phase, to the mature response when the hair cell depolarises as the kinocilium is deflected away from the stereocilia. Mutants lacking kinocilia never show the initial reversed polarity phases, but do successfully develop the mature mechanotransductive response. This suggests that the initial immature reversed functional polarity requires the kinocilial links, the links between the stereocilia and kinocilium (Kindt et al., 2012). Confirming these findings in hair cells of the inner ear would be informative and allow comparison of the developmental timing of the onset of inner ear hair cell compared with lateral line hair cell function.

A stage of reversed functional polarity has not been described for amniote hair cell development. This may be because it is more technically challenging to investigate gain of hair cell function in amniote species as the embryos are developing within an egg or the mother. Alternatively, it is possible that amniote hair cells do not experience a stage of reversed functional polarity in immature hair cells. Studies in which SEM has been performed on developing teleost hair cells suggest that the stereocilia develop in a polarised manner (Sokolowski and Popper, 1987; Kindt et al., 2012), compared to the initial unpolarised production of microvilli seen in chick auditory (Tilney et al., 1992) and mouse vestibular hair cells (Denman-Johnson and Forge, 1999), indicating that teleost hair cell development proceeds in a slightly different manner to amniote hair cell development.

The reason for the differences between hair cell maturation in teleosts and amniotes may be because there are different environmental pressures on the larvae and embryo. An embryonic amniote is in a stable environment (egg or uterus) and does not need to react to risk of predation or to hunt. In contrast a fish embryo that develops outside the mother, with no parental care, matures to a larval stage very quickly (hatching occurs at 3dpf in the zebrafish). After hatching the fish larva will be capable of sensing and avoiding potential predators and hunting independently. Therefore hair cell maturation that makes an immature hair cell responsive to environmental stimulus should be advantageous in comparison to a lengthy maturation process. It would be interesting to test this hypothesis. One way to do this could be by comparing hair cell development between different fish species that need to live independently at different developmental stages. For example, a species with no parental care could be compared to a closely related species with parental care. A comparison of hair cell development in viviparous and egg scattering species within the family Poeciliidae (the family containing guppies, mollies, platyfish, and others) would satisfy this experiment.

6.4 Cilia-mediated signalling in the otic vesicle

Non-motile cilia are known to be the localisation site for components of several signalling pathways, including hedgehog (Hh) signalling (see Section 1.2.4). It was therefore interesting to investigate how disrupting cilia affected OV formation and morphogenesis. Mutants completely lacking cilia still formed an OV with anterior and posterior poles containing

hair cells, and were able to nucleate otolith formation on the apical surface of the hair cells. However, as ear formation progressed the ears showed signs of misregulation of the Hh signalling pathway consistent with a failure to fully repress Hh signalling. This is consistent with previous reports that cilia are required for Hh signalling in the zebrafish, and that when cilia are absent, high-level Hh activation is lost, but areas of low Hh activity are expanded (Huang and Schier, 2009). The normal formation of the otic vesicle in the absence of cilia supports the current understanding that the FGF signalling pathway does not involve cilia. Zebrafish that are mutant for *fgf3* or *fgf8* form a small OV, while fish mutant for both *fgf3* and *fgf8* fail to form an otic placode (Brand et al., 1996; Whitfield et al., 1996; Phillips et al., 2001). This implies that if cilia were required for FGF signalling in zebrafish there would be a defect in otic placode specification.

During OV development before 24hpf only a small subset (2–8%) of cilia are motile. The majority of these motile cilia are concentrated at the poles of the OV, next to the first hair cells. However, if development of the first hair cells is prevented by injection of *atoh1b* morpholino, motile cilia are still concentrated at the poles of the OV. This suggests that something other than signalling from the hair cells results in the differentiation of motile cilia at these locations. There are also normally a very few motile cilia on the medial wall of the OV, but how these motile cilia are specified when they are surrounded by many immotile cilia is not known. The signalling pathways required for establishing ciliary motility in the OV could be investigated by pharmaceutical up- and down-regulation of the various signalling pathways known to be involved in OV specification and growth, followed by observation of the OV by high-speed videomicroscopy to determine if there was any change in the distribution and number of motile cilia. Another approach could be to investigate signalling pathways regulating *foxj1b* expression, as the Foxj1 transcription factors are required for development of motile cilia on cells (Yu et al., 2008). *foxj1b* is expressed in the OV during the stages of development when motile cilia are present (Yu et al., 2011). Although Yu et al. (2011) did not report that *foxj1b* had a stage of expression where it was expressed in only a few cells on the medial wall of the OV as well as at the poles, it may be that there is some fine control of *foxj1b* expression or translation. Alternatively, factors downstream of *foxj1b* may be regulated in such a way that motile cilia are only produced on a small subset of cells.

It has been shown that *foxj1a* expression in Kupffer's Vesicle is directly regulated by Wnt/β-catenin signalling (Caron et al., 2012). Caron et al. (2012) showed that if Wnt/β-catenin signalling was downregulated in the zebrafish (using the transgenic heat-shock promoter line *Tg(hsp:dkk1-GFP)*), *foxj1b* expression in the OV is lost and otolith defects are seen. However, the size of the OV was significantly decreased when Wnt/β-catenin signalling was downregulated, so the reported otolith defects may have been partially due to the reduction in OV size as well as due to loss of motile cilia. This study does indicate that Wnt signalling may prove a useful avenue for investigation of the process responsible for specifying ciliary motility within the OV.

6.5 Imaging cilia in the otic vesicle

Research into the function of cilia in developing tissue and into the development of hair cell sensory bundles would be aided if it were possible to obtain better resolution than that possible by conventional light microscopy on living tissue. At present electron microscopy is not possible on living tissue, although some arthropod species have been observed live using SEM (Pease et al., 1966; Ishigaki et al., 2012). However, the high vacuum conditions and electron beam used in electron microscopy means that for most live animals this is not a feasible approach. More promising are the recent developments in super-resolution light microscopy, allowing visualisation of structures at better than 200nm resolution (reviewed in Schermelleh et al., 2010; Maglione and Sigrist, 2013). Although these applications were initially limited to fixed, thin samples, they are now being applied *in vivo*. Examples include: observation of dendritic remodelling in the somatosensory cortex of an adult mouse using stimulated emission depletion (STED) microscopy (Berning et al., 2012); and live 4D acquisition of microtubules in the zebrafish posterior lateral line using multifocal structured illumination microscopy (MSIM) (York et al., 2012). The theoretical lateral resolution limit of super-resolution microscopy can be as fine as 10–20nm for some techniques, though this cannot currently be met in live samples. These techniques may allow *in vivo* observation of hair cell stereociliary bundle development and the mechanism of polarisation in zebrafish lateral line hair cells in the future. It would be easier to observe hair cell development in the lateral line than in the inner ear because the lateral line is on the surface of the zebrafish embryo, allowing improved optics.

As I was not able to record ciliary motility in the OV over several hours it is not known if the motile cilia in the OV are a different cilia type, and always motile, or if the motility is transient, and perhaps dependent on some cue from the surrounding OV fluid or epithelial cells. I did try performing high-speed videomicroscopy on the OVs of zebrafish embryos mounted in low-melting point agarose in a glass bottomed dish (the set up favoured for timelapse of development over several hours). However, it was not possible to get the OV of the embryo close enough to the coverslip of the dish to allow observation with the close working distance 100× oil objective necessary for observation of ciliary motility. It is possible that with further practice and optimisation of the microscopy set up it would be possible to observe embryos mounted in low melting point agarose, thus allowing a time lapse of ciliary motility over several hours. The file sizes generated by high-speed movies are very large, so I doubt it would be possible to perform continual high-speed recording of the OV. An approach where a 100 frame movie was recorded once every 10 minutes, for example, would be more feasible.

Looking at cross sections of the microtubule axonemes of cilia throughout the zebrafish OV using TEM may also prove insightful as to whether or not the motile cilia in the OV are a transient or separate structure to the immotile cilia. Finding more than one type of microtubule axoneme in the OV (for example, if both 9+0 with no dynein arms, and

9+2 with dynein arms axonemes are found on the medial wall of the OV), would strongly suggest that motile cilia are specified in some way and that cells either have a motile or immotile cilium, and that there is no transition of motility.

6.6 Relation of my research to the understanding of ciliopathies, hearing loss, and vestibular disease

My findings regarding the role of cilia and hair cells in zebrafish ear development and otolith formation are valuable for increasing understanding of developmental biology of the zebrafish. In mammals, the otoconia form and embed in the otoconial membrane in a process that has not been connected to cilia. Mature hair cells in the mammalian cochlea lack kinocilia; however, cochlear hair cells fail to polarise normally during development in the absence of cilia (Jones et al., 2008). Increasing understanding of the role and requirement of cilia in zebrafish hair cell development may have implications for mammalian hair cell development and maintenance.

Vestibular disease is a major problem in the aging human population and is thought to be a contributory cause of falls in the elderly. However, resources allocated to research into vestibular disease are far outstripped by allocation to research into hearing loss. Research into zebrafish mutants that have defects in the establishment or maintenance of otolith tethering may prove valuable in identifying target genes or pathways to improve the stability of otoconia in older people.

There have been promising advances in research into gene therapy for ciliopathies (reviewed in McIntyre et al., 2013). One approach has been to target the olfactory sensory neurons (OSNs) in mice carrying a hypomorphic mutation in *Ift88*. These mice usually lack cilia on their OSNs, and are anosmic as a result. If the OSNs are targeted by adenoviral-mediated expression of *Ift88* in these mutants, cilia are restored and the mouse gains a sense of smell (McIntyre et al., 2012). The OSNs are accessible for pilot studies into gene therapy for ciliopathies, as they are situated in the nasal epithelium and can be targeted by an intranasal aerosol containing the adenovirus. Other cell types commonly affected by ciliopathies, such as cells lining the lumen in the kidney, are less easily accessible. Very few ciliopathies have either hearing loss or vestibular disorder as a symptom (Waters and Beales, 2011), and these symptoms are considered minor compared to other ciliopathy symptoms. Therefore I predict that developing specific treatments for any inner ear defects resulting from a ciliopathy is going to be low priority in comparison to developing treatment for the more common symptoms, such as retinal degeneration and kidney failure.

6.7 Ventral axis curvature in zebrafish cilia mutants

Most zebrafish cilia mutants have a ventral axis curvature (curly-down tail) phenotype, but the cause of this has not yet been established. Other animal models of ciliopathy do not have an axis curvature defect, so why the zebrafish embryo does is intriguing. It has been hypothesised (Supatto and Vermot, 2011) that the curved axis in cilia mutants is related to the abnormal extra cellular matrix production seen in *polycystin1+2* morphants (Mangos et al., 2010). In this case *polycystin* morphants overproduce the extracellular matrix protein Col2a1 around the notochord, leading to a dorsal axis curvature phenotype that can be rescued by genetically or pharmaceutically inhibiting *col2a1* production or function. However, Mangos et al. (2010) found that the ventral axis curvature seen in intraflagellar transport mutants *ift88* and *ift172* could not be rescued by knockdown of *col2a1*, unlike the rescue of dorsal axis curvature seen in *polycystin1* and *polycystin2* morphants.

It is interesting to note that the zebrafish *gli2a* mutant (*you-too*) also has a ventral axis curvature phenotype as most cilia mutants do (van Eeden et al., 1996; Karlstrom et al., 1999). This suggests that the curly-down tail phenotype of cilia mutant zebrafish may be largely due to misregulation of Hh signaling. Gli2a normally localises to the primary cilium, moving to the distal tip of the cilium in the presence of Hh pathway activity (Kim et al., 2010). In zebrafish igu^{ts294e} mutants Gli2a is localised to the basal body of the severely truncated cilium (Kim et al., 2010), which presumably means that Gli2a cannot function as normal and so Hh signalling is misregulated as a consequence, quite possibly in a very similar way to the misregulation seen in the *gli2a* mutant. The mechanism by which the *you-too* mutation leads to a ventrally curved body axis is not known, though the U-shaped somites and floor plate defects seen in the *you-too* mutant may be involved.

6.8 Concluding remarks

This study on the role of cilia and hair cells in inner ear development and otolith formation in the zebrafish has increased our understanding of zebrafish ear development and has led to further questions, as discussed above. My work has confirmed and clarified the requirement for cilia in normal zebrafish ear development. The role that cilia play in zebrafish ear development is, importantly, part of a larger process dependent on many factors. These factors include correct developmental signalling on both a tissue and cellular level as well as environmental and physical factors.

Using the zebrafish as a model organism in my studies of cilia and ear development has allowed me to do experiments that would not have been possible or as easy in other models. For instance, many mouse mutants that fail to form cilia die mid-gestation, before the formation of an otic vesicle. This means that to study the role of cilia in inner ear development in the mouse conditional knock out lines must be used. Studying cilia in the zebrafish is simpler, as embryos with a cilia defect are viable up to 4 or 5dpf, when many

of the structures present in the adult have already started to develop. The transparency of the zebrafish embryo and the fact it develops outside the mother also makes imaging cilia *in vivo* much easier than in amniotic models of development. The functions of cilia appear to be well conserved among vertebrates. In non-vertebrate model organisms, such as *Drosophila* and *C. elegans*, the roles of cilia in development are not conserved. Similarly, the vestibular structures of the inner ear are well conserved across vertebrates, so studying the development of this aspect of inner ear function in the zebrafish provides an easier and cheaper approach than studies in chick or mouse. It should be noted that the zebrafish is not a perfect model for understanding every aspect of mammalian ear development; zebrafish lack a cochlea and form aragonitic otoliths instead of calcitic otoconia. However, a lot of the molecular pathways involved in the specification and development of inner ear structures are conserved. This makes the zebrafish a valuable complementary model system for understanding ear development and disease.

Appendix A

Movie Legends

All movies were recorded at 300 frames per second (fps) and played back at 15fps.

Movie 1: 18S AB strain OV

Movie of Figure 3.3A. The left ear in dorsolateral view, with anterior to the right and dorsal to the top. A single motile cilium (white arrowhead) is present on the medial wall of the OV. Immotile cilia are also present, a subset of which are labelled (black arrowheads).

Movie 2: 19S LWT strain OV

Movie of Figure 3.3B. The left ear in dorsolateral view, with anterior to the right and dorsal to the top. Motile cilia can be seen near the forming otoliths (white arrowheads).

Movie 3: 22S LWT strain OV

Movie of Figure 3.3C. The left ear in dorsolateral view, with anterior to the right and dorsal to the top. Motile cilia are present on dorsomedial wall of OV (white arrowheads) as well as near the forming otoliths. Immotile cilia are also present (black arrowheads).

Movie 4: 23S LWT strain OV

Movie of Figure 3.3D. The left ear in dorsolateral view, with anterior to the right and dorsal to the top. The tether cilia of the posterior otolith (top left, black arrowheads) are immotile, with three motile cilia near the otolith.

Movie 5: 26S AB strain OV

Movie of Figure 3.3E. The left ear in dorsolateral view, with anterior to the right and dorsal to the top. Motile cilia move the otoliths passively as they brush past (white arrowheads).

Movie 6: 26S AB strain OV

Movie of inset of Figure 3.3F. The left ear in dorsolateral view, with anterior to the right and dorsal to the top. Different focal plane of same embryo as in Movie 5. A motile cilium is present on the medial wall of the OV that rotated first one way, and then the other, whilst recording (white arrowhead).

Movie 7: 25hpf LWT strain OV

Movie of Figure 3.3G. The left ear in dorsolateral view, with anterior to the right and dorsal to the top. Two motile cilia are present under the mineralised otolith (white arrowheads). The tether cilia supporting the otolith are immotile and longer (black arrowheads).

Movie 8: 22S LWT strain OV

Movie of Figure 3.3H. The left ear in dorsolateral view, with anterior to the right and dorsal to the top. An otolith precursor particle was observed bound to the tip of a motile cilium near the posterior otolith (white arrowhead).

Movie 9: 23S LWT strain OV

The left ear in dorsolateral view, with anterior to the right and dorsal to the top. The focal plane of the movie changes from the medial wall of the OV to the lateral of the OV.

Movie 10: 24S *kei* mutant OV

Movie of Figure 3.4E. The left ear in dorsolateral view, with anterior to the right and dorsal to the top. Two immotile anterior tether cilia (black arrowheads) are present with a nearby motile cilium (white arrowhead). Otolith precursor particles are present, but do not become bound to the tether cilia.

Movie 11: 24.5 hpf *kei* mutant OV

Movie of Figure 3.4F. The left ear in dorsolateral view, with anterior to the right and dorsal to the top. The anterior tether cilia are long and immotile (black arrowheads); four shorter motile cilia are present (white arrowheads).

Movie 12: 22S Z*ovl* sibling OV

Movie of Figure 4.1G. The left ear in dorsolateral view, with anterior to the right and dorsal to the top. Motile cilia are present near the forming otoliths.

Movie 13: 24S Z*ovl* mutant OV

Movie of Figure 4.1H. The left ear in dorsolateral view, with anterior to the right and dorsal to the top. Motile cilia are present near the forming otoliths, the Z*ovl* mutant OV shows no difference in ciliary presence or motility to the Z*ovl* sibling OV at this stage.

Movie 14: 22S *igu*^{tm79a} sibling OV

Movie of inset of Figure 4.3J. The left ear in dorsolateral view, with anterior to the right and dorsal to the top. Three motile cilia are present around the anterior otolith (white arrowheads).

Movie 15: 21S *igu*^{tm79a} mutant OV

Movie of Figure 4.3K. The left ear in dorsolateral view, with anterior to the right and dorsal to the top. No motile cilia are visible within the OV.

Movie 16: 25S *lrrc50* sibling OV

Movie of Figure 4.6E. The left ear in dorsolateral view, with anterior to the top and dorsal to the left. There is one motile cilium visible next to the anterior otolith (white arrowhead).

Movie 17: 26S *lrrc50* mutant OV

Movie of Figure 4.6F. The left ear in dorsolateral view, with anterior to the right and dorsal to the top. All cilia near the forming otolith are immotile (black arrowheads).

Movie 18: 20S *mib* mutant OV

Movie of inset of Figure 4.8F. The left ear in dorsolateral view, with anterior to the right and dorsal to the top. Several tether cilia nucleate the anterior otolith (black arrowheads). Motile cilia are still present around the otolith and have not been lost (white arrowheads).

Movie 19: 22S LWT *atoh1b* morphant OV

Movie of Figure 4.9F. The left ear in dorsolateral view, with anterior to the right and dorsal to the top. No otoliths have nucleated in the atoh1b morphant owing to the absence of tether cells. Several otolith precursor particles are visible; motile (white arrowheads) and immotile (black arrowheads) cilia are present.

Movie 20: 26S *slo* sibling OV

Movie of inset of Figure 4.12C. The left ear in dorsolateral view, with anterior to the right and dorsal to the top. There is one motile cilium next to the anterior otolith (white arrowhead).

Movie 21: 27S *slo* mutant OV

Movie of inset of Figure 4.12D. The left ear in dorsolateral view, with anterior to the right and dorsal to the top. There is one motile cilium next to the anterior otolith (white arrowhead).

Bibliography

Aamar, E. and Dawid, I. B. (2008). Isolation and expression analysis of foxj1 and foxj1. 2 in zebrafish embryos. The International Journal of Developmental Biology *52*, 985–991.

Abbas, L. and Whitfield, T. T. (2010). The zebrafish inner ear. In Zebrafish, (Perry, S. F., Ekker, M., Farrell, A. P. and Brauner, C. J., eds), chapter 4, pp. 123–171. Academic Press.

Afzelius, B. A. (2004). Cilia-related diseases. Journal of Pathology *204*, 470–477.

Ahmed, Z. M., Goodyear, R., Riazuddin, S., Lagziel, A., Legan, P. K., Behra, M., Burgess, S. M., Lilley, K. S., Wilcox, E. R., Riazuddin, S., Griffith, A. J., Frolenkov, G. I., Belyantseva, I. A., Richardson, G. P. and Friedman, T. B. (2006). The tip-link antigen, a protein associated with the transduction complex of sensory hair cells, is protocadherin-15. The Journal of Neuroscience *26*, 7022–34.

Bai, C. B., Auerbach, W., Lee, J. S., Stephen, D. and Joyner, A. L. (2002). Gli2, but not Gli1, is required for initial Shh signaling and ectopic activation of the Shh pathway. Development *129*, 4753–61.

Bang, P. I., Sewell, W. F. and Malicki, J. J. (2001). Morphology and cell type heterogeneities of the inner ear epithelia in adult and juvenile zebrafish (Danio rerio). The Journal of Comparative Neurology *438*, 173–90.

Bärenz, F., Mayilo, D. and Gruss, O. J. (2011). Centriolar satellites: busy orbits around the centrosome. European Journal of Cell Biology *90*, 983–9.

Basten, S. G. and Giles, R. H. (2013). Functional aspects of primary cilia in signaling, cell cycle and tumorigenesis. Cilia *2*, 6.

Baxendale, S., Holdsworth, C. J., Meza Santoscoy, P. L., Harrison, M. R. M., Fox, J., Parkin, C. A., Ingham, P. W. and Cunliffe, V. T. (2012). Identification of compounds with anti-convulsant properties in a zebrafish model of epileptic seizures. Disease Models & Mechanisms *5*, 773–84.

Berning, S., Willig, K. I., Steffens, H., Dibaj, P. and Hell, S. W. (2012). Nanoscopy in a living mouse brain. Science *335*, 551.

Billingsley, G., Bin, J., Fieggen, K. J., Duncan, J. L., Gerth, C., Ogata, K., Wodak, S. S., Traboulsi, E. I., Fishman, G. A., Paterson, A., Chitayat, D., Knueppel, T., Millán, J. M., Mitchell, G. A., Deveault, C. and Héon, E. (2010). Mutations in chaperonin-like BBS genes are a major contributor to disease development in a multiethnic Bardet-Biedl syndrome patient population. Journal of Medical Genetics *47*, 453–63.

Bisgrove, B. W. and Yost, H. J. (2006). The roles of cilia in developmental disorders and disease. Development *133*, 4131–4143.

Borovina, A. and Ciruna, B. (2013). IFT88 plays a cilia- and PCP-independent role in controlling oriented cell divisions during vertebrate embryonic development. Cell Reports *5*, 37–43.

Borovina, A., Superina, S., Voskas, D. and Ciruna, B. (2010). Vangl2 directs the posterior tilting and asymmetric localization of motile primary cilia. Nature Cell Biology *12*, 407–412.

Brand, M., Heisenberg, C. P., Warga, R. M., Pelegri, F., Karlstrom, R. O., Beuchle, D., Picker, A., Jiang, Y. J., Furutani-Seiki, M., van Eeden, F. J., Granato, M., Haffter, P., Hammerschmidt, M., Kane, D. A., Kelsh, R. N., Mullins, M. C., Odenthal, J. and Nüsslein-Volhard, C. (1996). Mutations affecting development of the midline and general body shape during zebrafish embryogenesis. Development *123*, 129–42.

Brignull, H. R., Raible, D. W. and Stone, J. S. (2009). Feathers and fins: non-mammalian models for hair cell regeneration. Brain Research *1277*, 12–23.

Buck, L. M., Winter, M. J., Redfern, W. S. and Whitfield, T. T. (2012). Ototoxin-induced cellular damage in neuromasts disrupts lateral line function in larval zebrafish. Hearing Research *284*, 67–81.

Cantagrel, V., Silhavy, J. L., Bielas, S. L., Swistun, D., Holden, K. R., Marsh, S. E., Bertrand, J. Y., Audollent, S., Attie, T., Dobyns, W. B., Traver, D., Al-gazali, L., Ali, B. R., Lindner, T. H., Caspary, T., Otto, E. A., Hildebrandt, F., Glass, I. A., Logan, C. V., Johnson, C. A., Bennett, C., Brancati, F., Joubert, T. I., Related, S., Jsrd, D., Group, S., Valente, E. M. and Woods, C. G. (2008). Mutations in the Cilia Gene ARL13B Lead to the Classical Form of Joubert Syndrome. The American Journal of Human Genetics *83*, 170–179.

Caron, A., Xu, X. and Lin, X. (2012). Wnt/β-catenin signaling directly regulates Foxj1 expression and ciliogenesis in zebrafish Kupffer's vesicle. Development *139*, 514–524.

Caspary, T., Larkins, C. E. and Anderson, K. V. (2007). The graded response to Sonic Hedgehog depends on cilia architecture. Developmental Cell *12*, 767–78.

Chang, N., Sun, C., Gao, L., Zhu, D., Xu, X., Zhu, X., Xiong, J.-W. and Xi, J. J. (2013). Genome editing with RNA-guided Cas9 nuclease in zebrafish embryos. Cell Research *23*, 465–72.

Clendenon, S. G., Shah, B., Miller, C. A., Schmeisser, G., Walter, A., Gattone II, V. H., Barald, K. F., Liu, Q. and Marrs, J. A. (2009). Cadherin-11 Controls Otolith Assembly: Evidence for Extracellular Cadherin Activity. Developmental Dynamics *238*, 1909 –1922.

Colantonio, J. R., Vermot, J., Wu, D., Langenbacher, A. D., Fraser, S., Chen, J.-N. and Hill, K. L. (2009). The dynein regulatory complex is required for ciliary motility and otolith biogenesis in the inner ear. Nature *457*, 205–9.

Cotanche, D. A. and Corwin, J. T. (1991). Stereociliary bundles reorient during hair cell development and regeneration in the chick cochlea. Hearing Research *52*, 379–402.

Deans, M. R. (2013). A Balance of Form and Function: Planar Polarity and Development of the Vestibular Maculae. Seminars in Cell & Developmental Biology *24*, 490–498.

Deans, M. R., Peterson, J. M. and Wong, G. W. (2010). Mammalian Otolin: A Multimeric Glycoprotein Specific to the Inner Ear that Interacts with Otoconial Matrix Protein Otoconin-90 and Cerebellin-1. PLoS ONE *5*, e12765.

Delaval, B., Bright, A., Lawson, N. D. and Doxsey, S. (2011). The cilia protein IFT88 is required for spindle orientation in mitosis. Nature Cell Biology *13*, 461–8.

Denman-Johnson, K. and Forge, A. (1999). Establishment of hair bundle polarity and orientation in the developing vestibular system of the mouse. Journal of Neurocytology *28*, 821–35.

Duldulao, N. A., Lee, S. and Sun, Z. (2009). Cilia localization is essential for in vivo functions of the Joubert syndrome protein Arl13b/Scorpion. Development *136*, 4033–42.

Dunkelberger, D. G., Dean, J. M. and Norimitsu, W. (1980). The Ultrastructure of the Otolithic Membrane and Otolith in the Juvenile Mummichog, Fundulus heteroclitus. Journal of Morphology *163*, 367–377.

Echeverri, K. and Oates, A. C. (2007). Coordination of symmetric cyclic gene expression during somitogenesis by Suppressor of Hairless involves regulation of retinoic acid catabolism. Developmental Biology *301*, 388–403.

Eggenschwiler, J. T. and Anderson, K. V. (2007). Cilia and developmental signaling. Annual Review of Cell and Developmental Biology *23*, 345–73.

Essner, J. J., Amack, J. D., Nyholm, M. K., Harris, E. B. and Yost, H. J. (2005). Kupffer's vesicle is a ciliated organ of asymmetry in the zebrafish embryo that initiates left-right development of the brain, heart and gut. Development *132*, 1247–60.

Feistel, K. and Blum, M. (2006). Three types of cilia including a novel 9+4 axoneme on the notochordal plate of the rabbit embryo. Developmental Dynamics *235*, 3348–58.

Flicek, P., Ahmed, I., Amode, M. R., Barrell, D., Beal, K., Brent, S., Carvalho-Silva, D., Clapham, P., Coates, G., Fairley, S., Fitzgerald, S., Gil, L., García-Girón, C., Gordon, L., Hourlier, T., Hunt, S., Juettemann, T., Kähäri, A. K., Keenan, S., Komorowska, M., Kulesha, E., Longden, I., Maurel, T., McLaren, W. M., Muffato, M., Nag, R., Overduin, B., Pignatelli, M., Pritchard, B., Pritchard, E., Riat, H. S., Ritchie, G. R. S., Ruffier, M., Schuster, M., Sheppard, D., Sobral, D., Taylor, K., Thormann, A., Trevanion, S., White, S., Wilder, S. P., Aken, B. L., Birney, E., Cunningham, F., Dunham, I., Harrow, J., Herrero, J., Hubbard, T. J. P., Johnson, N., Kinsella, R., Parker, A., Spudich, G., Yates, A., Zadissa, A. and Searle, S. M. J. (2013). Ensembl 2013. Nucleic Acids Research *41*, D48–55.

Flock, A. and Duvall, A. J. (1965). The Ultrastructure of the Kinocilium of the Sensory Cells in the Inner Ear and Lateral Line Organs. The Journal of Cell Biology *25*, 1–8.

Freshour, J., Yokoyama, R. and Mitchell, D. R. (2007). Chlamydomonas flagellar outer row dynein assembly protein ODA7 interacts with both outer row and I1 inner row dyneins. The Journal of Biological Chemistry *282*, 5404–12.

Fritzsch, B., Barald, K. F. and Lomax, M. I. (1998). Early Embryology of the Vertebrate Ear. In Development of the Auditory System, (Rubel, E. W., Popper, A. N. and Fay, R. R., eds), chapter 3, pp. 80–145. Springer-Verlag New York.

Gao, C., Wang, G., Amack, J. D. and Mitchell, D. R. (2010). Oda16/Wdr69 is essential for axonemal dynein assembly and ciliary motility during zebrafish embryogenesis. Developmental Dynamics *239*, 2190–7.

Geisler, R., Rauch, G.-J., Geiger-Rudolph, S., Albrecht, A., van Bebber, F., Berger, A., Busch-Nentwich, E., Dahm, R., Dekens, M. P. S., Dooley, C., Elli, A. F., Gehring, I., Geiger, H., Geisler, M., Glaser, S., Holley, S., Huber, M., Kerr, A., Kirn, A., Knirsch, M., Konantz, M., Küchler, A. M., Maderspacher, F., Neuhauss, S. C., Nicolson, T., Ober, E. A., Praeg, E., Ray, R., Rentzsch, B., Rick, J. M., Rief, E., Schauerte, H. E., Schepp, C. P., Schönberger, U., Schonthaler, H. B., Seiler, C., Sidi, S., Söllner, C., Wehner, A., Weiler, C. and Nüsslein-Volhard, C. (2007). Large-scale mapping of mutations affecting zebrafish development. BMC Genomics *8*, 11.

Glazer, A. M., Wilkinson, A. W., Backer, C. B., Lapan, S. W., Gutzman, J. H., Cheeseman, I. M. and Reddien, P. W. (2010). The Zn finger protein Iguana impacts Hedgehog signaling by promoting ciliogenesis. Developmental Biology *337*, 148–56.

Goetz, S. C. and Anderson, K. V. (2010). The primary cilium: a signalling centre during vertebrate development. Nature Reviews Genetics *11*, 331–44.

Goodyear, R. J. and Richardson, G. P. (2002). Extracellular matrices associated with the apical surfaces of sensory epithelia in the inner ear: molecular and structural diversity. Journal of Neurobiology *53*, 212–27.

Goodyear, R. J. and Richardson, G. P. (2003). A novel antigen sensitive to calcium chelation that is associated with the tip links and kinocilial links of sensory hair bundles. The Journal of Neuroscience *23*, 4878–87.

Granato, M., van Eeden, F. J., Schach, U., Trowe, T., Brand, M., Furutani-Seiki, M., Haffter, P., Hammerschmidt, M., Heisenberg, C. P., Jiang, Y. J., Kane, D. A., Kelsh, R. N., Mullins, M. C., Odenthal, J. and Nüsslein-Volhard, C. (1996). Genes controlling and mediating locomotion behavior of the zebrafish embryo and larva. Development *123*, 399–413.

Green, J. L., Inoue, T. and Sternberg, P. W. (2008). Opposing Wnt pathways orient cell polarity during organogenesis. Cell *134*, 646–56.

Guirao, B., Meunier, A., Mortaud, S., Aguilar, A., Corsi, J.-M., Strehl, L., Hirota, Y., Desoeuvre, A., Boutin, C., Han, Y.-G., Mirzadeh, Z., Cremer, H., Montcouquiol, M., Sawamoto, K. and Spassky, N. (2010). Coupling between hydrodynamic forces and planar cell polarity orients mammalian motile cilia. Nature Cell Biology *12*, 341–50.

Haddon, C., Jiang, Y., Smithers, L. and Lewis, J. (1998). Delta-Notch signalling and the patterning of sensory cell differentiation in the zebrafish ear: evidence from the mind bomb mutant. Development *125*, 4637–4644.

Haddon, C. and Lewis, J. (1996). Early Ear Development in the Embryo of the Zebrafish, Danio rerio. Journal of Comparative Neurology *365*, 113–128.

Haddon, C., Mowbray, C., Whitfield, T., Jones, D., Gschmeissner, S. and Lewis, J. (1999). Hair cells without supporting cells: further studies in the ear of the zebrafish mind bomb mutant. Journal of Neurocytology *28*, 837–50.

Hammond, K. L., Loynes, H. E., Folarin, A. A., Smith, J. and Whitfield, T. T. (2003). Hedgehog signalling is required for correct anteroposterior patterning of the zebrafish otic vesicle. Development *130*, 1403–1417.

Hammond, K. L., van Eeden, F. J. M. and Whitfield, T. T. (2010). Repression of Hedgehog signalling is required for the acquisition of dorsolateral cell fates in the zebrafish otic vesicle. Development *137*, 1361–1371.

Hammond, K. L. and Whitfield, T. T. (2011). Fgf and Hh signalling act on a symmetrical pre-pattern to specify anterior and posterior identity in the zebrafish otic placode and vesicle. Development *138*, 3977–87.

Hawkins, T. A., Haramis, A.-P., Etard, C., Prodromou, C., Vaughan, C. K., Ashworth, R., Ray, S., Behra, M., Holder, N., Talbot, W. S., Pearl, L. H., Strähle, U. and Wilson, S. W. (2008). The ATPase-dependent chaperoning activity of Hsp90a regulates thick filament formation and integration during skeletal muscle myofibrillogenesis. Development *135*, 1147–56.

Hirokawa, N., Tanaka, Y., Okada, Y. and Takeda, S. (2006). Nodal flow and the generation of left-right asymmetry. Cell *125*, 33–45.

Hoey, D. A., Chen, J. C. and Jacobs, C. R. (2012a). The primary cilium as a novel extracellular sensor in bone. Frontiers in Endocrinology *3*.

Hoey, D. A., Downs, M. E. and Jacobs, C. R. (2012b). The mechanics of the primary cilium: An intricate structure with complex function. Journal of Biomechanics *45*, 17–26.

Holley, M., Rhodes, C., Kneebone, A., Herde, M. K., Fleming, M. and Steel, K. P. (2010). Emx2 and early hair cell development in the mouse inner ear. Developmental Biology *340*, 547–56.

Hu, Z., Zhang, J. and Zhang, Q. (2011). Expression pattern and functions of autophagy-related gene atg5 in zebrafish organogenesis. Autophagy *7*, 1514–1527.

Huang, P. and Schier, A. F. (2009). Dampened Hedgehog signaling but normal Wnt signaling in zebrafish without cilia. Development *136*, 3089–98.

Huang, P., Zhu, Z., Lin, S. and Zhang, B. (2012). Reverse genetic approaches in zebrafish. Journal of Genetics and Genomics *39*, 421–33.

Huangfu, D., Liu, A., Rakeman, A. S., Murcia, N. S., Niswander, L. and Anderson, K. V. (2003). Hedgehog signalling in the mouse requires intraflagellar transport proteins. Nature *426*, 83–87.

Hughes, I., Blasiole, B., Huss, D., Warchol, M. E., Rath, N. P., Hurle, B., Ignatova, E., Dickman, J. D., Thalmann, R., Levenson, R. and Ornitz, D. M. (2004). Otopetrin 1 is required for otolith formation in the zebrafish Danio rerio. Developmental Biology *276*, 391–402.

Hughes, I., Thalmann, I., Thalmann, R. and Ornitz, D. M. (2006). Mixing model systems: using zebrafish and mouse inner ear mutants and other organ systems to unravel the mystery of otoconial development. Brain Research *1091*, 58–74.

Hwang, W. Y., Fu, Y., Reyon, D., Maeder, M. L., Tsai, S. Q., Sander, J. D., Peterson, R. T., Yeh, J.-R. J. and Joung, J. K. (2013). Efficient genome editing in zebrafish using a CRISPR-Cas system. Nature Biotechnology *31*, 227–9.

Ibsch, M., Anken, R. H., Vöhringer, P. and Rahmann, H. (2001). Vesicular bodies in fish maculae are artifacts not contributing to otolith growth. Hearing Research *153*, 80–90.

Inglis, P. N., Boroevich, K. A. and Leroux, M. R. (2006). Piecing together a ciliome. Trends in Genetics *22*, 491–500.

Ishigaki, Y., Nakamura, Y., Oikawa, Y., Yano, Y., Kuwabata, S., Nakagawa, H., Tomosugi, N. and Takegami, T. (2012). Observation of live ticks (Haemaphysalis flava) by scanning electron microscopy under high vacuum pressure. PLoS ONE *7*, e32676.

Itoh, M., Kim, C.-H., Palardy, G., Oda, T., Jiang, Y.-J., Maust, D., Yeo, S.-Y., Lorick, K., Wright, G. J., Ariza-McNaughton, L., Weissman, A. M., Lewis, J., Chandrasekharappa, S. C. and Chitnis, A. B. (2003). Mind bomb is a ubiquitin ligase that is essential for efficient activation of Notch signaling by Delta. Developmental Cell *4*, 67–82.

Jagger, D., Collin, G., Kelly, J., Towers, E., Nevill, G., Longo-Guess, C., Benson, J., Halsey, K., Dolan, D., Marshall, J., Naggert, J. and Forge, A. (2011). Alström Syndrome protein ALMS1 localizes to basal bodies of cochlear hair cells and regulates cilium-dependent planar cell polarity. Human Molecular Genetics *20*, 466–81.

Jékely, G., Colombelli, J., Hausen, H., Guy, K., Stelzer, E., Nédélec, F. and Arendt, D. (2008). Mechanism of phototaxis in marine zooplankton. Nature *456*, 395–9.

Jiang, Y. J., Brand, M., Heisenberg, C. P., Beuchle, D., Furutani-Seiki, M., Kelsh, R. N., Warga, R. M., Granato, M., Haffter, P., Hammerschmidt, M., Kane, D. A., Mullins, M. C., Odenthal, J., van Eeden, F. J. and Nüsslein-Volhard, C. (1996). Mutations affecting neurogenesis and brain morphology in the zebrafish, Danio rerio. Development *123*, 205–16.

Jones, C., Roper, V. C., Foucher, I., Qian, D., Banizs, B., Petit, C., Yoder, B. K. and Chen, P. (2008). Ciliary proteins link basal body polarization to planar cell polarity regulation. Nature Genetics *40*, 69–77.

Jones, G. P., Lukashkina, V. A., Russell, I. J. and Lukashkin, A. N. (2010). The Vestibular System Mediates Sensation of Low-Frequency Sounds in Mice. Journal of the Association for Research in Otolaryngology *11*, 725–32.

Kang, Y.-J., Stevenson, A. K., Yau, P. M. and Kollmar, R. (2008). Sparc protein is required for normal growth of zebrafish otoliths. Journal of the Association for Research in Otolaryngology *9*, 436–51.

Karlstrom, R. O. (2003). Genetic analysis of zebrafish gli1 and gli2 reveals divergent requirements for gli genes in vertebrate development. Development *130*, 1549–1564.

Karlstrom, R. O., Talbot, W. S. and Schier, A. F. (1999). Comparative synteny cloning of zebrafish you-too : mutations in the Hedgehog target gli2 affect ventral forebrain patterning. Genes & Development *13*, 388–393.

Kazmierczak, P., Sakaguchi, H., Tokita, J., Wilson-Kubalek, E. M., Milligan, R. A., Müller, U. and Kachar, B. (2007). Cadherin 23 and protocadherin 15 interact to form tip-link filaments in sensory hair cells. Nature *449*, 87–91.

Kim, H. R., Richardson, J., van Eeden, F. and Ingham, P. W. (2010). Gli2a protein localization reveals a role for Iguana/DZIP1 in primary ciliogenesis and a dependence of Hedgehog signal transduction on primary cilia in the zebrafish. BMC Biology *8*, 65.

Kimmel, C. B., Ballard, W. W., Kimmel, S. R., Ullmann, B. and Schilling, T. F. (1995). Stages of embryonic development of the zebrafish. Developmental Dynamics *203*, 253–310.

Kimmel, C. B., Patterson, J. and Kimmel, R. O. (1974). The development and behavioral characteristics of the startle response in the zebra fish. Developmental Psychobiology *7*, 47–60.

Kindt, K. S., Finch, G. and Nicolson, T. (2012). Kinocilia Mediate Mechanosensitivity in Developing Zebrafish Hair Cells. Developmental Cell *23*, 329–341.

Kramer-Zucker, A. G., Olale, F., Haycraft, C. J., Yoder, B. K., Schier, A. F. and Drummond, I. A. (2005). Cilia-driven fluid flow in the zebrafish pronephros, brain and Kupffer's vesicle is required for normal organogenesis. Development *132*, 1907–21.

Kunimoto, K., Yamazaki, Y., Nishida, T., Shinohara, K., Ishikawa, H., Hasegawa, T., Okanoue, T., Hamada, H., Noda, T., Tamura, A., Tsukita, S. and Tsukita, S. (2012). Coordinated Ciliary Beating Requires Odf2-Mediated Polarization of Basal Bodies via Basal Feet. Cell *148*, 189–200.

Larusso, N. F. and Masyuk, T. V. (2011). The role of cilia in the regulation of bile flow. Digestive Diseases *29*, 6–12.

Li, X., Anken, R. H., Wang, G., Hilbig, R. and Liu, Y. (2010). Effects of Wall Vessel Rotation on the Growth of Larval Zebrafish Inner Ear Otoliths. Microgravity Science and Technology *23*, 13–18.

Li, Y. and Hu, J. (2011). Small GTPases and cilia. Protein & Cell *2*, 13–25.

Li, Y., Wei, Q., Zhang, Y., Ling, K. and Hu, J. (2010). The small GTPases ARL-13 and ARL-3 coordinate intraflagellar transport and ciliogenesis. The Journal of Cell Biology *189*, 1039–51.

Louvi, A. and Grove, E. A. (2011). Cilia in the CNS: The Quiet Organelle Claims Center Stage. Neuron *69*, 1046–60.

Maglione, M. and Sigrist, S. J. (2013). Seeing the forest tree by tree: super-resolution light microscopy meets the neurosciences. Nature Neuroscience *16*, 790–7.

Malicki, J., Schier, A., Solnica-Krezel, L., Stemple, D., Neuhauss, S., Stainier, D., Abdelilah, S., Rangini, Z., Zwartkruis, F. and Driever, W. (1996). Mutations affecting development of the zebrafish ear. Development *123*, 275–283.

Mangos, S., Lam, P.-Y., Zhao, A., Liu, Y., Mudumana, S., Vasilyev, A., Liu, A. and Drummond, I. A. (2010). The ADPKD genes pkd1a/b and pkd2 regulate extracellular matrix formation. Disease Models & Mechanisms *3*, 354–65.

Mariño, G., Fernández, A. F., Cabrera, S., Lundberg, Y. W., Cabanillas, R., Rodriguez, F., Salvador-Montoliu, N., Vega, J. A., Germaná, A., Fueyo, A., Freije, J. M. P. and López-Otin, C. (2010). Autophagy is essential for mouse sense of balance. The Journal of Clinical Investigation *120*, 2331–44.

Marshall, J. D., Hinman, E. G., Collin, G. B., Beck, S., Cerqueira, R., Maffei, P., Milan, G., Zhang, W., Wilson, D. I., Hearn, T., Vettor, R., Veronese, C., Martin, M., So, V. and Nishina, P. M. (2007). Spectrum of ALMS1 Variants and Evaluation of Genotype-Phenotype Correlations in Alström Syndrome. Human Mutation *28*, 1114–1123.

McGrath, J., Somlo, S., Makova, S., Tian, X. and Brueckner, M. (2003). Two populations of node monocilia initiate left-right asymmetry in the mouse. Cell *114*, 61–73.

McIntyre, J. C., Davis, E. E., Joiner, A., Williams, C. L., Tsai, I.-C., Jenkins, P. M., McEwen, D. P., Zhang, L., Escobado, J., Thomas, S., Szymanska, K., Johnson, C. A., Beales, P. L., Green, E. D., Mullikin, J. C., Sabo, A., Muzny, D. M., Gibbs, R. A., Attié-Bitach, T., Yoder, B. K., Reed, R. R., Katsanis, N. and Martens, J. R. (2012). Gene therapy rescues cilia defects and restores olfactory function in a mammalian ciliopathy model. Nature Medicine *18*, 1423–8.

McIntyre, J. C., Williams, C. L. and Martens, J. R. (2013). Smelling the roses and seeing the light: gene therapy for ciliopathies. Trends in Biotechnology *31*, 355–63.

Millimaki, B. B., Sweet, E. M., Dhason, M. S. and Riley, B. B. (2007). Zebrafish atoh1 genes: classic proneural activity in the inner ear and regulation by Fgf and Notch. Development *134*, 295–305.

Mo, W., Chen, F., Nechiporuk, A. and Nicolson, T. (2010). Quantification of vestibular-induced eye movements in zebrafish larvae. BMC Neuroscience *11*, 110.

Molla-Herman, A., Ghossoub, R., Blisnick, T., Meunier, A., Serres, C., Silbermann, F., Emmerson, C., Romeo, K., Bourdoncle, P., Schmitt, A., Saunier, S., Spassky, N., Bastin,

P. and Benmerah, A. (2010). The ciliary pocket: an endocytic membrane domain at the base of primary and motile cilia. Journal of Cell Science *123*, 1785–95.

Moorman, S. J., Burress, C., Cordova, R. and Slater, J. (1999). Stimulus dependence of the development of the zebrafish (Danio rerio) vestibular system. Journal of Neurobiology *38*, 247–58.

Murayama, E., Herbomel, P., Kawakami, A., Takeda, H. and Nagasawa, H. (2005). Otolith matrix proteins OMP-1 and Otolin-1 are necessary for normal otolith growth and their correct anchoring onto the sensory maculae. Mechanisms of Development *122*, 791–803.

Murayama, E., Takagi, Y., Ohira, T., Davis, J. G., Greene, M. I. and Nagasawa, H. (2002). Fish otolith contains a unique structural protein, otolin-1. European Journal of Biochemistry *269*, 688–96.

Murcia, N. S., Richards, W. G., Yoder, B. K., Mucenski, M. L., Dunlap, J. R. and Woychik, R. P. (2000). The Oak Ridge Polycystic Kidney (orpk) disease gene is required for left-right axis determination. Development *127*, 2347–55.

Nauli, S. M., Jin, X. and Hierck, B. P. (2011). The mechanosensory role of primary cilia in vascular hypertension. International Journal of Vascular Medicine *2011*, 376281.

Nayak, G. D., Ratnayaka, H. S. K., Goodyear, R. J. and Richardson, G. P. (2007). Development of the hair bundle and mechanotransduction. The International Journal of Developmental Biology *51*, 597–608.

Neugebauer, J. M., Amack, J. D., Peterson, A. G., Bisgrove, B. W. and Yost, H. J. (2009). FGF signalling during embryo development regulates cilia length in diverse epithelia. Nature *458*, 651–4.

Ninkovic, J., Stigloher, C., Lillesaar, C. and Bally-Cuif, L. (2008). Gsk3beta/PKA and Gli1 regulate the maintenance of neural progenitors at the midbrain-hindbrain boundary in concert with E(Spl) factor activity. Development *135*, 3137–48.

Nonaka, S., Shiratori, H., Saijoh, Y. and Hamada, H. (2002). Determination of left right patterning of the mouse embryo by artificial nodal flow. Nature *418*, 96–99.

Nonaka, S., Tanaka, Y., Okada, Y., Takeda, S., Harada, A., Kanai, Y., Kido, M. and Hirokawa, N. (1998). Randomization of left-right asymmetry due to loss of nodal cilia generating leftward flow of extraembryonic fluid in mice lacking KIF3B motor protein. Cell *95*, 829–37.

Nonaka, S., Yoshiba, S., Watanabe, D., Ikeuchi, S. and Goto, T. (2005). De Novo Formation of Left–Right Asymmetry by Posterior Tilt of Nodal Cilia. PLoS Biology *3*, e268.

Obholzer, N., Swinburne, I. A., Schwab, E., Nechiporuk, A. V., Nicolson, T. and Megason, S. G. (2012). Rapid positional cloning of zebrafish mutations by linkage and homozygosity mapping using whole-genome sequencing. Development *139*, 4280–4290.

Oghalai, J. S., Manolidis, S., Barth, J. L., Stewart, M. G. and Jenkins, H. A. (2000). Unrecognized benign paroxysmal positional vertigo in elderly patients. Otolaryngology - Head and Neck Surgery *122*, 630–634.

Pan, J., Seeger-Nukpezah, T. and Golemis, E. A. (2012). The role of the cilium in normal and abnormal cell cycles: emphasis on renal cystic pathologies. Cellular and Molecular Life Sciences *70*, 1849–74.

Panizzi, J. R., Jessen, J. R., Drummond, I. A. and Solnica-Krezel, L. (2007). New functions for a vertebrate Rho guanine nucleotide exchange factor in ciliated epithelia. Development *134*, 921–31.

Pazour, G. J., Baker, S. A., Deane, J. A., Cole, D. G., Dickert, B. L., Rosenbaum, J. L., Witman, G. B. and Besharse, J. C. (2002). The intraflagellar transport protein, IFT88, is essential for vertebrate photoreceptor assembly and maintenance. The Journal of Cell Biology *157*, 103–13.

Pease, R., Hayes, T., Camp, A. and Amer, N. (1966). Electron Microscopy of Living Insects. Science *154*, 1185–1186.

Petko, J. A., Millimaki, B. B., Riley, B. B. and Levenson, R. (2008). Otoc1: A Novel Otoconin-90 Ortholog Required for Otolith Mineralization in Zebrafish. Developmental Neurobiology *68*, 209–222.

Phillips, B. T., Bolding, K. and Riley, B. B. (2001). Zebrafish fgf3 and fgf8 encode redundant functions required for otic placode induction. Developmental Biology *235*, 351–365.

Phillips, J. B., Blanco-Sanchez, B., Lentz, J. J., Tallafuss, A., Khanobdee, K., Sampath, S., Jacobs, Z. G., Han, P. F., Mishra, M., Titus, T. A., Williams, D. S., Keats, B. J., Washbourne, P. and Westerfield, M. (2011). Harmonin (Ush1c) is required in zebrafish Müller glial cells for photoreceptor synaptic development and function. Disease Models & Mechanisms *4*, 786–800.

Pisam, M., Jammet, C. and Laurent, D. (2002). First steps of otolith formation of the zebrafish: role of glycogen? Cell and Tissue Research *310*, 163–168.

Platt, C. (1993). Zebrafish inner ear sensory surfaces are similar to those in goldfish. Hearing Research *65*, 133–40.

Purves, D., Augustine, G. J., Fitzpatrick, D., Katz, L. C., LaMantia, A.-S., McNamara, J. O. and Williams, S. M., eds (2001). Neuroscience. 2nd edition, Sinauer Associates, Sunderland (MA).

Radosevic, M., Robert-Moreno, A., Coolen, M., Bally-Cuif, L. and Alsina, B. (2011). Her9 represses neurogenic fate downstream of Tbx1 and retinoic acid signaling in the inner ear. Development *138*, 397–408.

Riley, B. B. and Grunwald, D. J. (1996). A mutation in zebrafish affecting a localized cellular function required for normal ear development. Developmental Biology *179*, 427–35.

Riley, B. B. and Moorman, S. J. (2000). Development of utricular otoliths, but not saccular otoliths, is necessary for vestibular function and survival in zebrafish. Journal of Neurobiology *43*, 329–337.

Riley, B. B. and Phillips, B. T. (2003). Ringing in the new ear: resolution of cell interactions in otic development. Developmental Biology *261*, 289–312.

Riley, B. B., Zhu, C., Janetopoulos, C. and Aufderheide, K. J. (1997). A Critical Period of Ear Development Controlled by Distinct Populations of Ciliated Cells in the Zebrafish. Developmental Biology *191*, 191–201.

Robert, A., Margall-Ducos, G., Guidotti, J.-E., Brégerie, O., Celati, C., Bréchot, C. and Desdouets, C. (2007). The intraflagellar transport component IFT88/polaris is a centrosomal protein regulating G1-S transition in non-ciliated cells. Journal of Cell Science *120*, 918–918.

Rosenbaum, J. L. and Witman, G. B. (2002). Intraflagellar transport. Nature Reviews Molecular Cell Biology *3*, 813–25.

Ross, A. J., May-Simera, H., Eichers, E. R., Kai, M., Hill, J., Jagger, D. J., Leitch, C. C., Chapple, J. P., Munro, P. M., Fisher, S., Tan, P. L., Phillips, H. M., Leroux, M. R., Henderson, D. J., Murdoch, J. N., Copp, A. J., Eliot, M.-M., Lupski, J. R., Kemp, D. T., Dollfus, H., Tada, M., Katsanis, N., Forge, A. and Beales, P. L. (2005). Disruption of Bardet-Biedl syndrome ciliary proteins perturbs planar cell polarity in vertebrates. Nature Genetics *37*, 1135–40.

Satir, P. and Christensen, S. T. (2007). Overview of Structure and Function of Mammalian Cilia. Annual Review of Physiology *69*, 377–400.

Satir, P. and Sleigh, M. A. (1990). The Physiology of Cilia and Mucociliary Interactions. Annual Review of Physiology *52*, 137–55.

Schermelleh, L., Heintzmann, R. and Leonhardt, H. (2010). A guide to super-resolution fluorescence microscopy. The Journal of Cell Biology *190*, 165–75.

Schier, A. F., Neuhauss, S. C., Harvey, M., Malicki, J., Solnica-Krezel, L., Stainier, D. Y., Zwartkruis, F., Abdelilah, S., Stemple, D. L., Rangini, Z., Yang, H. and Driever, W. (1996). Mutations affecting the development of the embryonic zebrafish brain. Development *123*, 165–78.

Schindelin, J., Arganda-Carreras, I., Frise, E., Kaynig, V., Longair, M., Pietzsch, T., Preibisch, S., Rueden, C., Saalfeld, S., Schmid, B., Tinevez, J.-Y., White, D. J., Hartenstein, V., Eliceiri, K., Tomancak, P. and Cardona, A. (2012). Fiji: an open-source platform for biological-image analysis. Nature Methods *9*, 676–82.

Schwander, M., Kachar, B. and Müller, U. (2010). Review series: The cell biology of hearing. The Journal of Cell Biology *190*, 9–20.

Seeley, E. S. and Nachury, M. V. (2010). The perennial organelle: assembly and disassembly of the primary cilium. Journal of Cell Science *123*, 511–8.

Sekimizu, K., Nishioka, N., Sasaki, H., Takeda, H., Karlstrom, R. O. and Kawakami, A. (2004). The zebrafish iguana locus encodes Dzip1, a novel zinc-finger protein required for proper regulation of Hedgehog signaling. Development *131*, 2521–32.

Serluca, F. C., Xu, B., Okabe, N., Baker, K., Lin, S.-Y., Sullivan-Brown, J., Konieczkowski, D. J., Jaffe, K. M., Bradner, J. M., Fishman, M. C. and Burdine, R. D. (2009). Mutations in zebrafish leucine-rich repeat-containing six-like affect cilia motility and result in pronephric cysts, but have variable effects on left-right patterning. Development *136*, 1621–31.

Shiao, J. C., Lin, L. Y., Horng, J. L., Hwang, P. P. and Kaneko, T. (2005). How can teleostean inner ear hair cells maintain the proper association with the accreting otolith? The Journal of Comparative Neurology *488*, 331–341.

Sieger, D., Tautz, D. and Gajewski, M. (2003). The role of Suppressor of Hairless in Notch mediated signalling during zebrafish somitogenesis. Mechanisms of Development *120*, 1083–1094.

Siemens, J., Lillo, C., Dumont, R. A., Reynolds, A., Williams, D. S., Gillespie, P. G. and Müller, U. (2004). Cadherin 23 is a component of the tip link in hair-cell stereocilia. Nature *428*, 950–955.

Sokolowski, B. H. A. and Popper, A. N. (1987). Gross and Ultrastructural Development of the Saccule of the Toadfish Opsanus tau. Journal of Morphology *194*, 323–48.

Söllner, C., Burghammer, M., Busch-Nentwich, E., Berger, J., Schwarz, H., Riekel, C. and Nicolson, T. (2003). Control of crystal size and lattice formation by starmaker in otolith biomineralization. Science *302*, 282–6.

Söllner, C., Schwarz, H., Geisler, R. and Nicolson, T. (2004). Mutated otopetrin 1 affects the genesis of otoliths and the localization of Starmaker in zebrafish. Development Genes and Evolution *214*, 582–90.

Sorokin, S. (1962). Centrioles and the Formation of Rudimentary Cilia by Fibroblasts and Smooth Muscle Cells. The Journal of Cell Biology *15*, 363–377.

Spoor, F., Garland, T., Krovitz, G., Ryan, T. M., Silcox, M. T. and Walker, A. (2007). The primate semicircular canal system and locomotion. PNAS *104*, 10808–12.

Stooke-Vaughan, G. A., Huang, P., Hammond, K. L., Schier, A. F. and Whitfield, T. T. (2012). The role of hair cells, cilia and ciliary motility in otolith formation in the zebrafish otic vesicle. Development *139*, 1777–1787.

Sullivan-Brown, J., Schottenfeld, J., Okabe, N., Hostetter, C. L., Serluca, F. C., Thiberge, S. Y. and Burdine, R. D. (2008). Zebrafish mutations affecting cilia motility share similar cystic phenotypes and suggest a mechanism of cyst formation that differs from pkd2 morphants. Developmental Biology *314*, 261–75.

Sumanas, S., Larson, J. D. and Miller Bever, M. (2003). Zebrafish chaperone protein GP96 is required for otolith formation during ear development. Developmental Biology *261*, 443–455.

Supatto, W. and Vermot, J. (2011). From cilia hydrodynamics to zebrafish embryonic development. Current Topics in Developmental Biology *95*, 33–66.

Takagi, Y. and Takahashi, A. (1999). Characterization of Ootolith Soluble-Matrix Producing Cells in the Saccular Epithelium of Rainbow Trout (Oncorhynchus mykiss) Inner Ear. The Anatomical Record *254*, 322–9.

Tanimoto, M., Ota, Y., Inoue, M. and Oda, Y. (2011). Origin of inner ear hair cells: morphological and functional differentiation from ciliary cells into hair cells in zebrafish inner ear. The Journal of Neuroscience *31*, 3784–94.

Tay, S. Y., Yu, X., Wong, K. N., Panse, P., Ng, C. P. and Roy, S. (2010). The iguana/DZIP1 protein is a novel component of the ciliogenic pathway essential for axonemal biogenesis. Developmental Dynamics *239*, 527–534.

Thisse, C. and Thisse, B. (2005). High Throughput Expression Analysis of ZF-Models Consortium Clones.

Tilney, L. G., Cotanche, D. A. and Tilney, M. S. (1992). Actin filaments, stereocilia and hair cells of the bird cochlea. VI. How the number and arrangement of stereocilia are determined. Development *116*, 213–26.

Tsui, S., Dai, T., Roettger, S., Schempp, W., Salido, E. C. and Yen, P. H. (2000). Identification of two novel proteins that interact with germ-cell-specific RNA-binding proteins DAZ and DAZL1. Genomics *65*, 266–73.

Tsujikawa, M. and Malicki, J. (2004). Intraflagellar transport genes are essential for differentiation and survival of vertebrate sensory neurons. Neuron *42*, 703–16.

van Eeden, F. J., Granato, M., Schach, U., Brand, M., Furutani-Seiki, M., Haffter, P., Hammerschmidt, M., Heisenberg, C. P., Jiang, Y. J., Kane, D. A., Kelsh, R. N., Mullins, M. C., Odenthal, J., Warga, R. M., Allende, M. L., Weinberg, E. S. and Nüsslein-Volhard, C. (1996). Mutations affecting somite formation and patterning in the zebrafish, Danio rerio. Development *123*, 153–64.

van Rooijen, E., Giles, R. H., Voest, E. E., van Rooijen, C., Schulte-Merker, S. and van Eeden, F. J. (2008). LRRC50, a conserved ciliary protein implicated in polycystic kidney disease. Journal of the American Society of Nephrology *19*, 1128–38.

Veland, I. R., Awan, A., Pedersen, L. B., Yoder, B. K. and Christensen, S. T. (2009). Primary cilia and signaling pathways in mammalian development, health and disease. Nephron Physiology *111*, p39–53.

Verhey, K. J., Dishinger, J. and Kee, H. L. (2011). Kinesin motors and primary cilia. Biochemical Society Transactions *39*, 1120–5.

Vio, M. M. and Holme, R. H. (2005). Hearing loss and tinnitus: 250 million people and a US$10 billion potential market. Drug Discovery Today *10*, 1263–5.

Wallingford, J. B. (2010). Planar cell polarity signaling, cilia and polarized ciliary beating. Current Opinion in Cell Biology *22*, 597–604.

Wallingford, J. B. and Mitchell, B. (2011). Strange as it may seem: the many links between Wnt signaling, planar cell polarity, and cilia. Genes & Development *25*, 201–13.

Waters, A. M. and Beales, P. L. (2011). Ciliopathies: an expanding disease spectrum. Pediatric Nephrology *26*, 1039–56.

Wetmore, S. J., Eibling, D. E., Goebel, J. A., Gottshall, K. R., Hoffer, M. E., Magnusson, M. and Raz, Y. (2011). Challenges and opportunities in managing the dizzy older adult. Otolaryngology - Head and Neck Surgery *144*, 651–6.

Wheatley, D. N. (2005). Landmarks in the first hundred years of primary (9+0) cilium research. Cell Biology International *29*, 333–9.

Whitfield, T. T. (2002). Zebrafish as a model for hearing and deafness. Journal of Neurobiology *53*, 157–71.

Whitfield, T. T., Granato, M., van Eeden, F. J., Schach, U., Brand, M., Furutani-Seiki, M., Haffter, P., Hammerschmidt, M., Heisenberg, C. P., Jiang, Y. J., Kane, D. A., Kelsh, R. N., Mullins, M. C., Odenthal, J. and Nüsslein-Volhard, C. (1996). Mutations affecting development of the zebrafish inner ear and lateral line. Development *123*, 241–54.

Whitfield, T. T. and Hammond, K. L. (2007). Axial patterning in the developing vertebrate inner ear. The International Journal of Developmental Biology *51*, 507–520.

Whitfield, T. T., Riley, B. B., Chiang, M.-Y. and Phillips, B. (2002). Development of the zebrafish inner ear. Developmental Dynamics *223*, 427–58.

Wilkinson, C. J., Harris, W. A. and Carl, M. (2009). Cep70 and Cep131 contribute to ciliogenesis in zebrafish embryos. BMC Cell Biology *10*, 17.

Wolff, C., Roy, S., Lewis, K. E., Schauerte, H., Joerg-rauch, G., Kirn, A., Weiler, C., Geisler, R., Haffter, P. and Ingham, P. W. (2004). iguana encodes a novel zinc finger protein with coiled-coil domains essential for Hedgehog signal transduction in the zebrafish embryo. Genes and Development *18*, 1565–1576.

Wood, C. R., Huang, K., Diener, D. R. and Rosenbaum, J. L. (2013). The Cilium Secretes Bioactive Ectosomes. Current Biology *23*, 906–911.

Woods, C., Montcouquiol, M. and Kelley, M. W. (2004). Math1 regulates development of the sensory epithelium in the mammalian cochlea. Nature Neuroscience *7*, 1310–1318.

Wu, D., Freund, J. B., Fraser, S. E. and Vermot, J. (2011). Mechanistic Basis of Otolith Formation during Teleost Inner Ear Development. Developmental Cell *20*, 271–8.

Xiang, M., Gan, L., Li, D., Chen, Z. Y., Zhou, L., O'Malley, B. W., Klein, W. and Nathans, J. (1997). Essential role of POU-domain factor Brn-3c in auditory and vestibular hair cell development. Proceedings of the National Academy of Sciences of the United States of America *94*, 9445–50.

Xiao, T., Roeser, T., Staub, W. and Baier, H. (2005). A GFP-based genetic screen reveals mutations that disrupt the architecture of the zebrafish retinotectal projection. Development *132*, 2955–67.

Yang, A. and Hullar, T. E. (2007). Relationship of semicircular canal size to vestibular-nerve afferent sensitivity in mammals. Journal of Neurophysiology *98*, 3197–205.

Yang, J., Gao, J., Adamian, M., Pawlyk, B., Zhang, L., Sanderson, M. J., Makino, C. L., Li, T., Wen, X.-h. and Zuo, J. (2005). The Ciliary Rootlet Maintains Long-Term Stability of Sensory Cilia. Molecular and Cellular Biology *25*, 4129–4137.

Yoder, B. K., Tousson, A., Millican, L., Wu, J. H., Bugg, C. E., Schafer, J. A. and Balkovetz, D. F. (2002). Polaris, a protein disrupted in orpk mutant mice, is required

for assembly of renal cilium. American Journal of Physiology: Renal Physiology *282*, F541–52.

York, A. G., Parekh, S. H., Nogare, D. D., Fischer, R. S., Temprine, K., Mione, M., Chitnis, A. B., Combs, C. A. and Shroff, H. (2012). Resolution Doubling in Live, Multicellular Organisms via Multifocal Structured Illumination Microscopy. Nature Methods *9*, 749–754.

Yu, X., Lau, D., Ng, C. P. and Roy, S. (2011). Cilia-driven fluid flow as an epigenetic cue for otolith biomineralization on sensory hair cells of the inner ear. Development *138*, 487–94.

Yu, X., Ng, C. P., Habacher, H. and Roy, S. (2008). Foxj1 transcription factors are master regulators of the motile ciliogenic program. Nature Genetics *40*, 1445–1453.

Zeddies, D. G. and Fay, R. R. (2005). Development of the acoustically evoked behavioral response in zebrafish to pure tones. The Journal of Experimental Biology *208*, 1363–72.

Zimmermann, K. W. (1898). Beitrage zur Kenntniss einiger Drusen und epithelien. Arch Mikrosk Anat *52*, 552–706.